Magnetic Resonance Imaging Assessment of Skeletal Muscle Changes Following Chronic Denervation in the Dog

Olga Vasilievna Krivonogova DVM

Submitted in fulfilment of the requirements for the degree of

Master of Veterinary Medicine

University of Glasgow

School of Veterinary Medicine

February 2014

Abstract

This study sought to evaluate the effect of presumed chronic denervation (due to brachial plexus mass lesions) on the magnetic resonance imaging (MRI) appearance of muscle in the dog. One of the features of denervation that has been described is fat infiltration; prior to defining the effect of the brachial plexus mass lesions, this study first attempted to define the normal patterns of fat deposition with increasing body condition scores. MRI assessment of subcutaneous and intramuscular fat deposition was compared against two previously described methods of body condition scoring in the dog. There was a significant relationship between the 9-point body score (BCS) assessment and body fat percentages calculated on the basis of girth and hock measurements. Both of these methods correlated well with MRI determination of subcutaneous fat (SCF) thickness in the dorsal lumbar area and with total (dorsal and ventral) SCF in the cervical area. What was evident from the MRI evaluation of fat deposition was that the pattern of fat deposition in these regions differed, being predominantly subcutaneous in the lumbar region, but with fat deposition in both the subcutaneous and intermuscular regions in the cervical region. In both regions the amount of fat deposition increased from cranial to caudal. Intramuscular fat deposition assessed in terms of T1W signal hyperintensity in the lumbar epaxial muscles correlated well with BCS, though for cervical muscles the correlation was weaker and increasing BCS appeared to have less effect on MRI signal change in normal neck muscle. Having decided to focus on brachial plexus mass lesions, the ability to identify the individual proximal thoracic limb muscles by MRI was assessed. Proximal thoracic limb muscles identification and MRI appearance were found to depend on the MRI plane position, relative to the spine of the scapula. Better results for the identification of individual muscles were achieved on images with the plane aligned parallel to the spine of the scapula or at 90 degree angle to it, and with the limbs positioned in extension along the body and symmetrically to each other. Transverse images permitted better muscle detection. MRI of the proximal thoracic limb of 19 dogs with brachial plexus mass lesions showed a mixed pattern of T1W and T2W hyperintensity and variable degrees of muscles atrophy. Mass lesions were found in three shapes – globoid, tubular and fusiform. Multiple lesions were detected in 9 cases, and in 6 out of 9 cases these included lesions within the thoracic cavity. In 9 cases vertebral canal involvement was evident. Mass lesions were best detectable on the short tau inversion recovery sequence (STIR) followed by T2W and T1FatSat with contrast.

Tables of Contents

List of Chapters

List of Tables

List of Figures

Dedication

To the memory of Dr Lawrence Caruana.

Declaration

I, Olga Vasilievna Krivonogova, declare that the work in this thesis is original, was carried out solely by myself or with due acknowledgements. It has not been submitted in any form for another degree or professional qualification.

Acknowledgements

I would like to express my sincere and deep gratitude to my supervisors, Professor Jacques Penderis and Professor Martin Sullivan for their guidance and invaluable help during my research. I would not be able to fulfil this programme without their advice, patience and moral support.

I would like to thank the Diagnostic Imaging unit staff – Nicola Brannan, Gil Cameron and Mr Gawain Hammond for their assistance in obtaining MR images.

I would like to give thanks to Karen Bell for her participation in the clinical part of my research.

I am especially thankful to Dr Alison King, who was very helpful with the shoulder anatomy evaluation.

I am very grateful to Dr Tim Parkin for his valuable advice in statistics.

Above all, I am very thankful to the all staff of Small Animal Hospital for direct and indirect help.

I would like to thank Mrs Marie Henderson for her kindness and support.

As well, I would like to thank my fellow postgraduate students of the Veterinary School for their help and friendship, special thanks go to Alexane Durand, Marlene Finck, Mariam Ariffin, Intan Shafie and Yao Qi.

1. Introduction

1.1 Review of Magnetic Resonance Imaging (MRI) Sequences Commonly Used in Veterinary Medicine

Magnetic resonance imaging (MRI) is widely used as a diagnostic investigative tool across a wide variety of pathological conditions, including in the investigation of disorders of the peripheral nervous system and muscle. MRI is in general non-invasive and safe, and within the muscle is even capable of identifying subtle changes (Lovitt et al., 2006). The basic source of MRI signal in muscle (and in most tissues) is fat and water.

1.1.1 **T1-Weighted Images**

T1-weighted images are obtained due to differences in T1 relaxation times between different tissues. 90° Radiofrequency (RF) pulses are used to displace protons, which rotate into the x-y plane and move along it in phase; in diphase the decaying signal is released during the return of protons back to the z line. In other words, the T1 signal originates during the relaxation time, and this relaxation time is related to the recovery of magnetisation along z direction after the application of a RF pulse (Gavin & Bagley, 2009). On T1-weighted images fat appears as hyperintense and fluid appears as hypointense. Hyperintensity unrelated to fat can be caused by a paramagnetic substance. Healthy muscle has long T1 relaxation time in contrast to fat, which has a relatively short T1 relaxation time, and this explains why T1-weighted images are very sensitive for the detection of fat. Water has a relatively long T1 relaxation time, and for this reason T1-weighted sequences are not useful for detecting water (Lovitt et al., 2006).

1.1.2 **T1-Weighted Images after Contrast Administration**

After the administration of paramagnetic contrast agents, T1-weighted images may demonstrate improved signal differences between tissues, and in particular as contrast enhancement in inflammatory and neoplastic lesions (Liney, 2005).

1.1.3 **T2-Weighted Images**

T2-weighted images are the result of differences in T2 relaxation time in different tissues. T2 relaxation time is related to the decay of magnetisation in the transverse plane after RF pulses: first a 90° RF pulse is applied while the protons are in phase, then, as the protons go into diphase, a 180° degree RF pulse is applied, and this sequence identifies the tissues which remain in phase for a longer time. Fat and fluid both appear hyperintense on T2-weighted images. Healthy muscle has a short T2 relaxation time, while fat and water have long T2 relaxation times. T2-weighted images are useful to identify early muscle changes (Lovitt et al., 2006).

1.1.4 **FLAIR Images**

FLAIR is a method of fluid attenuated inversion recovery with a very long inversion (TI) time (around 2 seconds) which is useful to suppress bright fluid signal, for example the cerebrospinal fluid (CSF) signal in the brain ventricular system (Liney, 2005) and improve visualization of the periventricular lesions (Gavin & Bagley, 2009). FLAIR technique produces strong T2-weighted images that are highly sensitive to T2 prolongation in tissues, which may result from a high protein content due to the presence of blood and inflammation (Bakshi et al., 1999). A number of studies showed the value of FLAIR imaging to reveal subarachnoid hemorrhage, meningitis, chemical irritation of the meninges, and subarachnoid seeding of neoplasm (Mohamed et al., 2004).

1.1.5 **T2* Images (Gradient Echo)**

T2* relaxation is one of the main determinants of image contrast with gradient-echo sequences and refers to the decay of transverse magnetisation seen with the sequences. T2* relaxation is a combination of T2 relaxation and relaxation caused by magnetic field inhomogeneities, and it is shorter than T2 relaxation. T2* based imaging includes making gradient-echo sequences more sensitive to T2* decay by changing selectable parameters such as echo time (TE), flip angle, and repetition time (TR) so that lesions, structures or areas of dephasing are shown as dark areas. The usual T2* protocol aims for a hyperintense tissue signal, similar to the usual T2-weighted sequences, in order to contrast with the areas of dephasing that appear dark.

T2*-weighted sequences are used to depict paramagnetic deoxyhaemoglobin, methaemoglobin and haemosiderin in tissues. Pathologic conditions in which this sequence is useful include cerebral hemorrhage, arterio-venous malformations, haemorrhage within neoplasms, punctate foci of haemorrhage in diffuse axonal injury, old intraventricular haemorrhage, thrombosed aneurysms and some calcifications (Chavhan et al., 2009).

1.1.6 **Fat Suppression Sequences**

Fat suppression techniques are used to suppress the signal from adipose tissue and to reduce chemical shift artifact, which allows better signal to be obtained from other tissues. Fat suppression techniques are based on differences in behaviour of lipid and hydrogen water protons. The optimal technique depends on the amount of lipid that requires signal suppression (Delfaut & Beltran, 1999).

1.1.6.1 Fat Saturation (Fat Sat) pulse

Fat saturation pulse is lipid specific and can be used with any imaging sequence for nulling the signal arising from fat. Fat-saturation pulses are affected by magnetic field inhomogeneities (e.g. differences between skin and air). Incomplete fat saturation is sometimes observed when such pulses are used, because of "imperfect selective excitation of the resonance frequency of fat". The addition of a fat-saturation pulse to a fast spin echo (SE) sequence during musculoskeletal MRI can result in highly sensitive depiction of oedema and also highlight the extent of pathologic change in bone marrow (Bitar et al., 2006).

1.1.6.2 Short Tau Inversion Recovery (STIR) Images

An alternative method for achieving fat saturation is by using the inversion-recovery pulse to null the signal arising from fat. When the net magnetisation vector of fat just passes the null point, little or no longitudinal magnetisation is present in fat; thus, when the net magnetisation vector for fat is flipped by the 90° RF pulse, the transverse magnetisation of fat is insignificant, and no signal is generated from it (Bitar et al., 2006). This is the only method that is insensitive to magnetic field inhomogeneities and can be used with low- field-strength magnets (Delfaut & Beltran, 1999).

STIR is very useful for better distinguishing adipose tissue, particularly in the presence of concurrent oedema. The signal is acquired as fat reaches the null point but water still has a non-zero magnetisation (Liney, 2005). Prior to applying the 90° pulse, a 180° pre-pulse is applied. Vascular and fluid-filled structures are seen as hyperintense against a dark background (Gavin & Bagley, 2009). STIR has homogeneous fat suppression but a relatively low signal to noise ratio (SNR); the signal-suppression in STIR is not specific for fat, but rather for tissues with a particular T1 value. Muscle oedema will show as increased signal intensity within the substance of the muscle (McMahon et al., 2010).

1.2 Normal Skeletal Muscle Structure

1.2.1 **Muscle fibres**

Muscle fibres are most commonly typed using 3 different methods: histochemical staining for myosin ATPase, myosin heavy chain isoform identification, and biochemical identification of metabolic enzymes (Monti et al., 2001; Scott et al., 2001).

On the basis of their metabolic and histochemical characteristics, muscle fibres can be classified into two main types:

Type I fibres are slow-twitch and slow-fatigue. They derive energy from oxidative metabolism. They contain many mitochondria and a high concentration of myoglobin.

Type II fibres are fast-twitch and fast fatigue. These are glycolytic. Type II fibres have fewer mitochondria and less myoglobin than type I fibres. Type II fibres are also subdivided into Type IIa (oxidative-glycolytic), which are fast contracting and fatigue resistant (there are more mitochondria than IIb), and Type IIb (glycolytic), which are also fast contracting but fatigue-susceptible due to rapid accumulation of lactic acid. However, the correlation for type IIb with fast glycolytic and type IIa with fast oxidative is not straightforward (Scott et al., 2001).

The type of muscle fibre (I or II) in a given muscle depends exclusively on the type of motor neuron innervation (Zachary & McGavin, 2012).

Classification on the basis of myosin heavy chains isoforms (MyHC) allowed for

muscle fibre typing into different groups due to the fact that each muscle fibre can contain more than one MyHC (Scott et al., 2001). Type IIx, a third fast fibre type with MyHC differs from IIa and IIb fibres in that its resistance to fatigue is intermediate between of them (Schiaffino & Reggiani, 2011).

Canine skeletal muscle has distinct characteristics, in that all fast fibre types are moderately to highly oxidative, and pure glycolytic fibres are not a feature (Acevedo & Rivero, 2006).

1.2.2 **Plasticity**

Fibre phenotype predetermines structural and functional properties of the muscle. Importantly, fibre phenotype can undergo modification under hormonal (especially thyroid) and nerve supply influence (Schiaffino & Reggiani, 2011). This allows for modification according to neuromuscular activity and for adaptation according to the functional demands (unloading or increased activity), and reflect the muscle's intrinsic plasticity. The most typical transformation occurs between IIB and IIA, and from type I to type II during spinal cord damage (Scott et al., 2001). It is believed that the population of fibres within each muscle is constantly adapting to the current demands being placed on that particular muscle. They are in a permanent dynamic state and are capable of expressing a hybrid phenotype (Jeon et al., 1997). Moreover, in a study of the muscle plasticity of Greenlandic sled dogs, fully reversible seasonal (during summer) atrophy in skeletal muscles was found, which correlated with the activity levels of the dogs and lower dietary quality (Gerth et al., 2009).

On the other hand, neurogenic fibre transformation alters not only the contractile muscle properties, but also induces qualitative and quantitative changes on the molecular level within the muscle. Nerve cross-union experiments have demonstrated the crucial role of innervation on muscle phenotype, though the mechanism of fibre transformation is not fully established and probably involves multiple pathways (Pette, 2001).

1.2.3 **Motor unit**

Mammalian skeletal muscles are composed of a mixture of motor unit types. A motor unit consists of its cell body within the ventral grey column of the spinal cord, or the motor nucleus of a cranial nerve, peripheral axon, neuromuscular junctions and

hundreds of muscle fibers innervated by the branches of the axon (Windhorst & Mommaerts, 1996; Fuglevand & Segal, 1997). The axons leave the grey matter between the ventral and lateral funiculi of the spinal cord to form the ventral roots, which join the respective dorsal roots to form the spinal nerves. Several spinal nerves often unite as a single peripheral nerve. Axons of the peripheral nerve split into branches to supply myofibres. A group of myofibres innervated by one neuron is called a motor unit (Dewey, 2008). Individual muscles are composed of a mixture of motor unit types, and their proportion is variable in different muscles (Delp & Duan, 1996), though this distribution has territory boundaries depending on a muscle and motor unit type (Monti et al., 2001).

For effective function, an appropriate number and type of motor units are required to be activated (Hodson-Tole & Wakeling, 2008). There are two main patterns of activation which correspond to two classes of motor neurons 1) a tonic pattern of activation with a relatively low frequency of firing (slow and fatigue resistant fibres), and 2) a phasic pattern of activation with a higher frequency of firing (fast fibres) (Schiaffino & Reggiani, 2011).

1.2.4 **Intramuscular fat and connective tissue**

Connective tissue plays an important role in normal muscle function. Connective tissue surrounds the muscle fibres (endomysium) and provides space and paths for blood vessels and nerves. Groups of muscle fibres, fascicles, are enveloped by perimysium, and a whole muscle is covered by epimysium, which continues into the fascia between adjacent muscles and between muscles and skin. Fascia helps movement between the structures, while also allowing the passage of nerves and blood vessels. The superficial fascia is attached to the deep fascia, which provides the origin for many muscles, and in some areas is represented by the intermuscular septa; it forms retinacular or annular ligaments encircling flexor tendons, holds them close to the bone, and prevents tendon bending during muscle contraction (Johnston, 1985).

Muscle fibre distribution plays an important role in the degree of lipid composition, with higher lipid contents in type I fibres, and which may correlate with different muscle functions, for example the deep and superficial neck muscles. It has been demonstrated in man that there is a significant difference in the muscle/fat index when

comparing cervical flexors and extensors, with the muscle/fat index being much higher in the dorsal muscles than in the ventral muscles (Cagnie et al., 2009). Direct measurement of intramyocellular lipid content in humans showed a higher lipid content in type 1 fibres. Nevertheless, considerable variation in lipid content was reported within every muscle, and in each fibre type within specific muscle groups (Goodpaster et al., 2004).

1.1.2 **Sex variations**

Although the fibre type composition of most skeletal muscles is similar in males and females, some muscles display a striking sexual dimorphism in certain species: for example in the jaw muscles (temporalis and masseter). In humans, like in most mammals, there is obvious gender diversity in skeletal muscle mass, due to testosterone levels, which are responsible for the greater hypertrophy of type II fibres in males (Schiaffino & Reggiani, 2011). A striking example of sexual dimorphism is evident in the levator ani muscle of the rat, which disappears during development of in the female, but can be maintained by testosterone administration (Souccar et al., 1982). In cows testosterone has been shown as a driver for rapid body weight gain, with a greater gain of lean muscle (Schreurs et al., 2008).

1.1.3 **Individual variations**

Significant individual variation in the fibre type composition has been reported for human skeletal muscles (Schiaffino & Reggiani, 2011). This variability in part explains the differences in physical ability and athletic performance between different indviduals, as well as the association between skeletal muscle fibre type composition and particular disease states, including obesity and insulin resistance (Zierath & Hawley, 2004).

1.3 Pathological Processes Affecting Muscle

1.2.5 **Myopathies**

Neuromuscular diseases can affect the muscle, the neuromuscular junction, the peripheral nerves, and the ventral horn cells of the spinal cord and are referred to as myopathies, junctionopathies, peripheral neuropathies and motor neuron diseases

respectively. A combined approach including history, physical and neurologic examinations, laboratory testing, muscle imaging, electrodiagnostic examinations, muscle biopsy or DNA analysis has been suggested to reach a diagnosis (Shelton, 2010). In man muscle disorders have been classified into heritable, traumatic, inflammatory, metabolic and neoplastic myopathies (Garcia, 2000). In veterinary medicine myopathies are classified into groups: degenerative/developmental; metabolic; inflammatory/infectious; nutritional, toxic, immunological, neoplastic, ischemic and traumatic myopathies (Dewey, 2008).

1.2.6 **Degenerative/developmental disorders**

1.2.6.1 Selected inherited myopathies

Muscular dystrophies

These are a group of inherited disorders characterised by different degrees and distribution of muscle atrophy or hypertrophy in man and in dogs. Dystrophies associated with the absence of, or abnormalities in, dystrophin, sarcoglycans, and laminin alpha 2 have been recognised in several breeds (Shelton, 2007).

Duchenne muscular dystrophy is the commonest and one of the most serious, a lethal X-linked recessive disorder, in which the loss of dystrophin causes progressive degeneration of skeletal and cardiac muscle. Golden Retriever Muscular Dystrophy is the closest animal counterpart of Duchenne muscular dystrophy in humans (Kornegay et al., 2012) and is used as a model for this disease (Thibaud et al., 2007).

Overall, muscular dystrophy can be found in any young dog or cat of any sex and breed (as well as mixed breeds) with persistent muscle weakness, gait abnormality and starting from the first months of life (Shelton, 2007). Comparing the composition of healthy and dystrophic muscles in dogs Mehta et al (1989) found that affected muscles contained more water and fat and were type II fibre deficient.

Nemaline rod myopathy

Nemaline rod myopathy is associated with rod-shaped structures in muscle fibres. At least seven distinct clinical forms have been described in humans and mutations have

been identified in five different thin-filament genes (Kube et al., 2006). A similar myopathy was described in cats and dogs (Delauche et al., 1998).

1.2.6.2 Metabolic myopathies

Normal mscle function depends on energy supply by adenosine triphosphatase through glycogen metabolism, lipid metabolism, phosphocreatine stores and purine nucleotide cycle,and will be altered in case of enzymatic, hormonal or toxic disruption of these pathways, leading to metabolic myopathies (Preedy & Peters, 2002). Specific types havebeen identified in humans and animals (Vitale & Olby, 2007). Myopathies can be caused by hyperadrencorticism (Type 2 fibre atrophy and deposition of perimysial and endomysial fat ave been described), adrenal insufficiency, primary hyperparathyroidism and diabetes mellitus (Platt, 2002). Electrolyte abnormalities have also been described as a cause of a group of myopathies (Cuddon, 2002).

Lipid storage myopathy is infrequently encountered in dogs; the precise biochemical defect has not yet been discovered. The lipid accumulation in the muscles has been suggested as the main pathological event (Shelton et al., 1998). It produces non-specific signs of muscle atrophy, weakness and sometimes myalgia.

Glycogen storage diseases are caused by inborn errors in glycogen metabolism and accumulation of glycogen-like material in the muscles and other tissues, causing muscular weakness, exercise intolerance and sometimes seizures (Dewey, 2008).

Defects in the mitochondrial energy generating pathway are implicated in a number of degenerative diseases in humans and in dogs. The organs which are highly dependent on oxidative metabolism, the brain, skeletal and cardiac muscles and kidneys, are most severely affected (Paciello et al., 2003). The marked variability of the clinical signs reflects the heterogeneity of these disorders, which may involve a single or multiple organs (Platt, 2002).

1.2.6.3 Inflammatory/infectious myopathies

Inflammatory and infectious myopathies in both dogs and humans are characterised by excessive inflammation, muscle necrosis, and fibrosis. Inflammatory myopathies can be classified into two groups: idiopathic inflammatory myopathies and secondary

inflammatory myopathies associated with other diseases. Clinical signs reflect the degree of inflammation within the muscle, the number of muscles affected, the location of these affected muscles and the presence of an underlying systemic disease (Podell, 2002). They can be focal (e.g. masticatory muscle myositis, extraocular myositis) or generalised (e.g. immune mediated polymyositis). Infectious myositis is considered when more than one muscle group is involved, though a focal form of infectious myositis is possible too (Lorenz et al., 2011). Pathogens such as *Neospora caninum, Hepatozoon americanum, Hepatozoon canis, Leishmania infantum, Ehrlichia canis, Toxoplasma gondii, Borrelia burgdorferi, Rickettsia rickettsii,* and *Leptospira australis* have all been reported as causes of infectious myopathies (Evans et al., 2004; Pumarola et al., 2004; Shelton, 2007).

Masticatory muscle myositis is a focal, immune-mediated inflammatory myopathy that affects the muscles of mastication innervated by the mandibular branch of the trigeminal nerve selectively (temporalis, masseter, pterygoid, rostral portion of digastricus) due to differences in histochemical and biochemical properties of the masticatory muscles (Lorenz et al., 2011). These muscles have a different embryologic origin from appendicular myofibres and contain a unique muscle fibre 2M and protein composition when compared with limb muscle (Dewey, 2008). Histopathological findings consist of inflammation, atrophy, necrosis, regeneration and fibrosis in the absence of infectious agents (Bishop et al., 2008). Other immune-mediated inflammatory myopathies include polymyositis, dermatomyositis with extra-muscular manifestations and inclusion-body myositis. They can be differentiated on the basis of clinical presentation, distribution and phenotypes of infiltrating cells and the auto-aggressive behaviour of the infiltrating mononuclear cells. In polymyositis, inflammatory cells are concentrated in the endomysium and surround and invade non-necrotic fibres. In dermatomyositis, the inflammatory cells are concentrated in the perimysium, where they are either perivascular or are scattered diffusely with predominance of B cells and CD4 cells (Pumarola et al., 2004).

In generalised autoimmune polymyositis the cause is usually unknown, although systemic lupus erythematosus, thymomas with acquired myaesthenia gravis and the use of trimethoprim-sulfa drugs in Dobermann pincher dogs have been associated with this condition (Dewey, 2008). It affects appendicular muscles, can mimic low motor neuron

(LMN) disease, but rarely causes tetraplegia, and the spinal reflexes are usually intact. Large breeds are predisposed with no sex or age prevalence though middle-aged dogs are more commonly affected (Dewey, 2008). Muscle biopsy usually demonstrates necrosis of muscle cells, with macrophages and prominent lymphoplasmacytic interstitial inflammation, which confirms the diagnosis (deLahunta & Glass, 2009).

1.2.6.4 Traumatic myopathies

Muscle injuries are sporadically encountered in dogs, mainly in hunting and working breeds, such as racing greyhounds. These are regarded as myotendinous strains with three broad degrees of severity: no functional deficits, mild functional deficits, or complete loss of muscle function. Stretch injury corresponds to a first degree injury, a partial tear corresponds to a second degree injury, and a complete tear corresponds to a third degree injury (Steiss, 2002) Stahl et al., 2010). Predisposition factors for injury to an individual muscle include: extension across two joints, a long fusiform shape, having a high composition of fast contracting type II fibres and an eccentric action. The muscle's origin or insertion is the most vulnerable to damage, but the muscle belly can also be damaged. Post-traumatic inflammation, oedema, and localised hemorrhage promote the development of muscle ischemia and compartment syndrome (Steiss, 2002). Strain injury with subsequent muscle contracture have been described in the muscles ilipsoas, quadriceps and gastrocnemius muscles and have been proposed as a cause of fibrotic (gracilis) myopathy (Steiss, 2002). Muscle healing depends on survival of the sarcolemnal cells and the endomysial connective tissue sheath (Stahl et al., 2010).

Pathologic conditions of the rotator muscles of the shoulder, the subscapularis, supraspinatus, infraspinatus and teres minor are very common in man, but rarely encountered in dogs. If they are encountered in dogs then this is largely in working and hunting breeds (Fusco et al., 2007). The reported findings consist of chronic non-progressive lameness and pronounced atrophy of the shoulder muscles leading later to contracture. It has been found to be different from neurogenic atrophy as there is an absence of angular atrophic fibres, which are typical of muscle denervation (Bruce et al., 1997). Fibrotic contracture of the infraspinatus muscle is a primary muscle disorder

characterised by atrophy and replacement by fibrotic tissue (Orellana-James et al., 2013).

Exertional myopathy (exertional rhabdomyolisis) has been described primarily in racing greyhounds with the supposed pathogenesis involving abnormal myofibre glycogen metabolism or electrolyte disturbances (Steiss, 2002).

1.2.7 **Neuropathies**

A number of peripheral nervous system (PNS) diseases of degenerative, nutritional, metabolic, toxic, immunological, neoplastic or infectious origin are recognised in dogs (Cuddon, 2002). The features of peripheral nerve disease reflect a failure of the lower motor neuron such as paresis, muscle atrophy, hypotonia and hyporeflexia (Dewey, 2008). Generally, there are two main pathological changes in peripheral neuropathies: axonal degeneration and demyelination with or without remyelination (Cuddon, 2002). Inherited neuropathies are classified according to their histopathological phenotype, mode of inheritance and motor or sensory clinical characteristics. The classical motor signs are weakness, hypotonia and muscle atrophy, but this depends on the degree of motor or sensory fibres involvement (Granger, 2011).

Acquired canine peripheral neuropathies are usually divided into acute and chronic-progressive neuropathies. The primary acute canine neuropathy is canine polyradiculoneuritis, which should be differentiated from three other major causes of acute lower motor neuron disease: botulism, tick paralysis and fulminant myasthenia gravis. Causes of chronic peripheral neuropathies include endocrinopathies (diabetes mellitus, hypothyroidism, hyperadrenocorticism), paraneoplastic syndrome (e.g. insulinoma, lymphosarcoma, carcinomas), intoxications, iatrogenic (as an adverse reaction to chemotherapy), infection, immune-mediated disease and idiopathic (Cuddon, 2002).

Entrapment neuropathies in humans are lesions of an individual peripheral nerve resulting from direct compression, stretch, angulation, or vascular compromise. Due to their anatomical location some nerves are particularly vulnerable, for example the long thoracic nerve in man. Following trauma involving shoulder depression in man the long thoracic nerve can be damaged, leading to isolated serratus ventralis muscle atrophy

(Watson & Schenkman, 1995). Neuropathies may be difficult to differentiate clinically from junctionopathies and myopathies, hence the terms 'motor unit disease' and 'neuromuscular disease' are used by some authors to describe these clinical presentations (Davies & Irwin, 2003).

1.2.7.1 Age Related Muscle Changes

Structural muscle changes occur not only in pathological conditions, but also during natural aging. These changes manifest as loss of skeletal muscle bulk and an accompanying increase in fat mass, and are termed sarcopaenia. Researchers on human sarcopaenia have elucidated that the causes are multifactorial and can include disuse, changing endocrine function, chronic disease, inflammation, insulin resistance, and nutritional deficiencies with involvement of such mechanisms as reduction in muscle cell number, centralisation of muscle nuclei, reduction of muscle membrane excitability, decrease in the number of motor neurons and their firing rate, decline of regenerative capacity and fat accumulation within and around muscle cells (Volpi et al., 2004; Kan et al., 2011). Similar alterations are found in the muscles of small animals, but precise details are lacking for different breeds and related to the general health of the dogs (Freeman, 2012). Different groups of muscles were measured during research of sarcopaenia in Labrador retrievers, with the correction for vertebral height (13^{th} thoracic vertebrae) for epaxial muscles bulk. It was estimated that the mean epaxial muscle area was significantly lower in healthy old dogs, compared with healthy young dogs, while the quadriceps and temporal muscles were not significantly different. One possible explanation could be that the quadriceps muscles contain a mixture of type I and II fibres, whereas the epaxial muscles are primarily composed of type II fibres (glycolytic), which are more susceptible to atrophy (Hutchinson et al, 2012).

1.2.8 **Muscle atrophy**

Muscle atrophy is a clinical sign of lack of nourishment, disuse or denervation and is characterised by a decrease in protein content, fibre diameter and fatigue resistance (Jackman & Kandarian, 2004). Denervated muscles atrophy rapidly and more completely than in disuse, although it may be difficult to differentiate (DeLahunta & Glass, 2009). Causes of denervation atrophy include localised loss of nerve function or generalised loss of the entire motor unit (Pathria & Boutin, 2005). As such, the

denervation pattern may be focal (a single muscle) or multifocal (multiple muscles) (McMahon et al., 2010). The muscle fibre atrophy has been recognised to be fibre-type specific with type II fibres affected more rapidly and severely (Carlson, 2008). Acute stages of denervation are accompanied by oedema, which later can progress to volume loss, fatty atrophy and fibrosis (Biering-Sorensen et al., 2009; Pathria & Boutin, 2005). Muscle atrophy can progress to an irreversible stage, as has been demonstrated in the experimental setting (Carlson, 2008).

Muscle atrophy represents a complex and dynamic environment: there is an initial three-fold increase in the satellite cells population, which is followed by a steady decline. However, in chronic atrophy there are a variety of different processes taking place at the same time, including cellular atrophy, cell apoptosis, muscle fibre regeneration and the generation of new muscle fibres (Carlson, 2008). The newly formed fibres have been found to be small, incompletely differentiated and immature and probably arise as the result of repeated cycles of necrosis and regeneration (Doppler et al., 2008).

Disuse muscle atrophy is most frequently identified following limb immobilisation or paraplegia/tetraplegia (Psatha et al., 2012). Disuse muscle atrophy is characterised by non-specific findings, including progressive atrophy, fibre degeneration and fatty replacement (Scelsi, 2001).

1.3 Normal MRI Appearance of the Skeletal Muscle

MRI sequences for muscle imaging include T1-weighted, T2-weighted and/or STIR. In MRI the proton density reflects the water and fat content, and the contrast is caused by the relaxation differences between the tissues, so despite similar water content, the signal intensity of normal muscle and the brain are different (Garcia, 2000).

The signal intensity of normal muscle is described as

1) Somewhat intermediate between those of fat and cortical bone (Murphy et al., 1986).
2) Slightly higher than that of water and much lower than that of fat on T1-weighted images, and much lower than that of both fat and water on T2-weighted images. On inversion-recovery and fat-suppressed T2-weighted images, normal muscle signal

intensity is much lower than that of water but higher than that of fat (May et al., 2000).

3) Slightly higher signal intensity than water on T1-weighted and lower than fat or water on T2-weighted images. On fat-suppressed T2-weighted images or STIR images, the contrast between normal skeletal muscle and water increases much more (Kim et al., 2011).

On non–fat-suppressed T1W images, skeletal muscle shows a feathery or marbled appearance, which results from the high-signal fat situated between the muscle fibres and linear hypointense tendon (Costa et al., 2012).

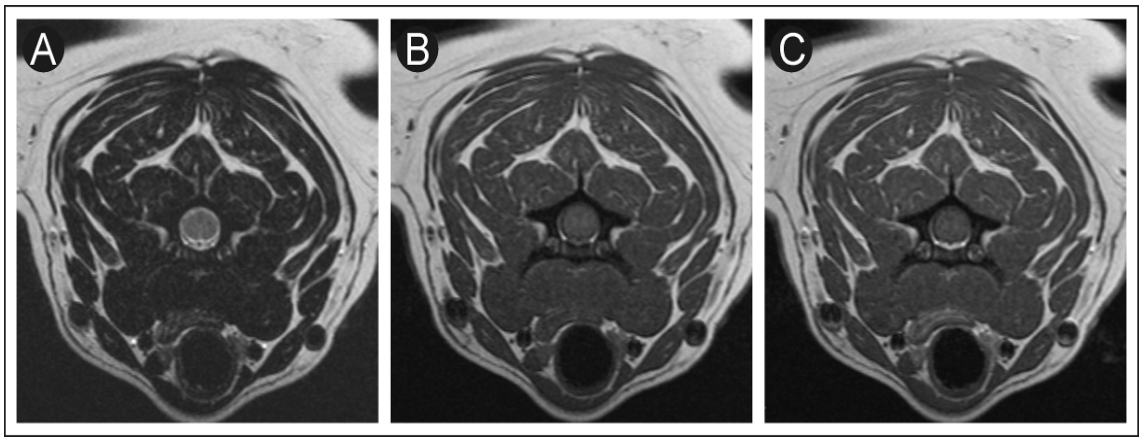

Figure 1-1 The appearance of the cervical muscles on transverse view on T2W(A), T1W (B) and T1W post contrast (C) magnetic resonance images.

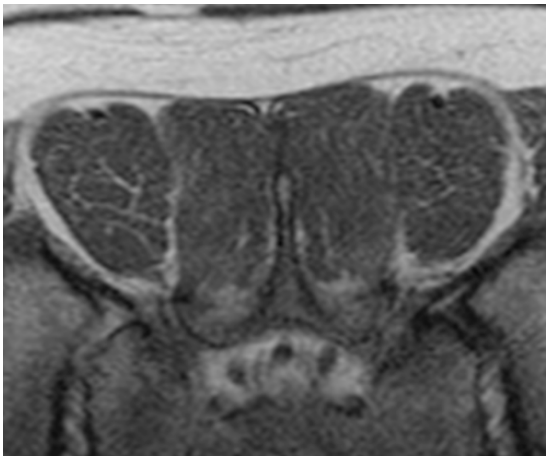

Figure 1-2 The lumbar epaxial muscles with intermuscular fat accumulation, evident as a marbling appearance.

1.4 MRI Appearance of Muscle Pathology

1.3.1 **Patterns**

Pathological muscle changes on MRI imaging usually correspond to patterns of oedema, fatty infiltration, mass affect or muscle size reduction, and reflect different conditions such as infectious, inflammatory, traumatic, neurologic and iatrogenic (May et al., 2000). Alterations in signal intensity are influenced by fat, water variations, electrolytes, pH, temperature and some other parameters (Mokrusch, 2002). Many diseases may look similar on MRI and on physical examination and additional diagnostic procedures may be necessary to reach a specific diagnosis. Nevertheless,

magnetic resonance imaging enables clear lesion description and localisation (Buhschwein et al., 2008).

Costa et al., (2012) described the following characteristic patterns of pathologic changes in the muscle:

1) Distribution within one muscle or multiple muscles: may be focal/multifocal/diffuse and symmetric/asymmetric.
2) Muscle size and shape: normal/reduced/enlarged; atrophy can be accompanied by compensatory hypertrophy.
3) T1W signal intensity typically increases due to fat replacement of a muscle: patchy fat replacement of muscle is usually seen in the early stage of disease; complete fatty replacement of muscle is usually seen in the later stage of disease, particularly in disorders such as complete tendon tear, denervation, long-term disuse, muscular dystrophies, congenital myopathies and some other conditions.
4) T2W and STIR signal for oedema detection which can be focal, patchy or diffuse and involving a single muscle or adjacent muscles or symmetrically non-adjacent muscles, or may be asymmetrical.

1.3.2 **Muscle dystrophy**

The first quantitative analysis of canine muscles using magnetic resonance imaging was performed on the extensor carpi radialis and the flexor carpi ulnaris muscles in golden retriever dogs with muscular dystrophy (Thibaud et al., 2007). In that study there was evidence of a T2/T1 ratio increase and oedema-like T2 hyperintensity with heterogeneity, reflecting patchy distribution of the pre-necrotic and necrotic fibres and inflammation.

1.3.3 **Inflammation**

The STIR sequence is useful for active disease localisation in inflammatory myopathies and for guiding muscle biopsy (Degardin et al., 2010). Early stages of inflammatory myopathies are accompanied by oedema and inflammatory cell accumulation which produce T2W hyperintensity and T1W isointensity or slight hypointensity (Bishop et al., 2008). Comparison of T1W and T2W images allows differentiation of fat from oedema (oedema has a high signal on T2W, but normal to reduced signal on T1W).

However, problems arise when trying to identify oedema superimposed on fat, and this is not possible without the use of a fat suppression technique or contrast medium (Platt et al., 2006). MR imaging of three dogs with inflammatory myopathies demonstrated FLAIR hyperintensity, low T1W, non-uniform T1 contrast uptake with non-enhanced center, consistent with necrosis, and a patchy appearance of T2W and T2* consistent with mineralisation or haemorrhage (Platt et al., 2006). In dogs with chronic inflammatory myopathies, accumulation of fibrous connective tissue is a feature, in contrast to the human patients (Bishop et al., 2008). MRI can reveal muscle and tendon trauma and associated morphologic disruption, intramuscular haematomas, abscesses or neoplasia that change normal muscle architecture and can produce variable signal characteristics (Buhschwein et al., 2008). Spinal muscles adjacent to a neoplasm may exhibit reactive inflammatory changes including myolysis and atrophy with fatty replacement (Bierry et al., 2008). In a case of necrotising myopathy the following abnormalities were detected: T2W hyperintensity in the serratus ventralis, subscapularis, supraspinatus and rhomboideus muscles and focal areas of hypointensity when compared with normal muscle on both T2W and T2* images and marked patchy enhancement of the abnormal muscles with areas of decreased or absent enhancement (de Risio et al, 2009).

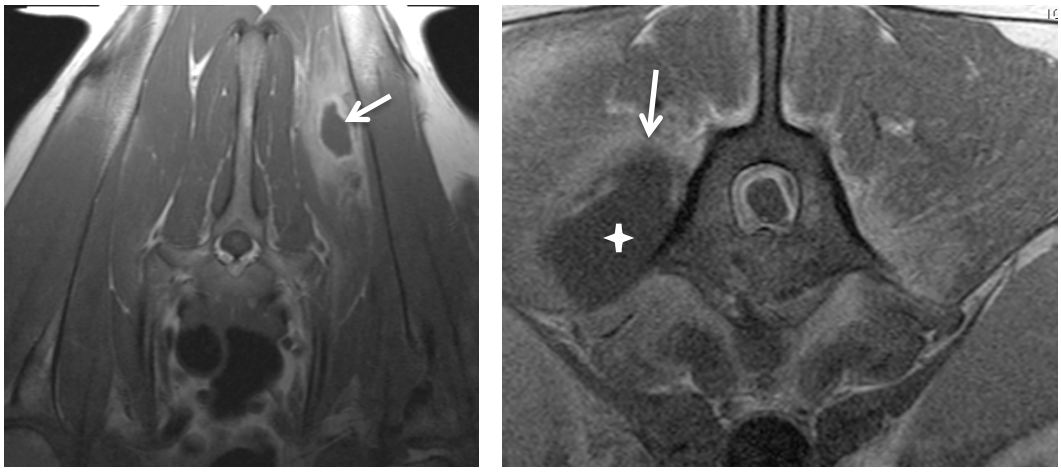

Figure 1-3 Focal muscle lesions MRI appearance (T2W images) is non-specific and characterised by a rim of hyperintensity (arrow) surrounding a hypointense centre (star): a) necrotizing myositis; b) – peritumoral muscle area.

1.3.4 **Denervation atrophy**

Muscle disorders associated with different pathological pathways such as generalised disuse atrophy, nerve root avulsion and chronic denervation, are being constantly investigated with the use of MRI imaging (Hayashi et al., 2002; Elliott et al., 2006). Early stages of muscle denervation are accompanied by an increase in vascular supply, as well as by an increase in extracellular fluid, probably due to impaired muscle cell membrane permeability. These events are responsible for the T2W signal hyperintensity, which may appear as early as 24 hours post denervation in man (Wessig et al., 2004; Kamath et al., 2008). In experimental mouse studies, the T2W abnormalities persisted until the renervation phase, and then decreased in parallel with the reduction in perfusion (Wessig et al., 2004). The point at which the T2W values began to decrease depended on the degree of nerve injury. In the irreversible neurotmesis group, T2W ratios remained high throughout the study (Pfirrmann, 2008). In the subacute phase, a denervated muscle had a relative increase in both the amount of fat and the extracellular water content (Kamath et al., 2008). The T2W signal intensity in experimental settings was found to have a good correlation with the severity of acute nerve damage (Yamabe et al., 2008). Denervation often results in mild, diffuse changes affecting the entire muscle, while during inflammation the changes tend to be multifocal (Platt et al., 2006). Chronic denervation is often best seen on T1W spin-echo images as

loss of muscle bulk and widespread areas of increased signal intensity resulting from fatty infiltration (Kamath et al., 2008).

1.4.2 **General Pathological Processes**

1.3.4.1 Oedema

Muscle oedema may be identified in many different conditions and can be classified as being secondary to increased delivery of fluid to the muscle ("hyperaemic") or secondary to impaired drainage of fluid from muscle ("congestive"); may occur secondary to direct injury ("traumatic"); or may occur due to infiltration by tumor ("tumorigenic"). Neural injury leads to a loss of muscle contractility, which impedes fluid egression from interstitial space (Napier et al., 2006). The main MRI feature of edema is T2W and STIR signal hyperintensity. Increased extracellular fluid results in T1W and T2W prolongation, because the relaxation time of water in the extracellular space of muscle is about four times that of the myoplasm (Polak et al., 1988).

Patterns of oedema distribution include diffuse (multiple muscles and muscle groups bilaterally, typically involving the entire muscle), focal (one muscle or muscle group or multiple adjacent muscles) or multifocal (patchy or nodular pattern) (McMahon et al., 2010). Focal oedema is usually posttraumatic, and may be seen near the myotendinous junction, superficially or at the muscle–bone interface. Diffuse oedema in a single muscle is seen in acute focal atrophy (Costa et al., 2012). The diffuse muscle oedema pattern encompasses noninfectious and immune-mediated inflammatory conditions affecting skeletal muscle (McMahon et al., 2010). Muscle oedema in adjacent muscles can be seen in deep venous thrombosis, compartment syndrome, eosinophilic myositis, pyomyositis, peripheral neuropathy (may not be entirely adjacent), vascular malformations, radiation and lymphoma (Costa et al., 2012). Multifocal muscle oedema pattern is typically associated with exercise involving lengthening muscle contractions, tumour metastasis and sarcoidosis in man displaying hyperintensity on the T2 with fat saturation and STIR images (McMahon et al., 2010).

1.3.4.2 Fat infiltration

Atrophy and fatty muscle replacement are the features of chronic denervation, disuse, complete or partial tears of tendon and muscle, and steroid therapy. Different methods have been applied to differentiate muscle and fat, to measure muscle size and to detect atrophy and fatty infiltration. In human medicine, indirect methods of measuring body density and conversion of these to the percent of body fat have been performed using generalised equations, include anthropometry, hydrodensitometry, air displacement plethysmography and bioelectric impedance. These techniques do not allow the differentiation of subcutaneous from visceral adipose tissue and ectopic fat. Such methods as dual energy X-ray absorptiometry (DEXA), CT, ultrasound, magnetic resonance spectroscopy (MRS), MRI, quantitative MR and chemical shift are direct techniques because they identify fat on the basis of the tissue's unique properties and signals in each modality (Hu et al., 2011).

MRI has been shown to be a reliable diagnostic tool for the determination of muscle size and structure. Researchers have been using T1W fat-saturated images (Dawson et al., 2013), fast spin-echo T1W and T2W sequences (Elliott et al., 2006; Okada et al., 2011). Accurate quantification of fat is based on the intrinsic differences between the T1 relaxation times of fat and other tissues (Sacha, 2003). Standard T1-weighted images provide visualisation of fatty septa in the muscle (intermuscular or extramyocellular lipid) and subcutaneous adipose tissue. However, the assessment of small concentrations of lipid within muscle tissue requires fat-selective MRI sequences with a high sensitivity for the signal arising from lipid (Goodpaster et al., 2004). Although, determination of the absolute concentration of fat is not possible by MRI, the T1 signal intensity provides a reliable indication of the amount of fat within the muscle (Cagnie et al., 2009).

The T1 signal of fat is one of the shortest amongst tissues *in vivo*, which has a very rapid recovery of its longitudinal magnetisation between successive radiofrequency excitations. Therefore, by using a T1-weighted sequence, strong tissue contrast can be achieved between short-T1 fat tissues: fat appears bright and muscles and organs with longer T1 values appear darker (Hu et al., 2011). As an example, in pigs T1 values (1.5T MRI) are about 260ms for fat and 900 ms for skeletal muscle, while T2 relaxation

times are around 44ms for muscle and 130ms for subcutaneous adipose tissue (Mitchell et al., 2001). The technique of T1W defining the relative content of fat in a muscle involves determining the ratio between the pixel intensities of each muscle to that of a standardised region of intermuscular fat and is based on the signal intensity difference between fat and water on T1W images (Elliott et al., 2005; Cagnie et al., 2009).

T2 relaxation times are prolonged in fat, necrotic tissue and connective tissue, and generally cannot easily distinguish between these states, which necessitates the use of fat-suppression techniques (Kobayashi et al., 2009). To enhance the contrast between the T1W and T2W characteristics of tissue, spin-echo pulse sequence can be used (Baulain, 1997). Utilising spin-echo pulse sequences to investigate body composition in pigs, it was estimated that the accuracy of the volume measurements by MRI depend on accurate tissue edge detection, slice thickness and the total volume of the region (Mitchell et al., 2001). In an MRI study investigating the muscle/fat index of the superficial and deep neck muscles at the level of C4-C5 in asymptomatic humans, it was found that flexor muscles had much less fat than extensor muscles. At the same time, significant differences were found in deep and superficial extensor muscles, but not in flexor muscles (Cagnie et al., 2009).

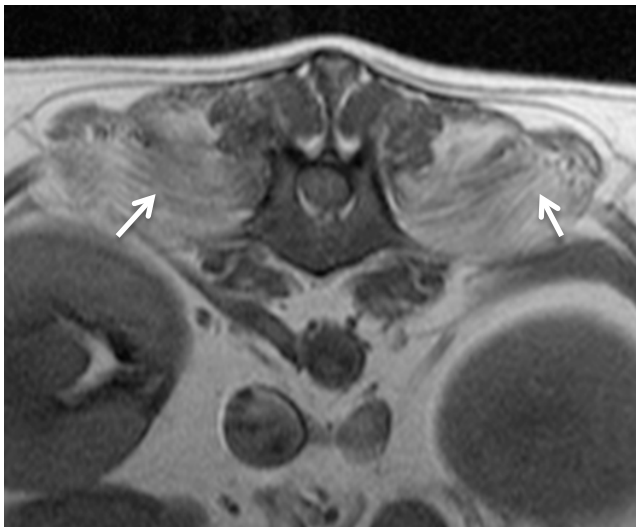

Figure 1-4 Diffuse T1W hyperintensity (arrows) suggestive of diffuse fat infiltration in the epaxial lumbar muscles.

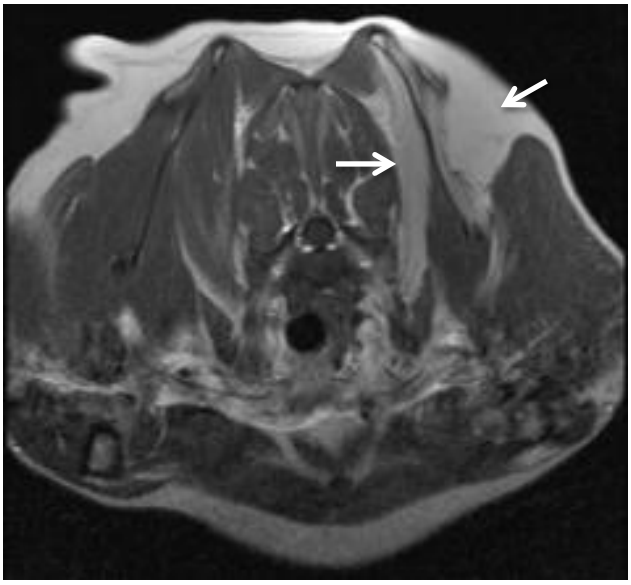

Figure 1-5 T1W transverse MR image. An example of complete replacement of the serratus ventralis and supraspinatus muscles by fat (arrows).

1.3.4.3 Mass effect

Mass effect is defined as a distortion of normal anatomy on MRI images, usually due to displacement by the extra volume (Gavin & Bagley, 2009). Relating to humans the mass lesion pattern may be seen in neoplasms, intramuscular abscesses, myonecrosis, traumatic injuries, myositis ossificans, muscular sarcoidosis, and parasitic infections (May et al., 2000).

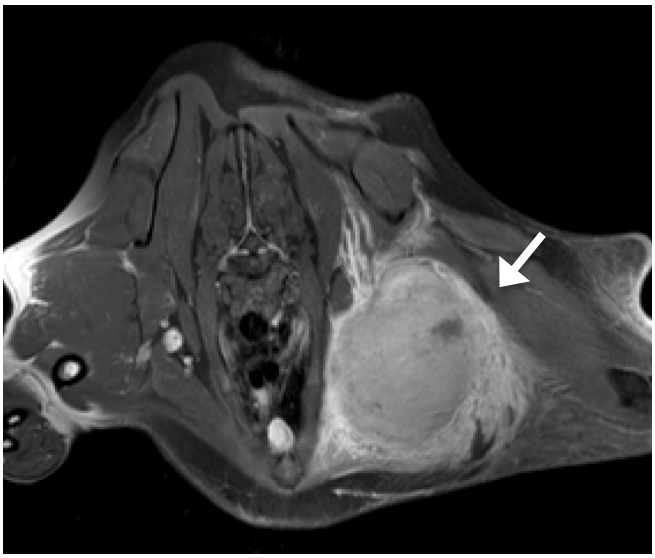

Figure 1-6 Example of mass effect produced by a tumour in the axilla (arrow).

Pathological processes	Most useful MRI sequences	Examples of disease processes
Oedema	T2, STIR, FLAIR	Polymyositis, dermatomyositis , mild injuries, infectious myositis, radiation therapy, acute denervation, compartment syndrome, myositis ossificans rhabdomyolysis
Fatty infiltration	T1, T1FatSat, T2	Chronic: denervation, disuse, tendon tear, corticosteroid use
Mass effect	T1, T2, STIR, T2*, Contrast	Neoplasms, intramuscular abscess, myonecrosis, traumatic injury, myositis ossificans, muscular sarcoidosis, parasitic infection.

Table 1-1 Main pathological effects that may be evident in muscle, the MRI sequences that are most useful in their characterisation and examples of disease processes where these effects may be evident.

1.4 Conclusion

Skeletal muscles in man and in dog are affected by a variety of pathological conditions which can be primary myopathic or neurogenic in origin. MRI has been shown to be a valuable diagnostic tool in the evaluation of these conditions, although the pattern of muscle response and the typical imaging changes are limited in character, with considerable overlap in features between different disorders. Nevertheless, the pattern

of alterations in the affected muscles and surrounding tissues may differ on certain MRI sequences and these differences may allow the list of differential diagnoses to be reduced. Combined with the presenting clinical complaint, signalment and the results of additional tests this will often allow a definitive diagnosis to be made.

1.5 Aims of the current work

This study sought to evaluate the utility of MRI for the assessment of muscle within the proximal thoracic limb of the dog, in health and disease. The effect of disease was examined in dogs with the mass lesions of the brachial plexus as a model of chronic denervation with the opposite normal limb acting as the control. One of the features of chronic denervation is infiltration of affected muscles with fat. Prior to understanding the effect of disease on the MRI anatomy and signal intensity of muscle, it was important to first examine the effect of body condition score (BCS) (as a measure of obesity) on normal muscle anatomy and signal intensity. This study therefore sought to:

1. Examine the MRI appearance of two soft tissue compartments: fat (subcutaneous, intermuscular and intramuscular) in the lumbar and cervical areas as a measure of BCS in a group of dogs (Chapter 2).
2. After quantification of the effect of differences in body condition, the anatomy of the skeletal muscles of the proximal thoracic limb where no pathology was present was examined using MRI (Chapter 3).
3. Finally, the effect of presumed chronic denervation on the MRI appearance of the skeletal muscles of the proximal thoracic limb was defined in cases of brachial plexus mass lesions (Chapter 4).

2 Assessment of Subcutaneous, Intermuscular and Intramuscular Fat by MRI and its Correlation with Body Condition Score

2.1 Introduction

2.1.1 **Adipose tissue**

The primary site of fat deposition is adipose tissue, which represents a specialised loose connective tissue, serving mainly as an energy store. In humans (Boettcher et al., 2009) and in dogs (Sagawa & Nakadomo, 2002) it has also been recognised as an endocrine organ which can influence physiological and pathological processes, for example immunity and inflammation. The following adipose tissue divisions have been recognised: subcutaneous fat (which is located between the dermis and aponeurosis and fascia of muscles) and interstitial fat (which surrounds and lies within the body organs or bone marrow) (Shen et al., 2003).

In man the patterns of adipose tissue distribution are considered an important biomarker of metabolic risk (Makrogiannis et al., 2012), in particular for the development of a number of inherited and acquired conditions such as lipodystrophies (Al-Attar et al., 2007), obesity associated coronary artery disease, type-2 diabetes, hypertension and stroke (Boettcher et al., 2009; Cornier et al., 2011).

Obesity has also been viewed as a low-grade inflammatory condition (Trayhurn & Wood, 2004). Obesity is common in companion animals, and has been shown to predispose to diseases such as osteoarthritis, hypertension, hyperlipidemia, cardiovascular and metabolic dysfunction, urinary disorders, mammary neoplasia, transitional cell carcinoma, exercise intolerance, increased general anaesthetic risk and dystocia (German, 2006; Toll et al., 2010; Corbee, 2013). Obesity in companion animals has also demonstrated a propensity to reduce median life expectancy (Stone et al., 2009). While the estimation of obesity in an otherwise healthy animal is usually easy to achieve, in the ill animal this can be problematic. In human patients muscle wasting is evident in a number of diseases, including prolonged immobilisation and various pathological conditions such as cancer, sepsis and diabetes. In these conditions the muscle atrophy is accompanied by replacement of the muscle tissue with adipose

tissue (Thibaud et al., 2007; Vettor et al., 2009). Whereas high body condition scores (BCS) are indicative of obesity, very low BCS in canine patients can either be caused by malnutrition or by a number of chronic diseases, including those affecting the kidneys and the gastrointestinal, cardiovascular and endocrine systems (Watson, 2003; Rucinsky et al., 2010; Lutz et al., 2013; O'Neill et al., 2013). While it is widely accepted that obesity is associated with an increased predisposition for a wide variety of disease, including cardiac disease, the "obesity paradox" has been reported in cardiology in human patients as well as in dogs. Here, increased BCS due to weight gain were associated with the longest survival times in some cardiac diseases. One of the proposed mechanisms to explain this was that adipose tissue-derived neuroendocrine molecules had a cardioprotective effect (Slupe et al., 2008). However, whether the increased survival was due to a lack of cachexia, rather than weight gain per se, was not completely clear.

In a study of BCS and cancer cachexia syndrome in 100 dogs (which is characterised by a lean body mass status with a BCS $\leq$3), Michel et al (2004) found that only 4% of the dogs included in their study exhibited cachexia (BCS $\leq$3), while 29% were classified as overweight (BCS $\geq$7). However, within this study, substantially more dogs demonstrated evidence of muscle wasting or weight loss, than were classified as underweight by the BCS (Michel et al., 2004). This highlights the limitations of the BCS system when used in ill animals, where there may also be muscle wastage. Intramuscular fat accumulation and the substitution of functional muscle tissue with fat also comprises one of the characteristic features of muscle atrophy secondary to denervation and disuse (Powers et al., 2007). This is particularly evident following spinal cord injury (Scelsi, 2001; Gorgey & Dudley, 2007), degenerative intervertebral disc disease, whiplash disorders (Elliott et al., 2005; Elliott et al., 2006; Cagnie et al., 2009), in inherited muscle defects and in ageing (Vettor et al., 2009).

Muscle atrophy with fat infiltration is encountered in myopathies of a variety of different aetiologies, in both human and companian animal patients (Hanson et al., 1998; Platt et al., 2006; Kobayashi et al., 2009; Olby et al., 2011). The degree of fatty infiltration of muscle has been found to be a marker for disease progression and severity in human muscular dystrophy (Phoenix et al., 1996). The molecular mechanism of the

muscular stem cell conversion into an adipose cell is still under investigation (Vettor et al., 2009).

2.1.2 **Body condition score (BCS)**

The body condition score (BCS) is a subjective method of estimation of body fat percentage, based on visual and palpable fatness assessment. The BCS correlates with the amount of subcutaneous & abdominal fat and the amount of superficial musculature, and takes into account the animal's frame size, independent of body weight. The reliability of the BCS depends on its repeatability, reproducibility and predictability (Burkholder, 2000). It can be formally defined as the ratio of fat to non-fat tissues in the body and thus can be used to estimate body fat percentage (German, 2006). For body condition scoring, 5-point and 9-point based scales have been described. It has been reported that a 9-point scale correlates better with objective methods such as dual-energy x-ray absorptiometry (DEXA) (Mawby et al., 2004). Results from several publications have shown that the ideal body fat (BF) percentage range is between 13% and 25% (average 20%) which relates to point 3 on the 5-point scale and points 4 to 5 on the 9-point scale. Obesity has been associated with a fat percentage between 15% and 40% (Burkholder & Toll, 1997; Sanderson, 2010; Toll et al., 2010). The difference between the 5- and 9-point scales has been determined as 10% of body fat per point on the 5-point scale or 5% on the 9-point scale (Diez, 2006). On the 9-point scale, animals with a BCS of 1 to 3 (Sanderson, 2010) or 1 to 4 (Diez, 2006) have been defined as underweight, and with the scores 6 to 9 as overweight. In any individual animal, particularly on the basis of a subjective assessment, a question might arise over assigning a particular animal to a specific BCS, particularly if they are borderline underweight or obese and where different studies have defined different cut-offs.

There are recognised differences in the body composition between dogs of different breeds, particularly related to a breed's functional classification. For example, Greyhounds (and the sighthounds and other racing dogs) have higher muscle mass than Rottweilers (which are classified as working dogs). Correspondingly, these breeds will differ in ideal body fat percentage. Consistent with this, Jeusette et al (2010) estimated 7.2% of body fat (with just 1.5% of fat difference between different body condition scores) for the ideal Greyhound, and 32% of body fat for the ideal Rottweiler. Not only

breed differences, but also gender and age can be important for the understanding what is normal. The BCS provides an overall qualitative assessment of body condition, but does not provide quantitative information on actual body fat versus body muscle composition, and cannot differentiate between body compartments (Elliot, 2006).

2.1.3 **Girth measurement as an alternative method for the estimation of body fat**

A different morphometric method of body fat quantification has been suggested by some researchers, based on the girth measurements (Mawby et al., 2004). This promising alternative method has been shown to positively correlate with the following plasma levels: insulin, non-esterified fatty acids, total cholesterol, triglycerides, blood urea nitrogen, creatinine and total protein (Li et al., 2012).

However, this method has similar limitations relating to a lack of objectivity, with the main concerns being operator technique (in particular the amount of tension on the tape measure) and detection of the precise location of potentially confusion anatomic landmarks (Toll et al., 2010). Nevertheless, an accuracy of ±2-4% has been reported for this method (Burkholder & Toll, 1997).

2.1.4 **Advanced methods of body fat estimation including MRI**

The gold standard for body composition assessment in dogs is chemical analysis of tissues from euthanised dogs, which is not a suitable method for diagnostic purposes in a clinical setting (Mawby et al., 2004). There are a number of more advanced methods of body fat estimation, although most are not applicable for clinical use, mainly due to technical complexity and the requirements for specialised equipment. It is also notable that the results obtained may demonstrate significant differences depending on the method employed. Using bioelectric impedance, one study calculated that a body fat percentage of 27% equated to a BCS of 5 (using the 9 point scale), and a BCS of 4 was assumed to represent a lean animal. The difference between the individual scores on the 9-point scale in this study was estimated as 4.8% of body fat (Stone et al., 2009). However, a study examining the measurement of body fat percentage by dual energy X-ray absorptiometry (DEXA) found that body fat percentages determined by this method were 15.8% higher on average than those calculated by the deuterium oxide dilution method (Son et al., 1998). The DEXA method has been considered by many

researchers to be the gold standard reference method, although variable results have been reported by the different workers (Jeusette et al., 2010). However, these methods are technically demanding and furthermore do not provide a solution for breed-associated differences in body fat percentage (Jeusette et al., 2010).

Other advanced methods for adipose tissue quantification include computed tomography (Ishioka et al., 2005; Marchadier et al., 2011; Samara et al., 2012), (MRI) (Khoury et al., 2008), ultrasound (Wilkinson & McEwan, 1991; Kramer et al., 1996; Stringer et al., 2010), and the Dixon MRI method of fat quantification based on the chemical shift phenomenon in MRI (Ross et al., 2000; Bley et al., 2010; Wokke et al., 2013). MRI is widely used for adipose tissue quantification because of intrinsic differences between the T1 relaxation times of fat and other tissues (Sacha et al., 2003; Wattjes et al., 2010; Hu, 2011). Strong tissue contrast between fat, muscles and organs allows for the precise measurement and topographic description of fat deposition (Cornier et al., 2011), as well as the objective quantification of intramuscular fat deposition (Cagnie et al., 2009). MRI provides a unique modality for water and fat-based tissue visualisation, and is considered to be the only in vivo technique for the accurate quantification of ectopic fat (Wattjes et al., 2010; Hu , 2011).

2.1.5 **Aims of the study**

The main aim of this part of the study was to compare the subjective estimation of body fat percentage by BCS and girth measurements, with the objective determination of the amount and pattern of fat deposition using MRI. In particular:

- To determine the correlation between BCS and girth measurements
- To describe the patterns of fat deposition on MRI in the cervical and lumbar regions with increasing BCS
- To examine the correlation between BCS and the objective MRI determination of fat deposition in the dorsal cervical and lumbar regions
- To define the correlation between increasing BCS and the change in MRI muscle signal intensity in the cervical and lumbar regions

2.2 Materials & Methods

2.2.1 **Animals**

The study was defined as sub-threshold for requiring formal ethical approval by the School of Veterinary Medicine Ethics and Welfare Committee. Data was collected over a period of 12 weeks in the University of Glasgow Small Animal Hospital. Dogs undergoing anaesthesia for an MRI study of the cervical or lumbar region were potential candidates for inclusion. Dogs with evidence of local vertebral column or spinal cord pathology on MRI that affected the regional anatomy or muscle innervation were excluded. Breed, gender, age and bodyweight were recorded. Descriptive statistics were reported as mean, median and range. All dogs were having the MRI study under anaesthesia as part of an unrelated clinical investigation. A variety of dog breeds, representing a cross-section of the hospital population, were included.

2.2.2 **Body condition scoring and girth measurements**

Body condition score (BCS) (Toll et al., 2010) was determined by two trained persons, and inter-observer variability was evaluated. The 9-point BCS scale was used, with the score for normal body condition defined as point 5, and characterised by:

- Normal body contours
- Bony prominences (ribs) that can be readily palpated but not seen
- Intra-abdominal fat which is insufficient to obscure or interfere with abdominal palpation
- Waist viewed from above and abdominal tuck evident

Morphometric (girth) measurements and total body fat percentage calculation were performed as previously described (Mawby et al., 2004). Pelvic circumference (PCcm) was measured around the level of the flank and hock-to-stifle length was measured from tuber calcaneus to midpatellar ligament (HScm):

Males (%BF) = -1.4 (HScm) + 0.77 (PCcm) + 4
Females (%BF) = -1.7 (HScm) + 0.93 (PCcm) + 5

2.2.3 **Magnetic resonance imaging**

MR imaging was performed using a 1.5 Tesla system. T1-weighted (360-870/10-15; range TR/TE) and T2-weighted (2160-5890/86-130; range TR/TE) images were acquired in both sagittal and transverse planes.

All dogs were placed in dorsal recumbency with the thoracic limbs extended either caudally or cranially. In all MR imaging studies, the transverse plane images were orientated perpendicular to the vertebral canal. The field of view ranged from 36x36cm to 51.2x51.2cm (sagittal plane) and 13x13cm to 51.2x51.2cm (transverse plane). The slice thickness varied from 3.5-4mm (transverse plane) and 3-4mm (sagittal plane) with an interslice interval of 0.3-0.5mm. Additional MRI sequences obtained included T1 FAT SAT and STIR weighted images.

MR images were evaluated using an open-source PACS Workstation DICOM viewer. Two regions were analysed; cervical and lumbar. Images from the sagittal and transverse planes, and lastly whole body cross-section images where available were evaluated.

2.2.4 **MRI patterns of fat deposition in lumbar and cervical region**

For the fat measurements in the lumbar and cervical regions a different approach was employed reflecting their anatomical characteristics: there was much less intermuscular connective tissue in the lumbar region comparing to the cervical region. In the lumbar region the fat distribution was mainly confined to the subcutaneous region. In the cervical region, due to the large amount of intermuscular fat, a separate method was employed to additionally determine the amount of intermuscular fat (in addition to the subcutaneous fat). Sagittal images of the cervical area were not analysed due to the frequent presence of an artifact created by identity chip placement.

2.2.5 **Correlation of body condition score with MRI fat determination**

2.2.5.1 Lumbar region

In the lumbar area, measurement of subcutaneous fat thickness and area were performed at the vertebral column level corresponding to intervertebral disc spaces L1-L2 and L3-L4 on the transverse images, and L1-L2, L3-L4 and L6-L7 on the sagittal images.

Regions of interest were set manually. Fat/muscle interfaces were excluded as containing both tissues (Monziols et al., 2006) and the assumption was made that the accuracy of the volume measurement by MRI was primarily a function of edge detection or tissue separation (Mitchell et al., 2001).

Subcutaneous perivertebral fat on the transverse images was measured from a line parallel to the level of spinal canal floor to the edge of the skin (Figure 2-1). The thickness of the subcutaneous fat was measured on the transverse images between the skin and the top of the vertebral spinous process, as well as paravertebraly at 45° to the middle vertical line, and on sagittal images in the dorsal midline (Figure 2-2).

All measurements were repeated 3 times by the same observer. Sagittal images were used to calculate the ratio of subcutaneous fat (SCF) to L2 vertebral body length. Perivertebral measurements on transverse images were used to calculate mean values and corrected for L2 vertebral body length. Statistical analysis was conducted based on the generated data.

Inhomogeneities on the images consisted of fascia, fat/muscle edge effects and inclusions in the fat and were not considered as significant.

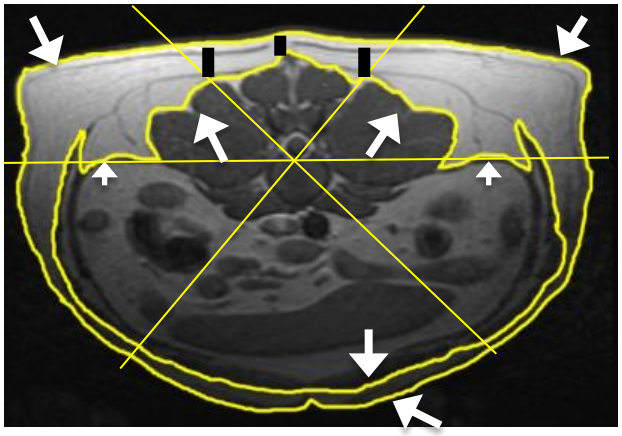

Figure 2-1. Transverse T1W MR image of a dog (BCS 5) at L2-L3 vertebral level showing the sites of linear measurements of SCF thickness (black lines at the dorsal muscles border), cross section fat area between the borders (shown by the long arrows) outlining the outer body surface, muscles and abdomen; and dorsal fat area starting from the horizontal line (small arrows).

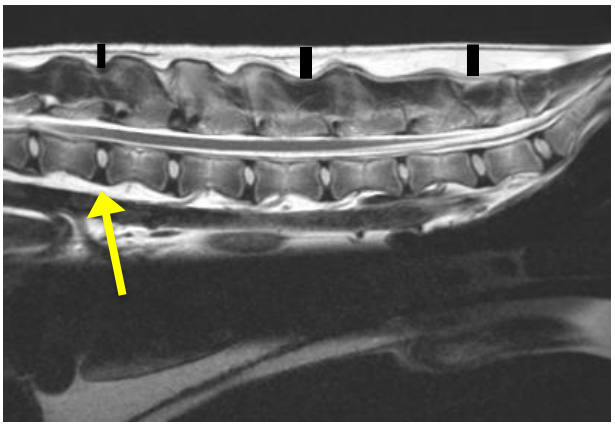

Figure 2-2. Sagittal T1W MR image of a dog (BCS 5) showing the sites of measurement of subcutaneous fat thickness (black vertical lines) at L1-L2 (arrow), L4-L5, L6-L7 respectively.

2.2.5.2 Cervical region

For SCF determination, transverse images used were at the level of C2/C3 and C4/C5 intervertebral disc spaces. Subcutaneous fat depth was measured by generating a set of radii to describe different points for measurement. The centre of the circle was taken as the ventral aspect of the spinal canal in midline (Figure 2-3). Radii were dorsal midline and 45° from the dorsal midline to both sides. The values generated were corrected to

C4 vertebral body length. Ventral, dorsal and intermuscular fat was measured along the radii to allow estimation of total fat. In the second set of measurements, in order to avoid skin folds, the radii were continued vertically in parallel to each other starting from the muscle edge. These three measurements were used to determine the dorsal fat thickness.

SCF and dorsal SCF cross sectional area were segmented manually and percentage differences calculated. Sagittal images were not included due to frequent ID chip artefact interference, but were used occasionally only for comparative purposes.

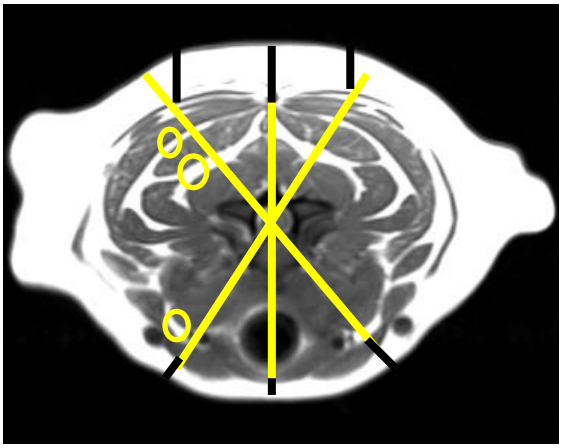

Figure 2-3 T1W transverse cervical (C4-C5 level) image of a dog: subcutaneous fat dorsal and ventral linear measurements at the midline and at 45° to the midline bilaterally (black lines). Intermuscular fat was measured along the lines drawn at a 45° through the floor of spinal cord canal in all cervical cases (intermuscular fat intersected by the 45° lines are highlighted by the yellow circles). Lumbar cases were not calculated in this manner due to the lack of intermuscular fat deposition in the lumbar area (Figure 2-4).

2.2.6 **Correlation of body condition score with muscle T1W signal intensity on MRI**

Muscle MR signal intensity relative to the spinal cord signal intensity was measured using ImageJ, a Java-based version of the public domain NIH Image software (Okada et al., 2011). In manually segmented muscles the signal intensity was calculated relative to the signal intensity of the spinal cord in the same transverse image. In the spinal

cord, regions of interest were segmented for every image using the round tool carefully avoiding the edges of the spinal cord. These measurements were conducted in the cervical and lumbar epaxial muscles and the muscles were grouped as follows:

- Dorsal inner layer – these included the epaxial muscles adjacent to the vertebra lamina, and which included the vertebral level C2/3 – obliquus capitis caudalis, longissimus muscles; at the level C4/5 - multifidus; semispinalis cervicis; longissimus capitis, longissimus cervicis muscles.
- Dorsal intermediate layer - epaxial group of muscles between the deep and medial fascia that included the semispinalis capitis muscles (biventer and complexus).
- Lumbar epaxial muscles – multifidus, longissimus and iliocostalis muscles.

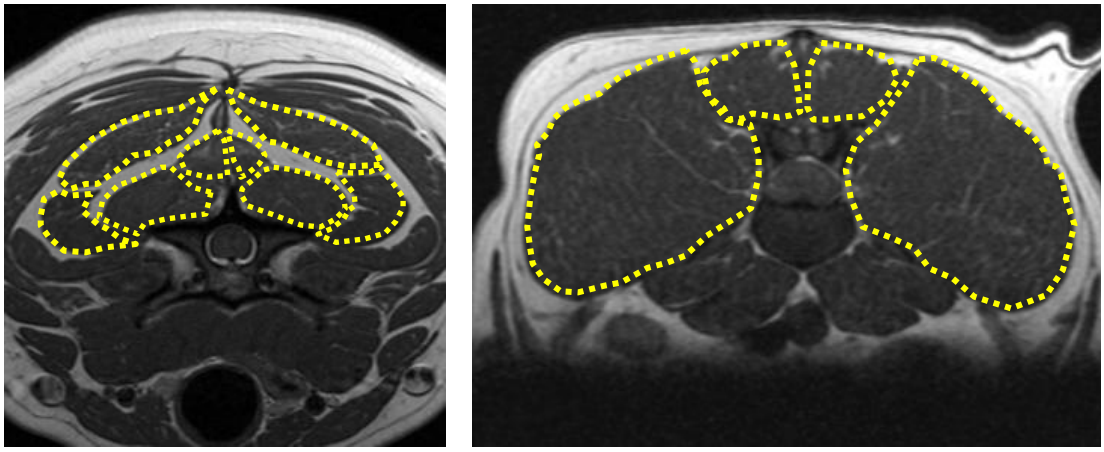

A B

Figure 2-4. Cervical (A) and lumbar (B) muscle segmentation for MR signal intensity measurement

2.2.7 **Statistical analysis**

GraphPad Prism 5.00 was used for statistical analysis. The descriptive statistics included mean, standard deviation and range. The statistical analysis was performed using Spearman correlation test.

2.3 Results

2.3.1 **BCS and Girth measurements**

2.3.1.1 Body condition scoring and inter-observer variability

BCS was assessed in 66 dogs, in 45 this was performed by two separate observers (the same two observers for all 45 dogs) and these were therefore available for inter-observer variability evaluation (group 1), while BCS and girth measurements were performed by one observer in 21 dogs (group 2). Mean age of these dogs was 6.75 years (range 12 months to 14 years); mean body weight was 20.29kg, (range 3.2-70); 31 were females (20 neutered, 11 entire), 36 males (14 neutered, 22 entire). Of the 45 dogs where the BCS was performed by two observers, 32 underwent lumbar area MR imaging, 22 cervical, 6 had both and 7 were not screened for the regions of interest in this study.

Breeds presented included: 6 cross breeds, 5 Dachshunds, 4 Jack Russell Terriers and 4 Cavalier King Charles Spaniel (CKCS). Three each of the following breeds: Cocker spaniel, Dalmatian, Labrador retriever, Pointer, Lhasa Apso, Collie. Two each of the following breeds: Boxer, Golden retriever, Shi-tsu, Lurchers, Boxer. One each of the following breeds: Poodle, Pomeranian, Springer spaniel, Great Dane, Border terrier, Pug, Irish Wolfhound, Basset hound, Husky, Rottweiler, Chihuahua, Irish setter, Yippet, Tibetan spaniel, Kerri Blue terrier, Patterdale, Maltese terrier, Dandy Dinmont terrier, Dobermann pincher.

Of the 45 dogs available for assessment of the inter-observer variability (group 1), 17 (37.7%) were scored equally by both observers, in 25 dogs (55.5%) a one point difference in BCS was noted and in 6.6% (3 dogs) a 2 point difference in BCS was noted. Correlation coefficient 0.718, p-value=0.008 (Figure 2-5).

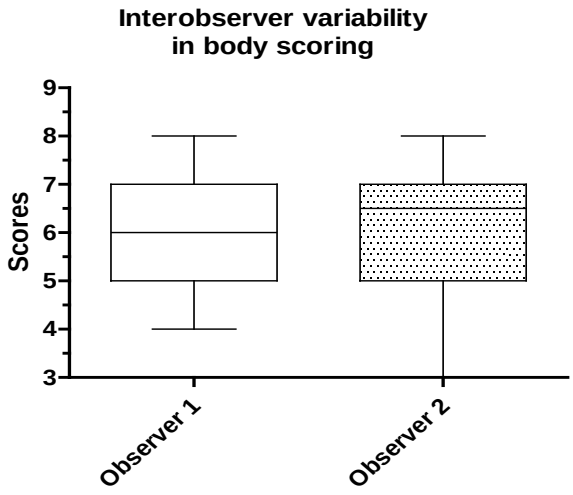

Figure 2-5 Box and whisker plot presents the inter-observer variability in body condition score assignment (r= 0.718, p-value=0.008).

Girth measurement and total body fat percentage were calculated in the group of 21 dogs (13 males and 8 females) (group 2) using the equation shown in the Materials & Methods section. Assuming that normal (BCS 5) body fat percentage lies between 13-20% and the difference between scales is around 5%, the following values could be calculated with an overlap of 7%:

- BCS 3 = 3-10% of fat
- BCS 4 = 8-15% of fat
- BCS 5 = 13-20% of fat
- BCS 6 = 18-25% of fat
- BCS 7 = 23-30% of fat
- BCS 8= 28-35% of fat
- BCS 9 = 33-40% and higher.

2.3.1.2 Correlation of BCS and body fat percentage calculated from the Girth measurements

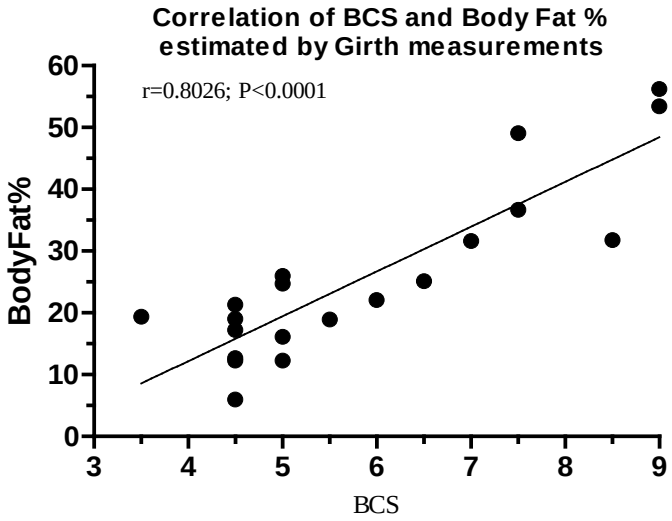

Figure 2-6 Scatterplot shows good correlation of the body condition score assigned with the body fat % as estimated by the girth measurements regardless of breed differences.

The body fat % calculated using the girth measurements appeared to be in good correlation with the BCS and was not affected by breed differences (Figure 2-6).

2.3.2 **Patterns of fat deposition**

2.3.2.1 Lumbar region

Subjectively there was a general tendency for SCF distribution in lumbar region to increase in thickness caudally, starting at L5-L6. In more lean animals (BCS 3.5), subcutaneous fat was limited to a thin, almost even layer along the dorsal lumbar area. This is demonstrated in Figures 2-7 to 2-12.

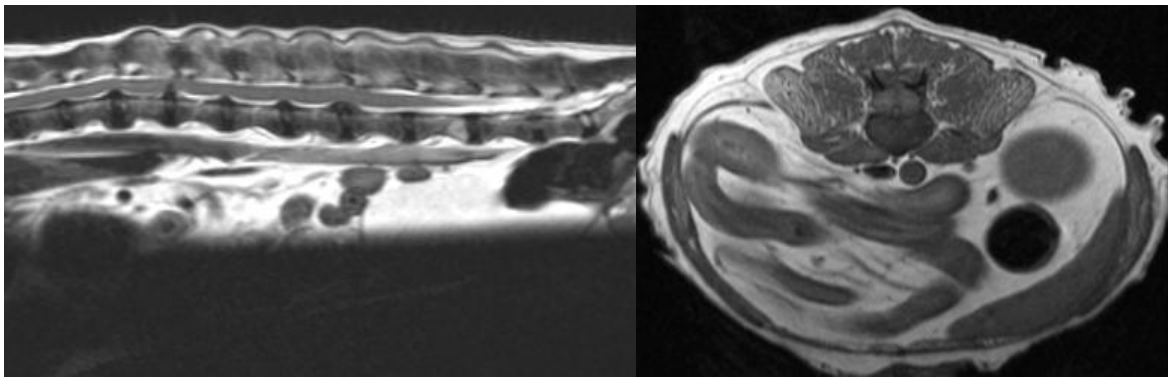

A B

Figure 2-7 T1W sagittal (A) and transverse (B) MR images of the dog a BCS 3.5 showing the patterns and thickness of SCF distribution in the lumbar region.

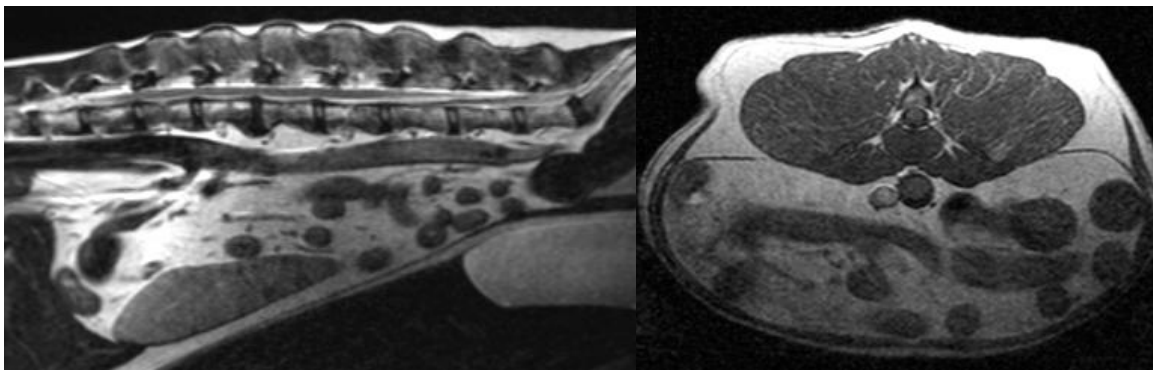

A B

Figure 2-8. T1W sagittal (A) and transverse (B) MR images of a dog with BCS 5. There is a mild increase in the subcutaneous fat thickness in lumbar area, but no substantive deposition of fat between the lumbar muscle groups.

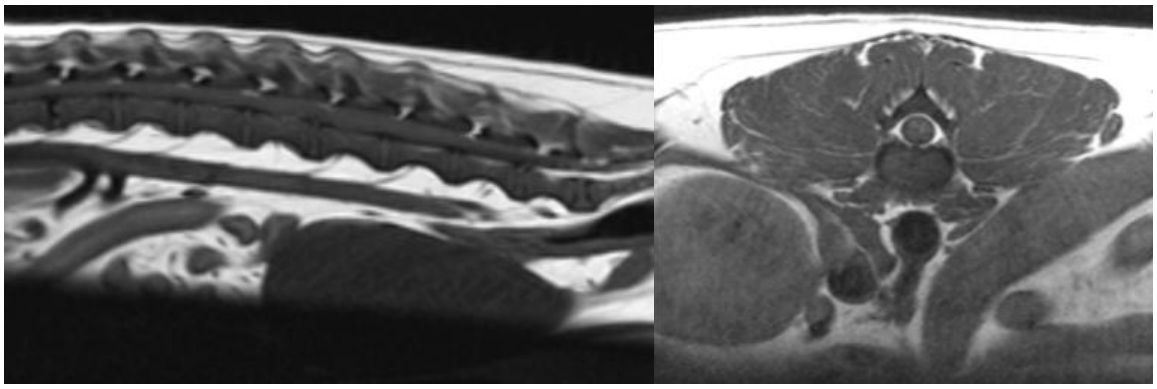

A B

Figure 2-9. T1W sagittal (A) and transverse (B) MR images of a dog with BCS 6: there is a marked increase in SCF thickness, with SCF covering the vertebral spinous processes more evenly, and with the main fat bulk starting from L5 level.

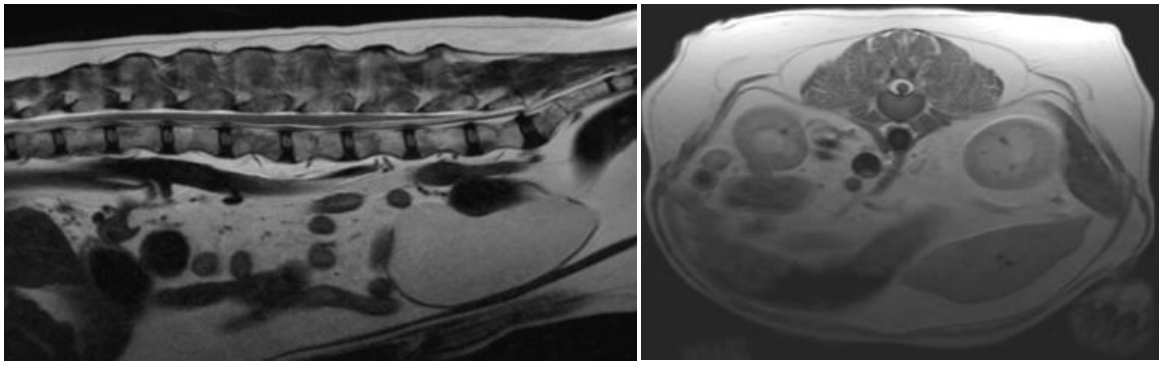

A B

Figure 2-10. T1W sagittal (A) and transverse (B) MR images of a dog with BCS 7. There is still no substantial fat deposition between the epaxial lumbar muscle bellies.

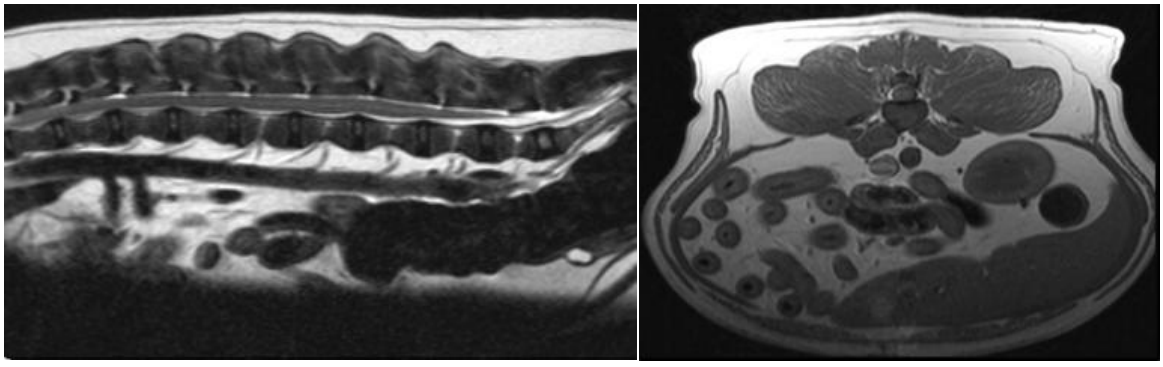

A B

Figure 2-11. T1W sagittal (A) and transverse (B) MR images of a dog with BCS 7 showing an even fat layer along the entire lumbar vertebral column. There is an obvious difference in the fat thickness between dogs with the same BCS (Figure 2-10 and 2-11).

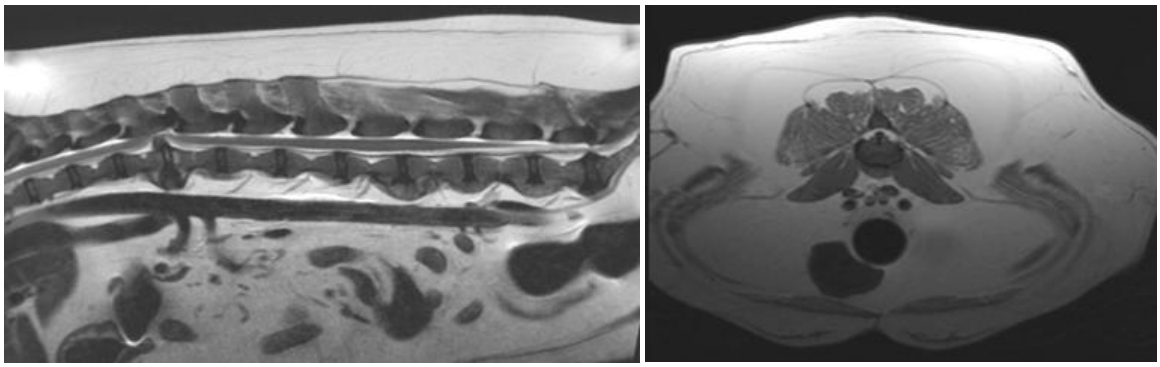

A B

Figure 2-12. T1W sagittal (A) and transverse (B) MR images of the lumbar area of a dog with BCS9. Obvious abundant fat accumulation over entire area is evident.

2.3.2.2 Neck region

There was an obvious visual difference in the amount of fat between extreme body scores: from an almost undetectable fat layer (BCS4) to excessive fat deposition in BCS9, in contrast the discrimination between adjacent scores was not immediately obvious.

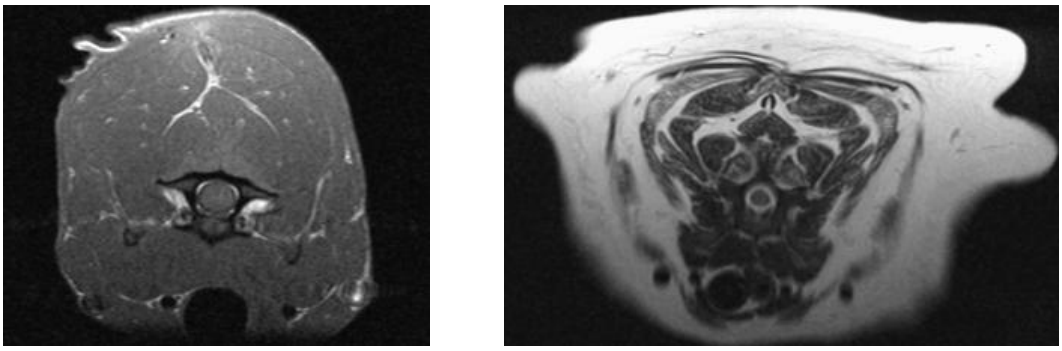

A B

Figure 2-13. A – T1W image of the neck of a Greyhound, with BCS 4. The MRI appearance of lean muscles and almost completely absent of subcutaneous and intermuscular fat results in muscles with a smooth appearance and poorly defined muscle edges. B – T2W image of the neck of a Labrador retriever with BCS 9. Subcutaneous fat deposition is marked, intermuscular fat is prominent and the muscles are more hyperintense relative to the intensity of the spinal cord than in A.

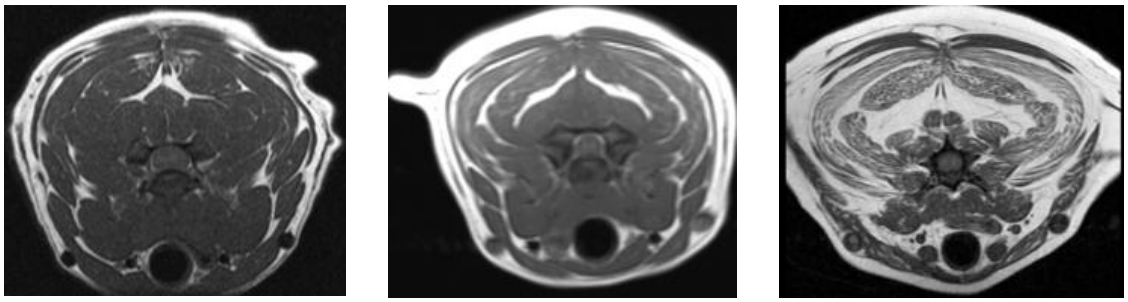

A B C

Figure 2-14. A – T1W cervical MR image of a Tibetan spaniel with BCS 3.5. B – T1W image of the Dalmatian with BCS 4.5. The difference between SCF layers is mild and there is moderate intermuscular fat distribution in both dogs, sufficient to define the borders of the individual muscles. C – T1W image of the neck of the dog with the BCS 9; the SCF fat layer is thicker than in dogs A and B, but the main difference is in the amount of intermuscular fat and the marked muscle hyperintensity.

2.3.3 **Correlation of BCS and fat deposition**

2.3.3.1 Lumbar region

The results of measurements performed on lumbar images are shown in figures 2-15 to 2-17.

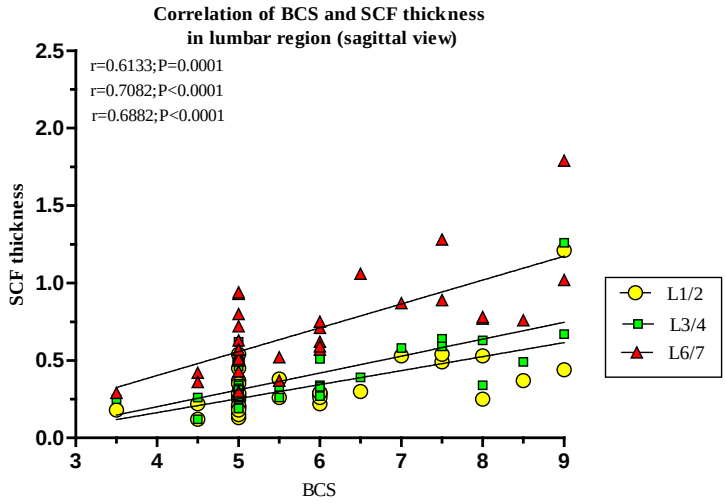

Figure 2-15. Scatterplot depicts the correlation between BCS and lumbar SCF thickness (relative to L2 vertebral body length) measured on the sagittal images at three levels – L1-L2, L3-L4 and L6-L7. BCS/ L1-2L2 level: r=0.6133, P=0.0001. BCS/L3-L4: r=0.7082, P<0.0001. BCS/L6-L7: r=0.6882, P<0.0001. Correlation is significant for all three levels.

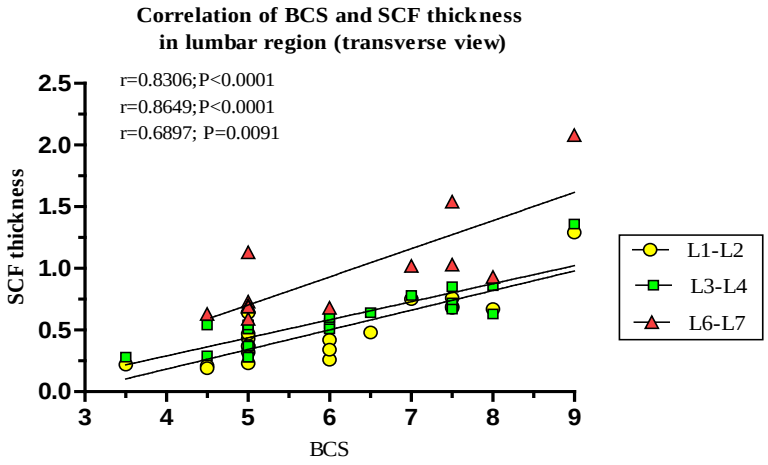

Figure 2-16. Scatterplot showing a positive correlation between increasing BCS and increasing SCF linear measurements (relative to L2 vertebral body length) on the transverse MR images (levels L1-L2, L3-L4 and L6-L7).

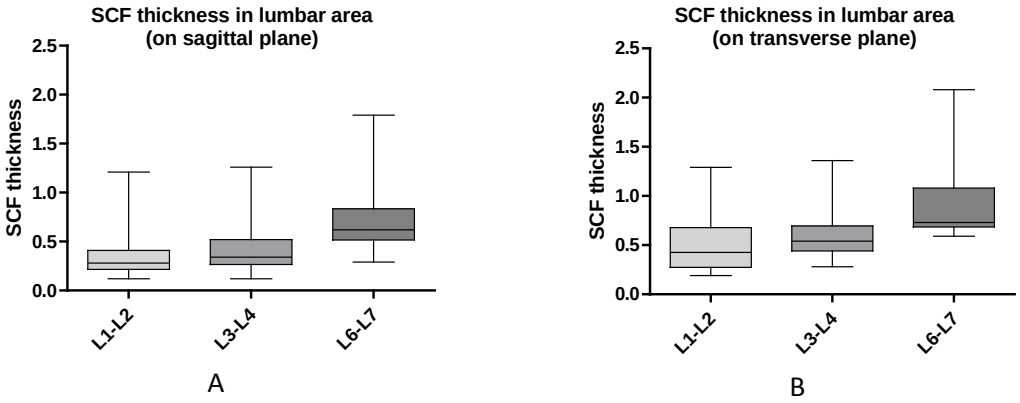

Figure 2-17. Box and whisker plots: A- SCF thickness (relative to L2 vertebral body length) in the lumbar region on sagittal plane images (median: 0.2800; 0.3400; 0.6200 respectively); B-SCF thickness in the lumbar region (relative to L2 vertebral body length) on transverse plane (median: 0.4250; 0.5400; 0.7300 respectively). There was a tendency for SCF to increase caudally on both sagittal and transverse planes.

2.3.3.2 Neck region.

The results of measurements performed on cervical images are shown in figures 2-18 to 2-20

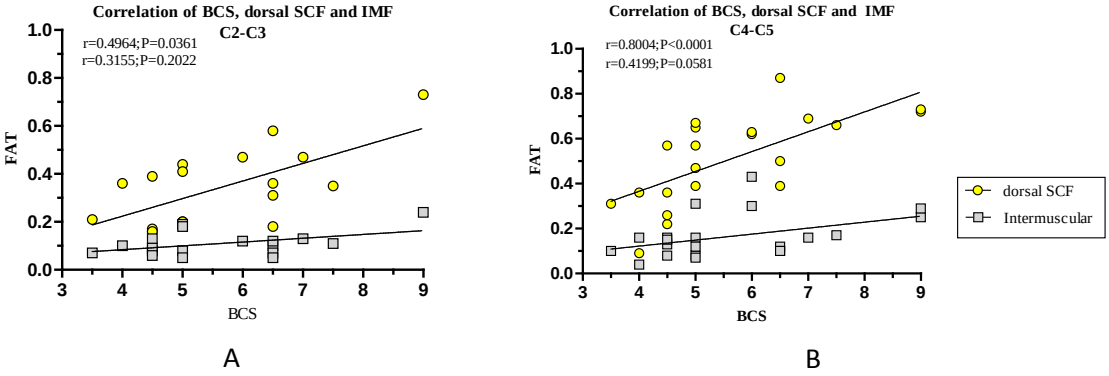

A B

Figure 2-18. Correlation of BCS and dorsal SCF thickness and intermuscular fat deposition (relative to L2 vertebral body length) for the levels C2-C3 (A) and C4-C5 (B). Increasing BCS resulted in increasing SCF deposition, and to a lesser extent increasing intermuscular fat deposition in the cervical region.

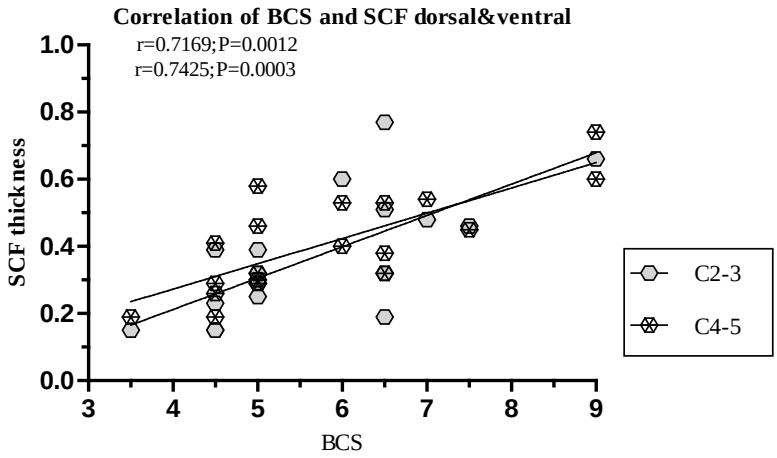

Figure 2-19. Correlation of the BCS and subcutaneous dorsal and ventral fat thickness (relative to L2 vertebral body length), measured along the 45° radii.

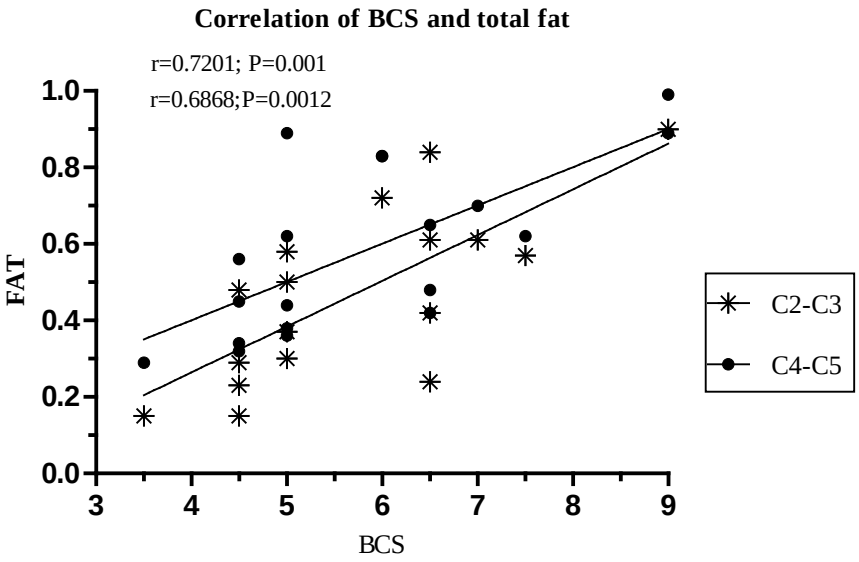

Figure 2-20. Scatterplot demonstrating the correlation between increasing BCS and increasing total (subcutaneous and intermuscular fat) (relative to L2 vertebral body length) in the neck region at the C2-C3 level and C4-C5 level. The C4-C5 level demonstrated the highest correlation (correlation line closest to the x-axis).

2.3.4 **Correlation of BCS and muscle signal intensity**

Signal intensity was measured in all the lumbar epaxial muscles as a combined group as it was not possible to accurately define different muscle groups due to the limited intermuscular fat deposition in this region. In the cervical region the muscles were divided into two large groups of muscles: the inner and intermediate dorsal layers. In the lumbar area the measurements were performed at the level of the L1-L2 and L3-L4 intervertebral disc space. In the cervical region the measurements were performed at the level of the C2-C3 and C4-C5 intervertebral disc spaces. For all measurements, muscle signal intensity was expressed relative to spinal cord signal intensity for each MR image. The results are demonstrated in figures 2-21 to 2-23.

2.3.4.1 Lumbar region

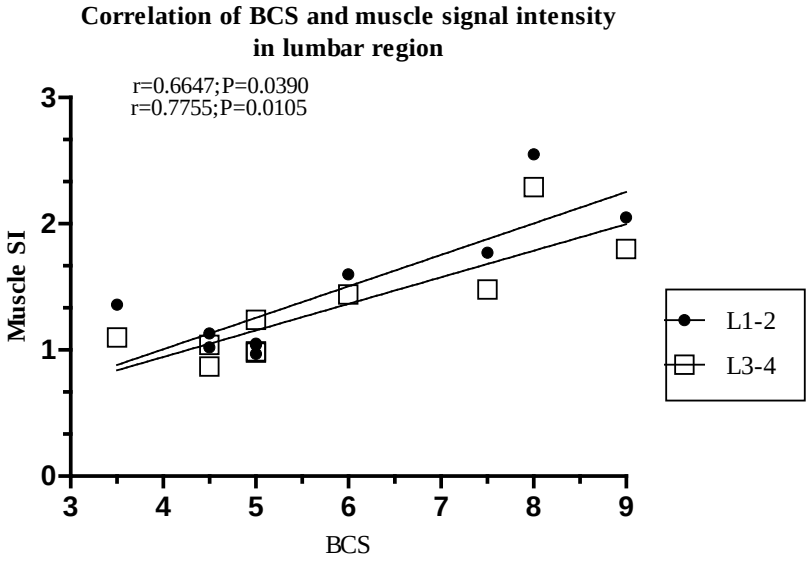

Figure 2-21. Scatterplot shows a good correlation between increasing BCS and increasing muscle signal intensity (relative to spinal cord signal intensity) at both lumbar region levels investigated.

2.1.1.1 Neck region

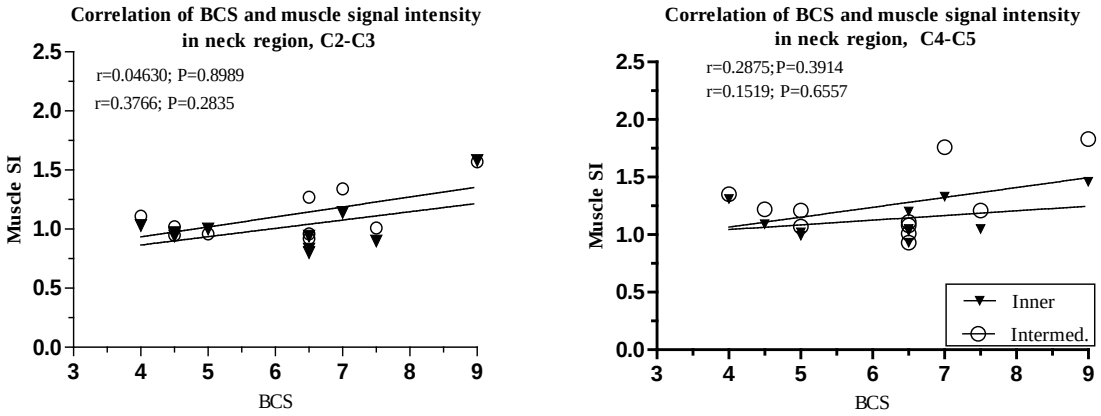

A B

Figure 2-22. Scatterplot showing correlation between increasing BCS and increasing signal intensity in the cervical muscles (relative to spinal cord signal intensity) at C2-C3 (A) and C4-C5 (B) vertebral levels.

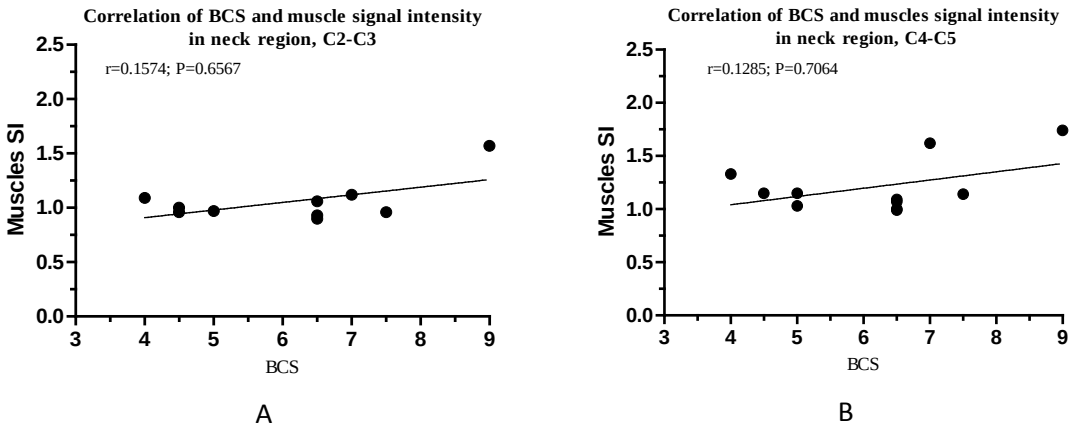

A B

Figure 2-23. Scatterplot showing a positive correlation between increasing BCS and increasing muscles signal intensity (relative to spinal cord signal intensity) measured in the neck region at C2-C3 (A) and C4-C5 (B) vertebral levels.

2.4 Discussion

Obesity is a growing problem in companion animals (McGreevy et al., 2005; Lund et al., 2006). The commonly reported health risks associated with obesity are diabetes mellitus, osteoarthritis and a shortened lifespan (German, 2006; Radin et al., 2009). Recent work has shown that obesity is associated with a low-grade chronic inflammation in adipose tissue, predisposing to insulin resistance and cardiovascular disease (Bastard et al., 2006). Most tissues have limited reserves of lipid, which is utilised as an energy source, for maintenance of membrane structure and intracellular signalling.With progressive obesity, lipid is deposited into non-adipose organs including the liver, pancreas, skeletal muscle, heart and kidneys thus forming ‘ectopic lipid’ and leading to impairment of cell function (lipotoxicity) and lipid-induced programmed cell death (lipoapoptosis) (Rasouli et al., 2007).

There are a variety of reported techniques for assessment of body composition in companion animals (German, 2006). The goals of this study were to assess two methods that readily translate into the clinical setting and compare them to MR imaging for fat determination: body condition scoring and girth measurements. These methods were used to examine the correlation between the body condition scores assigned to dogs on the 9-point BCS scale and:

- Body fat % calculated from girth measurements.
- Patterns of fat distribution in lumbar and cervical regions.

- Amount of fat detected on MRI images (subcutaneous in the lumbar and cervical regions; intermuscular in the cervical region).
- MRI signal intensity in the epaxial lumbar and cervical muscles.

Four types of measurements were performed on MR images in order to quantify fat composition within individual dogs:

1. Linear measurements of dorsal subcutaneous fat thickness on sagittal and transverse images in the lumbar region.
2. Linear measurements of dorsal and ventral subcutaneous fat in the cervical region.
3. Intermuscular fat measurements in the cervical region, which together with dorsal and ventral SCF was defined as "total" extramuscular fat
4. Epaxial muscle T1W MRI signal intensity (relative to spinal cord signal intensity).

Body condition scoring and Girth measurements

Clinical evaluation of body condition and assigning of BCS is complicated in dogs by differences between breeds and varying optimal body weights among dogs of the same breed depending on frame size (Burkholder & Toll, 1997). Gender and age dependant differences suggest a requirement for an individual approach to the body condition assessment. As an example, females are more prone to weight gain than males (Dorsten & Cooper, 2004). Furthermore, individual assessors' understanding of the norm may impact the scoring assigned. Differentiation between extremes is easier, while distinguishing between dogs in the overweight category of BCS 6-7 is harder, as is between obese dogs with BCS 8-9 or underweight dogs with BCS 3-4. The scoring system by itself contains some element of approximation, because the degree of emaciation or obesity can be variable, and as the result, animals with the same BCS can have different body fat percentages (Sanderson, 2010). However some clinical scoring systems do take into account breed, age and body conformation during scoring, and the 9-point system in particular has been shown as a reliable method in companion animals (Laflamme, 1997; Bjornvad et al., 2011).

In this study, inter-observer variability using the 9-point BCS system was evaluated in 45 dogs of different breeds, genders and ages, and revealed a discrepancy of only ±1

point in over half of the dogs evaluated and ±2 points in about 7% (3 dogs), which was considered a good level of agreement between observers (correlation coefficient 0.718, P-value=0.008) (Figure 2-5). Body fat percentage quantification based on the girth measurements has been reported to show good accuracy (Burkholder & Toll, 1997). In this study body fat percentage calculated using girth measurements in 20 dogs was significantly correlated with BCS for males (R= 0.74943) and females (R=0.74296), with the highest fat percentage corresponding to BCS 9 (53.42% in male and 56.24% in female dogs); the lowest fat percentage was found in BCS 3.5 (12.26%) male and BCS 4.5 (5.99%) female dogs (Figure 2-6). Importantly, there was a calculated 7% body fat overlap between the scores, which can allow for a breed, sex and age adjustments.

MR images analysis: patterns of fat distribution in the lumbar and neck regions

Magnetic resonance imaging has made an important contribution to the research of body composition in man (Ross et al., 2000). MR imaging can provide a more objective evaluation of SCF thickness, body fat distribution and the degree of muscle fatness; and thus can serve as a diagnostic tool for discrimination between normality and disease, when combined with clinical data. MRI analysis relies on the volume measurements of muscle and adipose tissue and has been used to predict body composition, not just in man (Ross et al., 2000), but also in pigs (Mitchell et al., 2001; Monziols et al., 2006), rabbits, chickens (Kover et al., 1998) and rodents (Tang et al., 2000).

In this study a clear difference between neck and lumbar regions was found. In the lumbar region fat accumulates in the dorsal subcutaneous area (Figure 2-7 to 2-11), while in the neck region the intermuscular space is an important site of fat deposition, which is evident from the comparison of the images of the dogs with different BCS (Figure 2-12 to 2-14). Interestingly, in man the amount of intermuscular adipose tissue has been shown to be as good a predictor of insulin sensitivity as visceral adipose tissue (Boettcher et al., 2009). Lumbar SCF thickness measurements correlated well with BCS. In the lumbar region it was evident that the main site of fat accumulation was dorsal and increased from cranial to caudal (2.24 times thicker at L6-L7 than at L1-L2). Fat measurements on the transverse images included perivertebral fat, and provided even better correlation with BCS than the sagittal view (Figure 2-1 to 2-3). Using ultrasound, Wilkinson & McEwan (1991), demonstrated a good correlation betweeen subcutaneous fat thickness and BCS in the midlumbar area in the dog (Wilkinson &

McEwan, 1991). However, in the present study, the difference between body condition scores is readily appreciated on the images of the neck region: from an almost undetectable subcutaneous fat layer (BCS 4) to a moderate, evenly distributed subcutaneous fat layer in BCS 6, and excessively deposited fat in BCS9 (Figure 2-13 and 2-14). Although, when comparing the lumbar and neck regions, the dorsal subcutaneous fat layer in the lumbar region had a higher correlation to BCS than the dorsal SCF in the neck region. When the SCF measurements included the ventral fat layer in the neck region, good correlation with BCS was obtained. Conversely, intermuscular fat accumulation was less well correlated with BCS, but increased for more caudal levels in both the lumbar and neck regions.

Correlation between BCS and T1W signal intensity in the dorsal lumbar and in the cervical regions

It is well recognised that the lipid content in skeletal muscle is altered with obesity (Ross et al., 2000). However, in an MRI and MR spectroscopy study of obesity-associated fat depositions in man, it was shown that variations in abdominal, subcutaneous and ectopic fat in the liver and skeletal muscle could not be predicted by anthropometric measurements (Thomas et al., 2012). In the study reported here, T1W MRI signal intensity was measured in the epaxial lumbar muscles: *mm. multifidus lumborum, longissimus* and *iliocistalis,* and in the neck region: *mm. multifidus cervicis, spinalis cervicis, semispinalis capitis* and *biventer cervicis* and *complexus*. It was found that lumbar, but not cervical, muscle signal intensity was significantly correlated to BCS. From these findings it can be implied that lumbar muscles are more prone to fat infiltration than the neck muscles with increasing BCS.

In conclusion, a positive correlation was found in this study between BCS and morphometric measurements to determine body fat (girth measurements), between body condition score and the amount of SCF deposition for both lumbar and cervical areas, and BCS and T1W MRI signal intensity of the lumbar epaxial muscles. SCF deposition, as well as muscle signal hyperintensity, appeared to increase caudally in each region with a better correlation for the lumbar area. This study indicates that investigation of lumbar and cervical areas should employ different approaches due to differences in intrinsic anatomical and physiological responses of these areas to increasing BCS.

3 Proximal thoracic limb muscle identification on MRI

3.1 Introduction

The shoulder area represents a very complex structure with different groups of muscles with different functions: stabilising the spine, attaching the thoracic limb to the body wall and moving the limb cranially, caudally, abducting, adducting and rotating. MRI is used for evaluation of the shoulder soft tissues and skeletal pathology in human and veterinary patients (Schaefer & Forrest, 2006; Murphy et al., 2008; Schaefer et al., 2010). Many authors have emphasised the significance of positioning for MR and CT imaging of the shoulder area in man and in dogs, primarily in connection with the glenohumeral joint and surrounding structures pathologies (Agnello et al., 2008). Correct positioning enables evaluation of normal anatomy and detection of lesions, which may affect diagnosis, surgery planning and follow up (Harder et al., 2008). In a study of the MRI and arthroscopy of the shoulder joint in humans problems of missed lesions were reported, including lesions that were overlooked, misinterpreted lesions and lesions that were difficult to identify or not present on images (even in retrospect) (Polster & Schickendantz, 2010).

A number of factors may affect imaging of the shoulder including potential artefact due to alignment of the supraspinatus tendon with the MR plane and abnormal signal in the supraspinatus muscle caused by narrowing of the interval between the supraspinatus and infraspinatus muscles if the limb is internally rotated (Carroll & Helms, 2002).

In a cadaveric study of 13 canine thoracic limbs, the CT detectability of the shoulder joint capsule, ligaments and deltoideus, teres minor, supraspinatus, infraspinatus, biceps brachii and subscapularis muscles was investigated. Good detectability of all muscles was evident when the shoulder joint was in an extended position (140 degrees), with poor visualization for some muscles in the neutral and flexed position (Silva et al., 2013). However the experimental settings, in particular the use of cadaveric limbs, have substantial limitations, and therefore do not allow clear extrapolation into live animals. One study recommended the following protocol for canine brachial plexus imaging: dorsal recumbency positioning with symmetrical limbs, and non-oblique body positioning (Kraft et al., 2007).

Detection of the muscle edges and their anatomical identification is of great importance for an accurate neuromuscular diagnostic workup. The above muscle groups can be detected on transverse and dorsal MRI planes with different degree of accuracy. Therefore, the main aim of this study was to assess the detectability of these muscles on clinically obtained images and examine the factors affecting their detection, with the following steps:

Aims of this study:

1. To review the proximal thoracic limb anatomy on MR images
2. To evaluate the appearance on MR images of these muscles on different imaging planes
3. To evaluate the effect of positioning, artefacts and field of view on muscle detectability
4. Review the clinical significance of these findings

3.1.1 **Anatomical review of the muscles of the proximal thoracic limb in a dog**

The ***serratus ventralis cervicis*** muscle is thick and fan-shaped, it starts from the facia serrata of the scapula, has five divisions each inserting on the transverse processes of C3 to C7. It continues with thoracic component, the serratus ventralis thoracis, incerting on the first seven or eight ribs. This muscle supports the trunk and carries the shoulder cranially and caudally with respect to the limb; and inspiration.

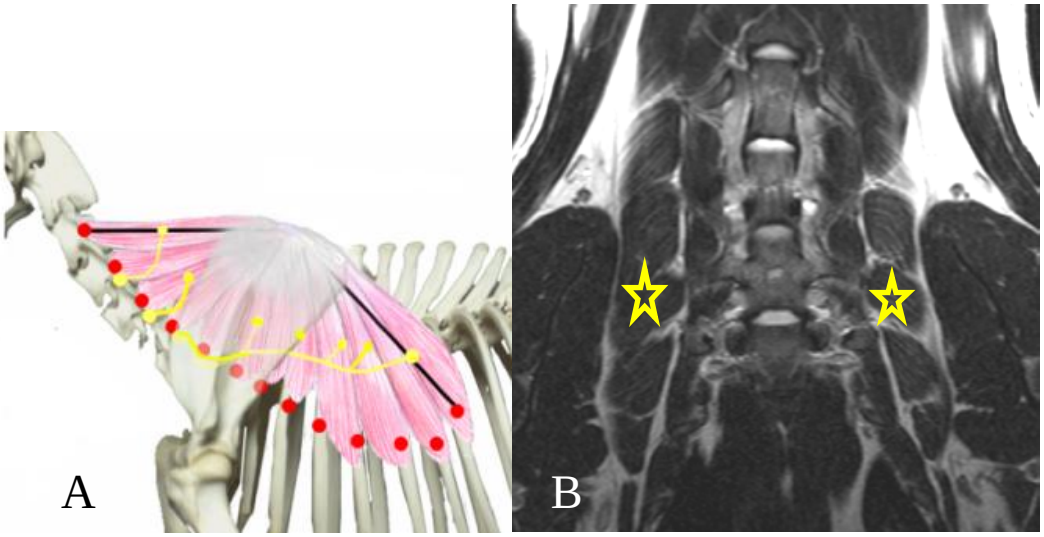

http://www.onlineveteriryatomy.net

Figure 3-1 The serratus ventralis muscle. A - schematic drawing; the yellow lines show the innervation pattern; the red dots - attachment sites; B- T2W dorsal image, the serratus ventralis m. is labeled by stars.

The ***supraspinatus muscle*** is covered by the trapezius cervicis and omotransversarius. It arises from the entire surface of the supraspinous fossa, spine of the scapula and from the edge of the neck of the scapula by numerous tendons. Then it passes around the neck of the scapula and crosses the medial surface of the shoulder joint. It inserts on the greater tubercle of the humerus. The role of this muscle is extension of the shoulder joint and advancement of the limb and lateral support of the shoulder joint.

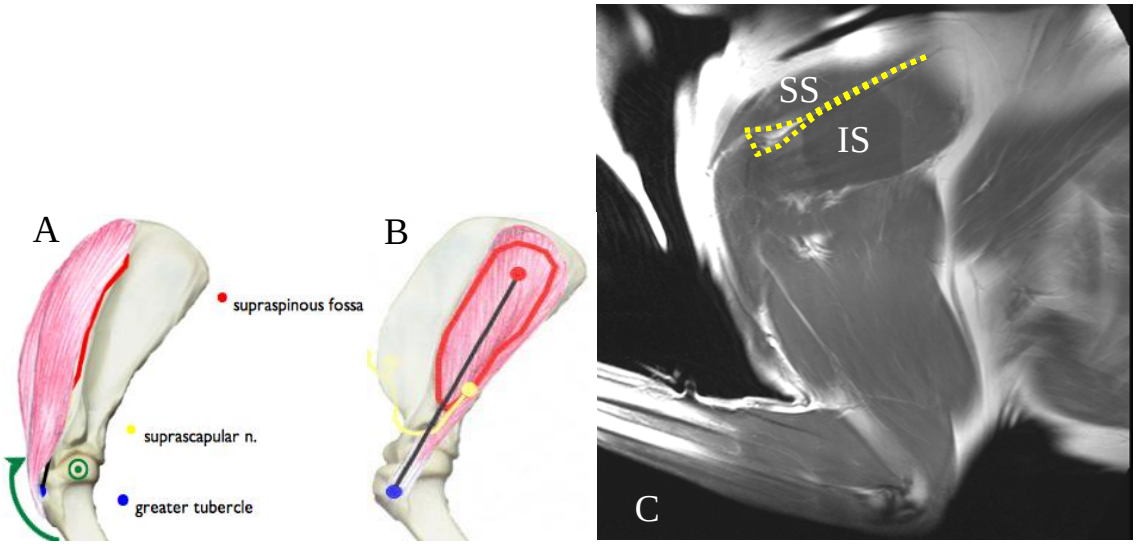

http://www.onlineveteriryatomy.net

Figure 3-2 A schematic drawing: A- The supraspinatus muscle; B-the infraspinatus muscle; the green arrow shows the mode of action – extension of the limb; C – T1W sagittal (parasagittal) image depicting the mm. supraspinatus (SS) and infraspinatus (IS). Dotted line indicates the spine of the scapula.

Th***e infraspinatus muscle*** originates from the infraspinous fossa, the scapular spine, the caudal border of the scapula. It is the lateral rotator and abductor of the humerus and a flexor/extensor of the shoulder joint and provides ideal collateral support to the joint.

The ***subscapularis*** muscle has a complicated system of fasciculi aligned in many different directions. Its origin is in the subscapular fossa, then it curves medially across the shoulder joint and inserts on the lesser tubercle of the humerus. Its function is adduction and extentioin of the shoulder joint and medial rotation of humerus, and provides medial collateral support to the shoulder joint. Innervation comes from nn. subscapularis and axillaris (Evans & de Lahunta, 2012).

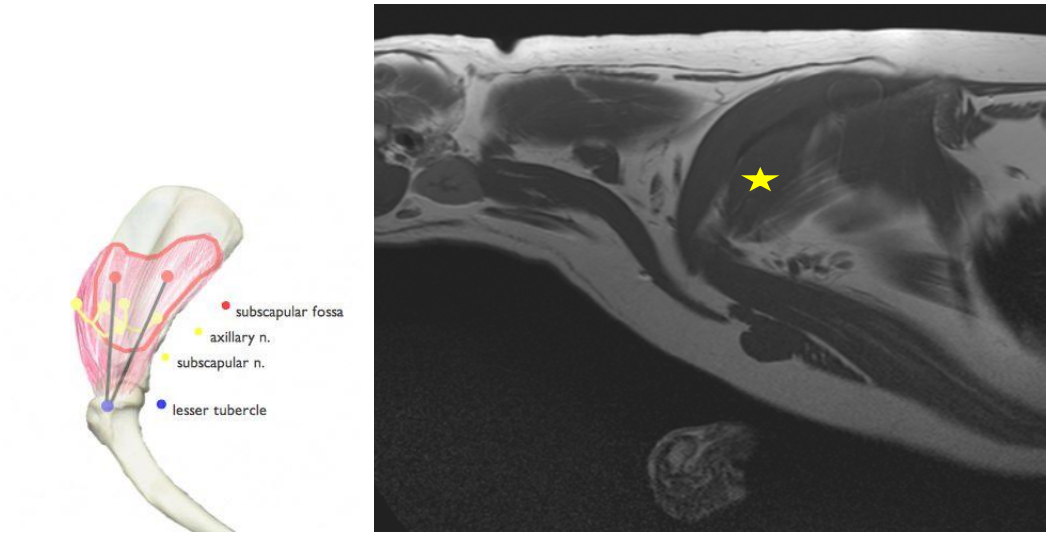

http://www.onlineveterinaryatomy.net

Figure 3-3 A-Schematic drawing and T1W MRI image showing the deltoideus muscle of a dog; yellow line shows innervation by the axillary nerve and subscapular nerve. B-T1W sagittal image: subscapularis muscle is labeled by a star.

The ***rhomboideus*** muscle fans out on the neck and cranial thorax between the median line of the neck and thorax, and the dorsal border of the scapula. The cervical part lies dorsolaterally on the neck from the second or third cervical vertebra to the third thoracic vertebra. It arises on the tendinous median raphe of the neck and the ends of the dorsal spinous processes of the first three thoracic vertebrae. It inserts on the rough medial surface and on the edge of the dorsal border of the scapula, including the scapular cartilage. It elevates the limb and pulls the limb and shoulder cranially or caudally; it draws the scapula against the trunk (Evans & de Lahunta, 2012).

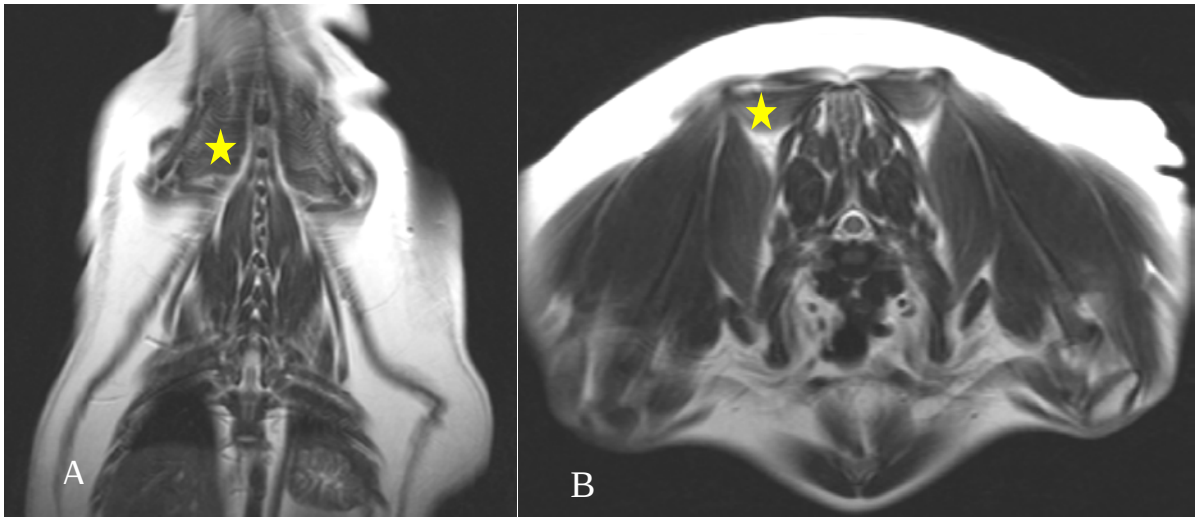

Figure 3-4 T2W dorsal (A) and transverse (B) images demonstrating the rhomboideus muscle (marked by the stars).

The muscle ***trapezius*** is a broad, thin, triangular muscle. It arises from the median fibrous raphe of the neck and the supraspinous ligament of the thora, extending from the third cervical vertebra to the ninth thoracic vertebra. It inserts on the spine of the scapula. It is divided into a cervical and a thoracic portion by a tendinous band extending dorsally from the spine of the scapula. It elevates the limb and draws it cranially ans rotates the scapula.

The ***deltoideus*** muscle has two parts; scapular and acromion. It is an abductor of the humerus and flexor of the shoulder joint. Innervation is provided by the axillary nerve (C7, C8).

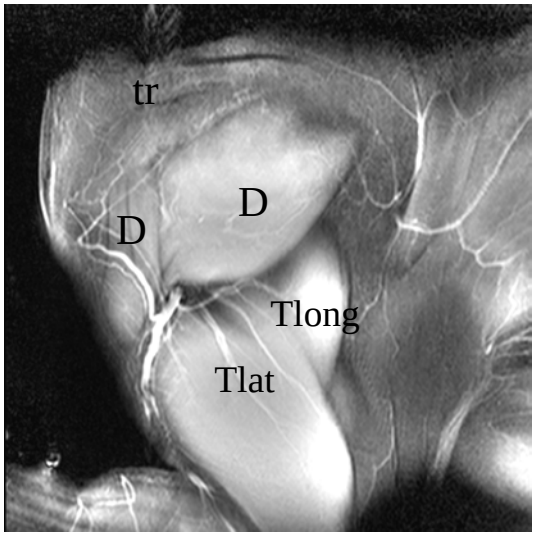

Figure 3-5 T1W parasagittal image shows the muscles: deltoideus(D) and triceps – lateral (Tlat) and long (Tlong); tr – trapezius.

The ***triceps*** muscle has four heads: long, lateral, medial, accessory, inserting on the olecranon tubercle. It extends the elbow joint and is innervated by the radial nerve (C7, C8, T1, T2). The long head arises on the caudal border of the scapula and by tendon on the infraglenoid tuberosity; the lateral head arises as an aponeurosis on the tricipital line between the tuberosity for the teres minor and the deltoid tuberosity. The medial head arises on the crest of the lesser tubercle between the point of insertion of the teres major and that of the muscle coracobrachialis. The accessory head arises from the proximal caudal part of the neck of the humerus, lies on the caudal side of the humerus between the other heads of the triceps muscle and the brachialis muscle (Evans & De Lahunta, 2012).

3.2 Materials and methods

Thirty two dogs with clinical signs attributable to caudal neck/shoulder region pathology were evaluated using a 1.5T magnet system. Of the 32, 13 were found to have no abnormalities, 1 had disc disease, 1 – histiocytic sarcoma, whilst 18 had a presumptive diagnosis of brachial plexus lesion.

Three groups of muscles for anatomy evaluation were selected: 1 - muscles, attaching the thoracic limb to the body wall; 2 - muscles of the medial aspect of proximal thoracic limb; 3 - muscles of the lateral aspect of proximal thoracic limb. Inclusion criteria were

established – detectability of the muscle on at least one MRI plane, bilaterally or unilaterally and readily differentiated from adjacent tissues margins. These groups included muscles: 1- rhomboideus, trapezius, serratus ventralis; 2- subscapularis, triceps; 3- supraspinatus, infraspinatus, deltoideus.

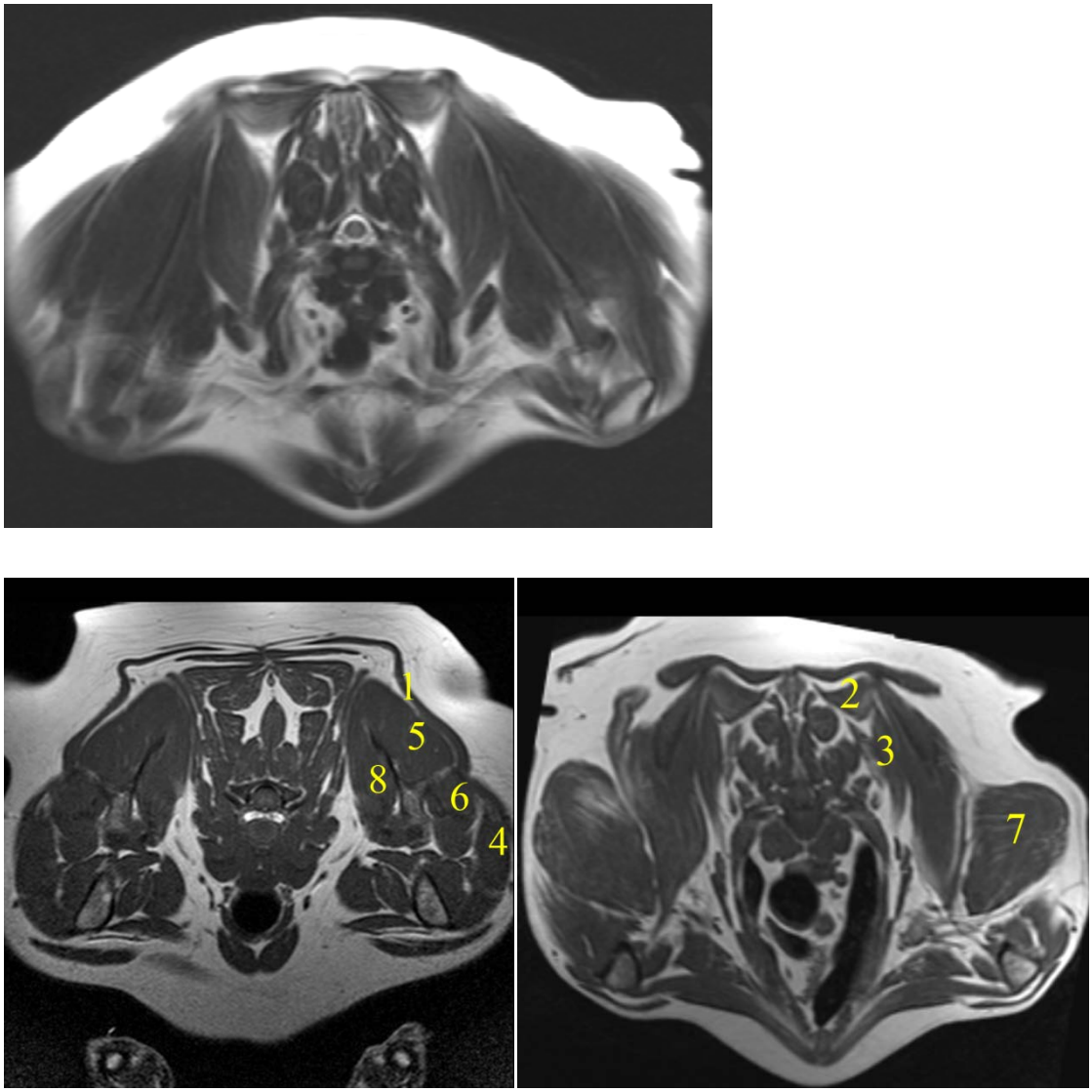

Figure 3-6 Muscles selected for anatomical description: 1- trapezius m, 2- rhomboideus m., 3- the serratus ventralis m, 4 –deltoideus m., 5- supraspinatus m., 6- infraspinatus m., 7 - triceps m., 8- subscapularis m.

For the anatomical study, the T1W sequence transverse plane was the standard cross-section image, and any available sequences in the dorsal plane were used as additional images. The sagittal plane was only used as a reference. The shoulder joint and scapula as bony structures were chosen as rigid identifiable landmarks. Muscles were detected according to their anatomical position in transverse and dorsal planes, and the difference in appearance was recorded.

3.3 Results

3.3.1 **Sequences and planes**

The results are shown in table 3-1.

Case / sequence	Transverse plane				Dorsal plane				Shoulder joint position
	T1	T2	FS	STIR	T1	T2	FS	STIR	
1	1	1	1	NA	NA	1	NA	NA	flexed
2	1	1	1	1	NA	1	1	NA	flexed
3	1	1	1	NA	NA	1	1	NA	flexed
4	1	1	1	1	NA	1	1	1	flexed
5	1	1	1	NA	1	1	NA	1	flexed
6	1	1	1	1	NA	1	NA	NA	flexed
7	1	1	1	NA	NA	NA	1	NA	flexed
8	1	1	NA	NA	NA	1	NA	NA	flexed
9	1	1	1	NA	NA	1	NA	1	extended
10	1	1	NA	1	1	1	NA	NA	extended
11	1	1	NA	NA	NA	NA	NA	1	extended
12	1	1	NA	1	NA	NA	NA	1	extended
13	1	1	NA	NA	NA	1	NA	NA	extended
14	1	1	NA	NA	1	NA	NA	1	extended
15	1	1	NA	NA	1	NA	NA	1	extended
16	1	1	NA	NA	NA	NA	NA	1	extended
17	1	1	NA	NA	1	NA	NA	1	extended
18	1	1	NA	NA	NA	NA	NA	1	flexed
19	1	1	1	1	NA	1	NA	NA	flexed
20	1	1	NA	NA	NA	NA	NA	NA	flexed
21	1	1	NA	NA	NA	NA	NA	NA	flexed
22	1	1	NA	NA	NA	NA	NA	NA	flexed
23	1	1	1	1	NA	1	1	1	flexed
24	NA	1	NA	1	NA	NA	NA	1	flexed
25	1	1	1	NA	NA	1	NA	NA	flexed
26	1	1	1	NA	NA	1	NA	1	flexed
27	1	1	1	1	NA	NA	NA	1	flexed
28	1	1	1	NA	NA	1	1	1	flexed
29	1	1	NA	NA	NA	NA	NA	NA	flexed
30	1	1	NA	NA	NA	NA	NA	NA	flexed
31	1	1	NA	1	NA	NA	NA	1	flexed
32	1	1	1	NA	NA	1	NA	1	flexed
Total	31	32	15	10	5	16	6	17	

Table 3-1 Sequences and planes used for the shoulder area screening in 32 dogs. FS=T1 with fat saturation; STIR=short T1 inversion recovery.

For the transverse images T1W (Figure 3-7A) and T2W (Figure 3-7B) sequences were available in 96.8 and 100% of cases. T1 with fat saturation were available in 46.8% of cases, followed by STIR (Figure 3-7C) in 31.2% of cases. For the dorsal plane STIR was available in 53% cases, T2 – in 50% of cases, while T1W – in just 15.6% and fat saturation – in 18.7% of cases.

Overall, transverse images were acquired in all cases, and dorsal images in 81.2% (26/32).

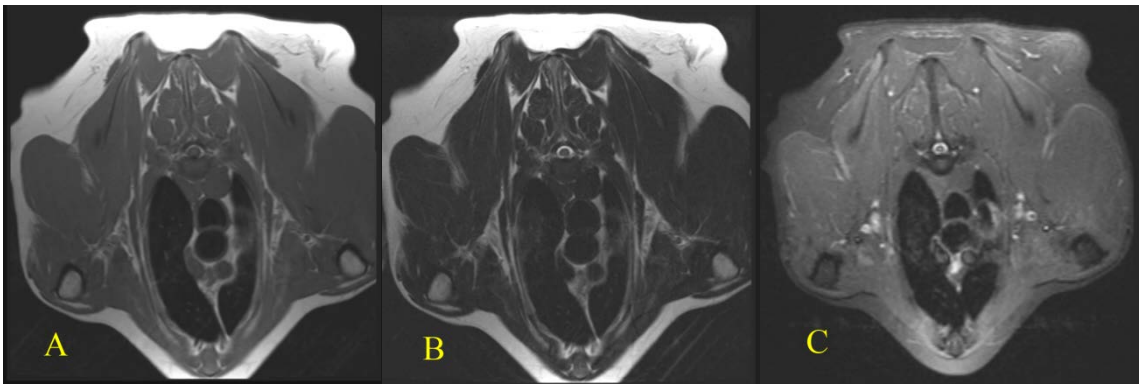

Figure 3-7 Transverse images of the shoulder in A - T1W, B - T2W and C - STIR sequences. All these sequences allow delineation of muscle.

3.3.2 **Planes and positioning**

During MRI examination a dog was typically placed in dorsal recumbency with flexed shoulder joint and limbs laid alongside the body. This positioning provided good access to the intravenous catheter throughout the procedure. However, occaisonally the limbs had to be extended cranially (table 3-1).

Due to the movable thoracic limb at the point of scapular attachment to the body wall and at the shoulder joint, the appearance of a muscle will depend on the angle between the spine of the scapula and the imaging plane. If the angle is close to 90°, the supraspinatus and infraspinatus muscles will be imaged in short axis. On the contrary, if the spine of the scapula is parallel to the plane, the muscles will be shown in long axis.

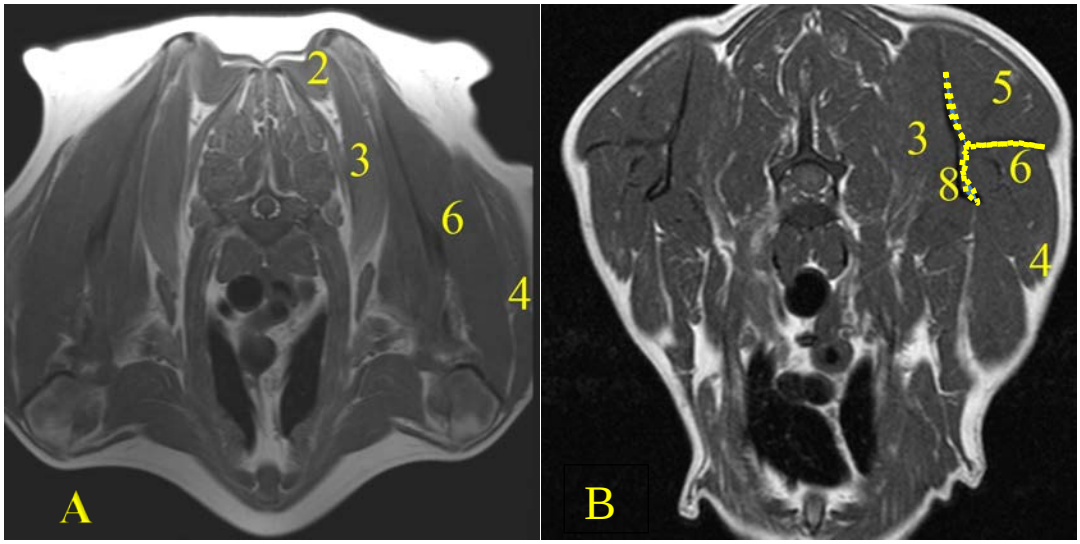

Figure 3-8 The appearance of the shoulder muscles on transverse plane images – with the plane parallel to the spine of the scapula (A) and perpendicular to it (B). In the infraspinatus (6) and supraspinatus (5) muscles are not evident in the same image. The dotted line labels the scapula.

Similar difference in the appearance can be seen on the dorsal plane.

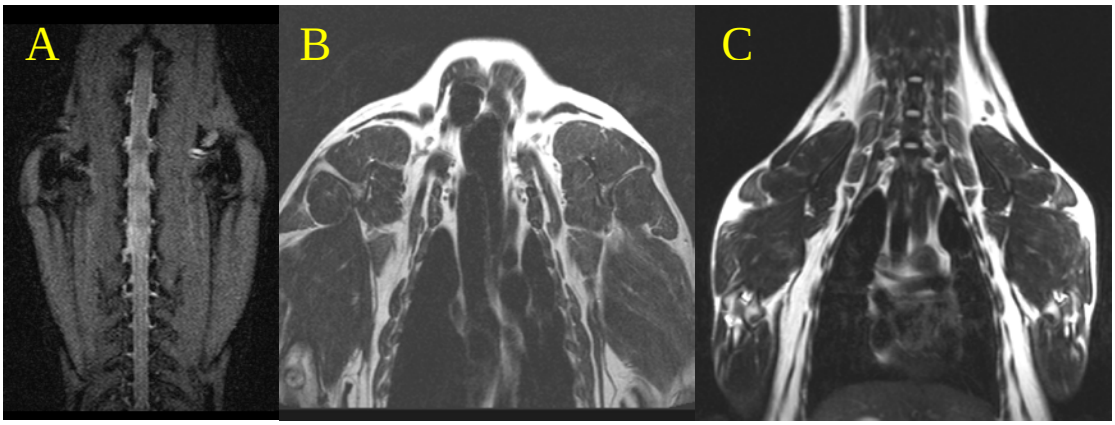

Figure 3-9 Dorsal images on STIR (A) and T2W (B+C) sequences: A - with the imaging plane parallel to the scapula and cranially extended limbs; B and C – plane is perpendicular to the scapula and limbs directed caudally.

These effects can be schematically shown in Figure 3-10.

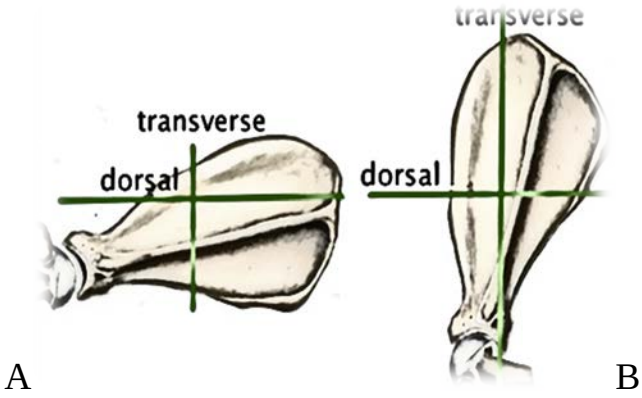

Figure 3-10 Horizontal and vertical lines show the image plane position on dorsal and transverse images in relation to the scapula when the limb is A- extended and B-flexed.

The appearance of triceps muscle depends on the flexion or extension of the shoulder joint and limb position at the time of imaging.

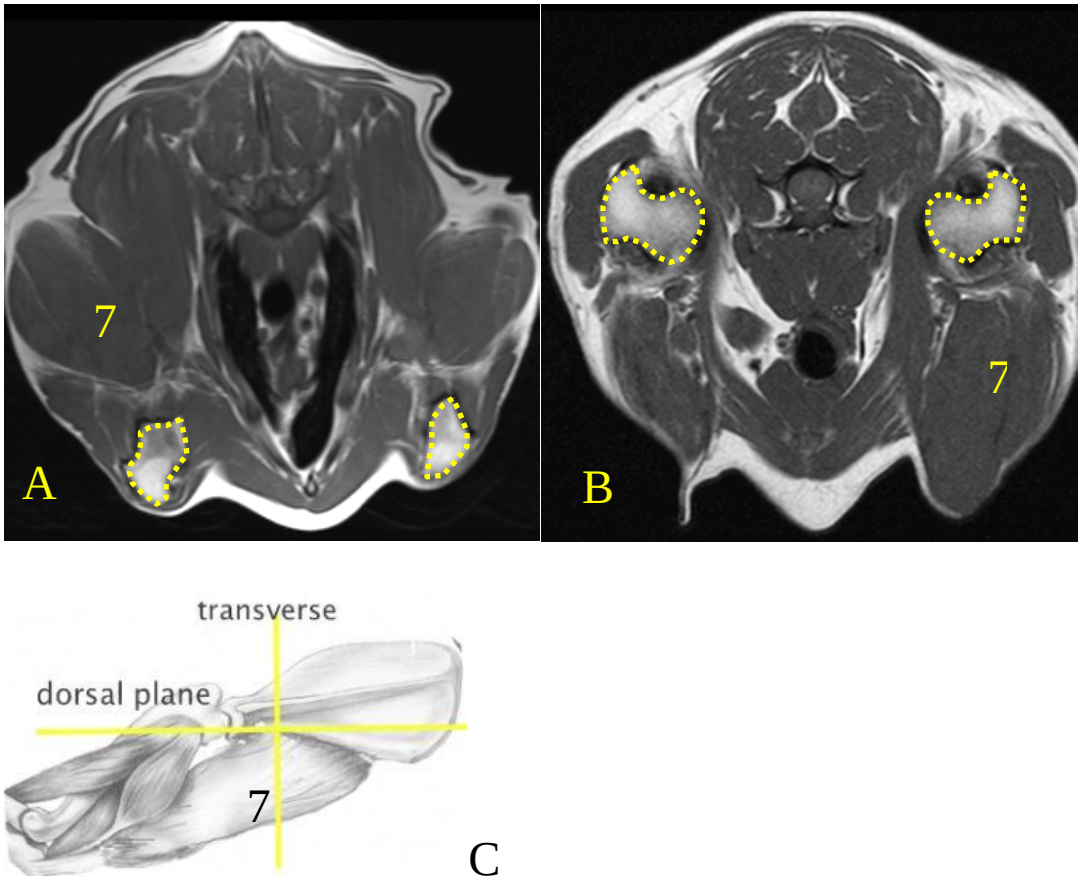

Figure 3-11 Appearance of the triceps muscle (7) on T1W transverse images with the shoulder joint in flexion (A) and extension (B). The dotted lines label bony landmarks – shaft of the humerus. C – represents a schematic position of the MR plane, scapula and the triceps

muscle. Notably, the image B depicts the triceps muscle at the C7 level. In cases with flexed limbs, the triceps muscle is seen at the T1-T3 level. However, on the majority of images the position of the limbs is not clearly visible, and their position relative to each other may differ (as on the Figure 3-11B).

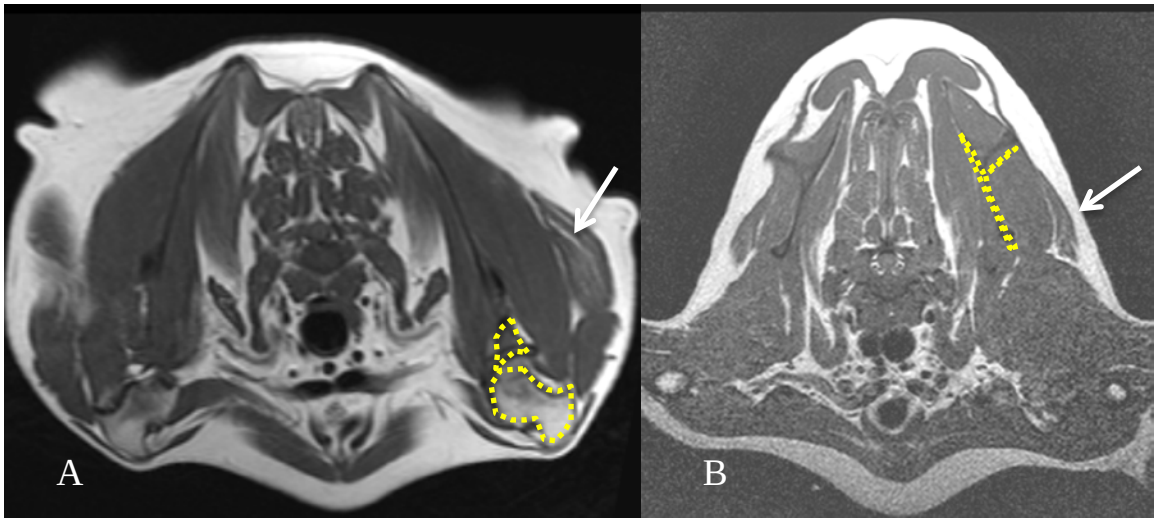

Figure 3-12 The degree of detectability of the deltoideus muscle depends on the scapula and limb position. The arrows indicate the deltoideus muscle, the dotted line – bony landmarks: glenoid cavity (A) and scapula (B).

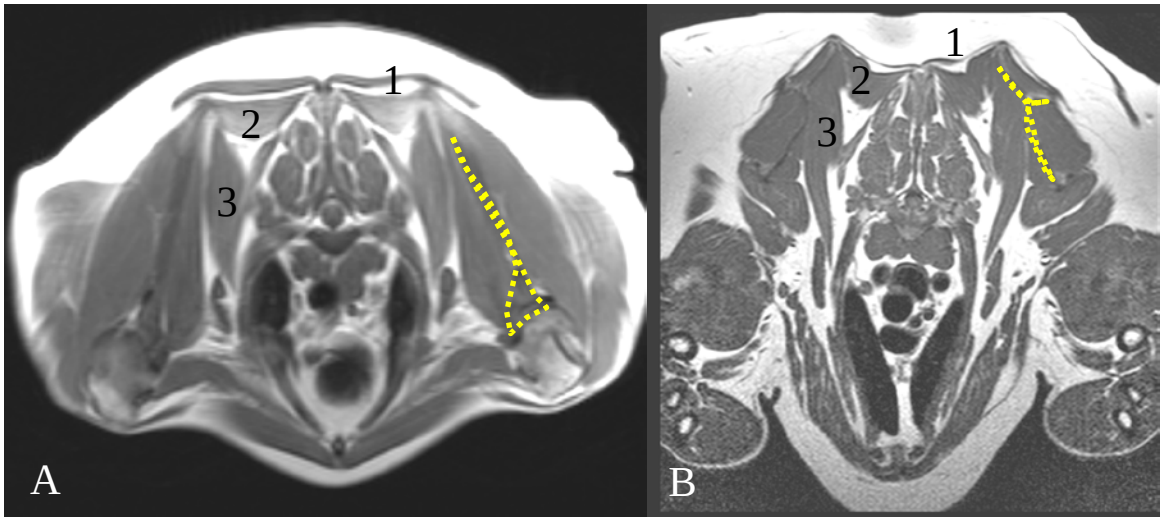

Figure 3-13 The appearance of the trapezius, rhomboideus and serratus ventralis muscle on the transverse plane is least altered by a change of scapula or limb position. A - T1W transverse

image with the imaging plane parallel to the scapula; B - with the imaging plane perpendicular to the scapula. 1 - trapezius, 2 - rhomboideus, 3 - serratus ventralis muscles. Dotted lined – label bony landmarks (scapula).

Muscles	Transverse (n=64;100%) n	%	Dorsal (n=54;100%) n	%
Rhomboideus	58	90.6	NA	NA
Trapezius	60	93.7	30	55
Serratus ventralis	64	100	32	59
Subscapularis	64	100	48	88.8
Supraspinatus	64	100	49	90.7
Infraspinatus	64	100	50	92.6
Deltoideus	47	73.4	37	68.5
Triceps	44	68.7	33	61

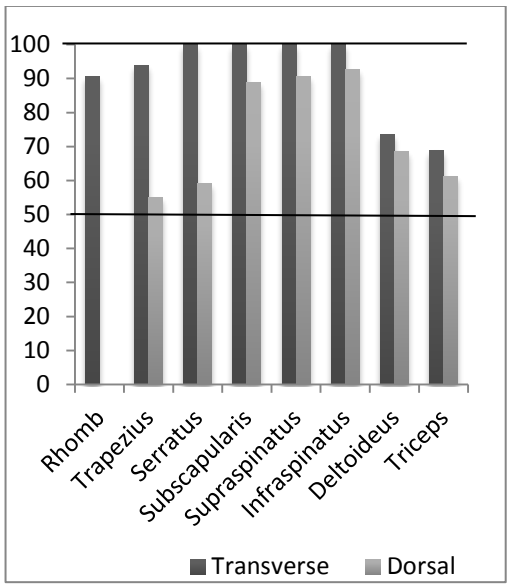

Table 3-2 Muscle detection on transverse and dorsal plane images. The table and graph show that on transverse images the serratus ventralis, subscapularis, supraspinatus and infraspinatus muscles were detected in all cases.

For the location of infraspinatus muscle in cases of parallel to the plane spine of scapula positioning, the sagittal view was necessary as a reference. On the dorsal plane the most detectable muscles were supraspinatus, infraspinatus and subscapularis. Unilaterally on the transverse plane were detected: the deltoideus muscle in 3 cases, the triceps – in two cases; on the dorsal plane – in one case each – the supraspinatus, deltoideus and triceps.

	Muscles detected partially				Muscles not detected			
Muscle	Parallel plane n21 =100% N	%	Perpendicular plane n11=100% N	%	Parallel plane n21=100% N	%	Perpendicular plane n11=100% N	%
Rhombo	1	4.70	1	9.00	1	4.70	2	18.80
Trapezius	3	14.30	3	27.30	0	0	2	18.80
Serratus	1	4.70	1	9.00	0	0	0	0
Subscap	1	4.70	0	0	0	0	0	0
Suprasp	1	4.70	1	9.00	0	0	0	0
Infrasp	1	4.70	2	18.20	0	0	0	0
Deltoideus	4	19.00	1	9.00	3	14.30	6	54.50
Triceps	5	23.80	2	18.20	3	14.30	7	63.30
Average		**10.08**		**14.24**		**11.10**		**38.85**
Overall muscle detection on parallel plane images N 168=100%	**17**	**1.01**			**7**	**0.41**		
Overall muscle detection on perpendicular plane images N 88=100%			**11**	**1.25**			**17**	**1.93**

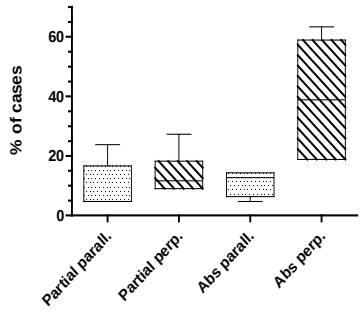

Table 3-3 The table shows the percentage of partially detected (not in full) and completely undetected muscles on the transverse images – 8 muscles on 21 "parallel" image planes and 11 -"perpendicular" image planes in relation to the spine of scapula MR studies.

There were more cases with partial detection of the deltoideus and triceps mm on the parallel plane, while the trapezius and infraspinatus mm were less detectable in full on the perpendicular plane. Overall, on the parallel plane the detectability was better (on average 10.08% of partially detected muscles) than on the perpendicular (14.24%). Totally undetected muscles on the parallel plane were the rhomboideus (4.7%), deltoideus (14.3%) and triceps (14.3%), while on the perpendicular plane rhomboideus

was missing in 18.8%, deltoideus in 54.5%, triceps in 63.3%, and additionally trapezius in 18.8%. On average, the muscles were missing on the parallel plane in 11.1% cases, and in 38.85% cases on the perpendicular. The percentage of completely undetected muscles on “parallel” to the scapula spine plane images was just 0.41% against 1.93% on “perpendicular” to scapula plane images. Overall, this data can illustrate that parallel alignment allows for a better muscles detectability.

3.3.3 **Field of view**

Field of view is very important for muscle detection. It depends on the goal of the study, and usually for transverse and dorsal imaging plane of the shoulder region, it is centered on the spinal cord or the brachial plexus, thus excluding some muscles from the study.

Figure 3-14 T1W (A and B) and T2W(C) transverse images without a full field of view. A and B are centered on the spinal cord, C – on the axilla. A narrow field of view can improve the quality of image, but some peripheral structures could be missed, especially if the animal is large. Most often in such cases the trapezius, rhomboideus, part or all of deltoideus, part of supraspinatus muscles are excluded from the view. The least affected are the more centrally situated serratus ventralis and subscapularis muscles.

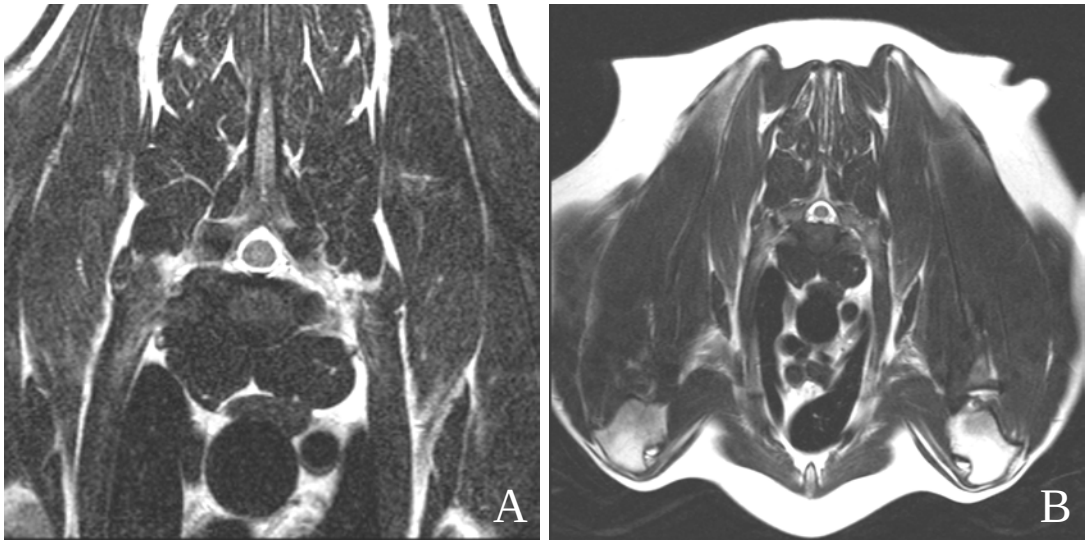

Figure 3-15 Narrow field of view allows for assessment of more muscle detail (A), than a wide one (B).

3.3.4 **Symmetry**

Some degree of limb asymmetry can be observed, and is explained by the difficulty in the imaging of both shoulders and in absolutely symmetrical positioning of the limbs. However, if comparison with the contralateral side is needed, matching images can be found when referenced to immobile landmarks, such as bony structures.

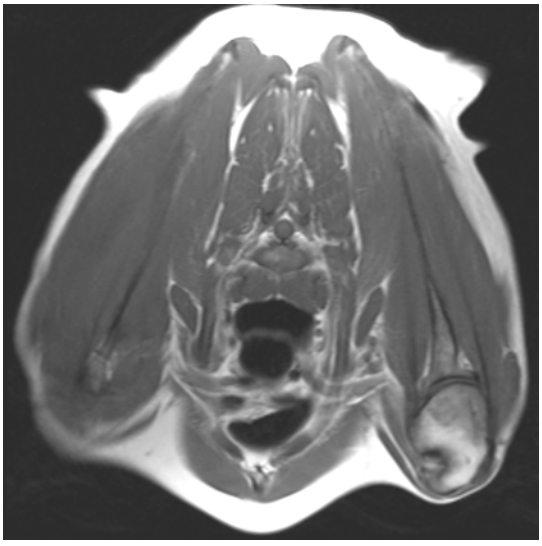

Figure 3-16 T1W transverse image shows discrepancy in limb position.

3.3.5 **Artefacts**

The most common found artefacts were pulsatile flow artifact (13 cases out of 32) due to respiration and blood flow (Fig. 3-17, A) and paramagnetic object e.g. ID chip(13 cases out of 32) (Fig. 3-17, B, C, D). The main effect of these artefacts was the creation of pseudolesions, masking of lesions or image distortion.

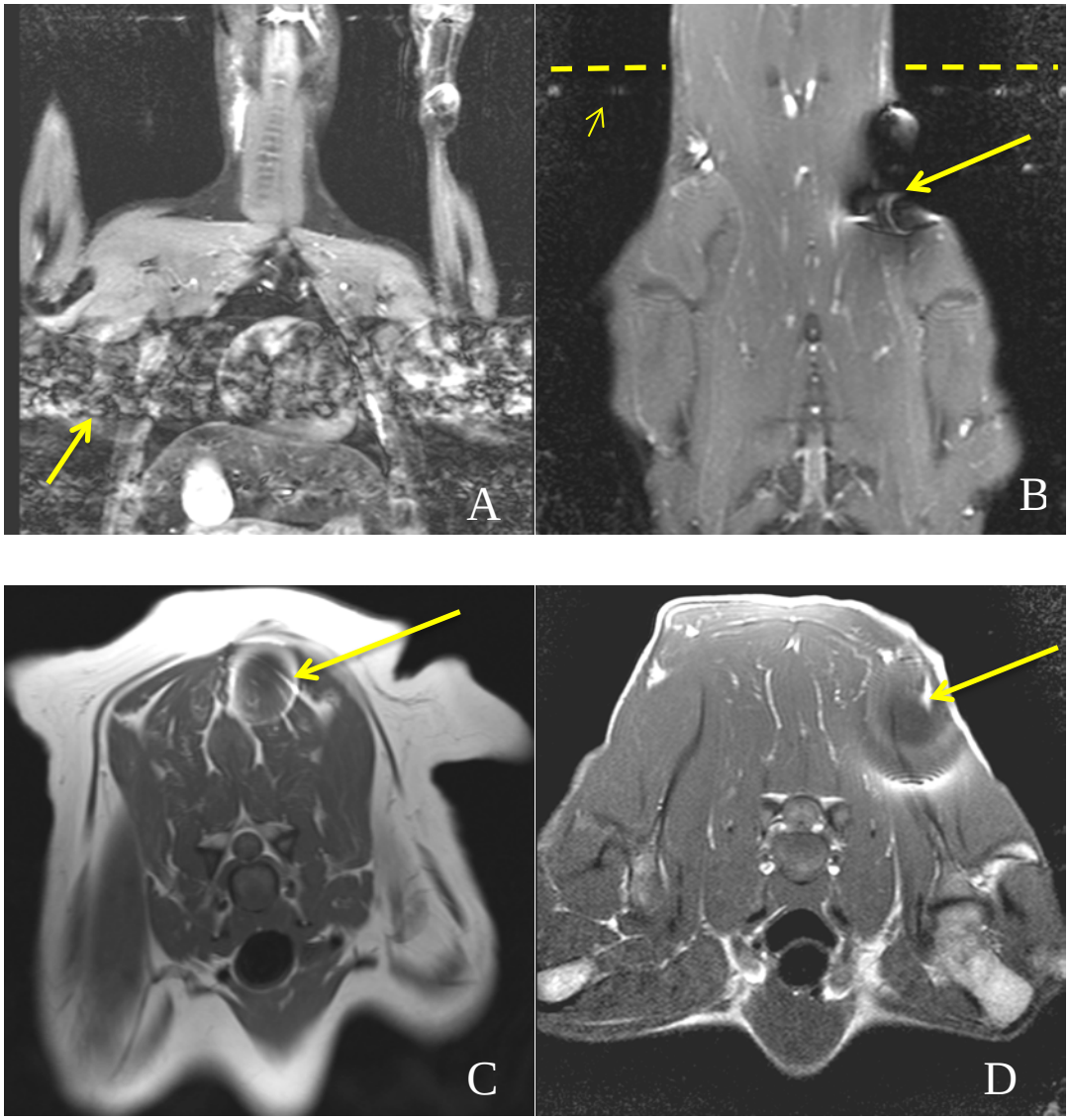

Figure 3-17 Artefacts: A- pulsatile flow artifact; B- ID microchip artifact and zip artifact: ID microchip artifact – C and D.

3.4 Discussion

Imaging methods are of great importance for the diagnosis of a variety of disorders demanding different approaches, as well, for therapy and surgery planning and for the follow up. MR imaging of the canine shoulder requires specific attention, because it is a complex anatomical structure with numerous soft tissue stabilising components (Schaefer & Forrest, 2006). For this reason consistent planning is very important. Agnello et al (2008) have proposed the MRI protocol for the humeroglenoid joint imaging. For imaging of the brachial plexus Kraft et al (2007) proposed the following planning – dorsal recumbency, symmetrical limbs, non-oblique body positioning, and both large and narrow field of view; and it was suggested by Platt et al (1999) to centre the field of view on the affected limb.

3.4.1 **Sequences**

In this study transverse and dorsal images of 32 dogs were used to analyse the detectability of the rhomboideus, trapezius, serratus ventralis; subscapularis, triceps; supraspinatus, infraspinatus and deltoideus muscles. These muscles can be divided into two functional groups – the muscles attaching the scapula to the body wall and the muscles of the proximal thoracic limb. The inclusion criterian was detectability on at least one plane with readily definable margins. It was found that for the transverse planes T1W and T2W sequences were used in 96.8 and 100% of cases. T1 with fat saturation was used in 46.8%, followed by STIR – 31.2% cases. For the dorsal plane STIR was used in 53% cases, T2W – in 50% of cases, while T1W – in just 15.6% and fat saturation – in 18.7% of cases. The best detectability was provided by the T2W and T1W sequences.

3.4.2 **Planes and positioning**

It was apparent that the appearance of a muscle depended on the angle between the spine of the scapula and the MR plane. If the angle is close to 90°, supraspinatus and infraspinatus muscles will be seen perpendicular to their fibers and inside their correspondent fossae. This may allow visualization of both muscles on one image. On the contrary, if the spine of the scapula is parallel to the imaging plane, the muscles will

be shown along their fibers, and in order to differentiate between supraspinatus and infraspinatus muscle a sagittal view is needed for reference.

Limb position also influenced muscles that can be seen on the image. Comparing these two types of limb positions in the transverse plane, it is clear that parallel plane positioning provides detectability of more muscles than the perpendicular plane. In 63.3% of cases the triceps muscle was not detected on the perpendicular images, while only in 18.2% of cases with parallel plane images was it not detectable. It was found that limb cranial protraction created different appearances of the images, which were occasionally very informative, especially for the triceps muscle (as it was found in one case), but may require many more images to perform in order to visualise the whole area, including the shoulder joint and axilla.

It was found that the transverse plane can provide better detectability for all muscles. The choice of sequence may also influence the frequency of artefacts, with the dorsal plane particularly affected by zip and motion artifacts across the cranial thorax, and caused by movement or blood flow. The rhomboideus muscle was difficult to identify accurately. Nevertheless, the dorsal plane may be highly informative. This can be especially true when combination with transverse plane images aligned parallel to the scapula, because, naturally in this case, the dorsal plane will become perpendicular and allow a contrasting view.

3.4.3 **Field of view.**

Field of view influenced whether a muscle could be identified on the image and if it could be visualised in full. It can depend on the goal of the study, and usually for the transverse and dorsal imaging plane of the shoulder region, it is centered on the spinal cord or the brachial plexus. Both wide and narrow planes have their advantages, and ideally would give more information if performed concurrently.

3.4.4 **Symmetry**

Symmetrical limb positioning is important in order to see any differences between the contralateral sides, though ideal symmetry might be difficult to achieve.

3.4.5 **Artifacts.**

The most common artifacts were found to be ID microchip artifact, zip and pulsatile flow. The significance of these corresponds to pseudolesion creation or masking and image distortion.

3.4.6 **Conclusion.**

In conclusion, the following addition to the protocol proposed by Kraft et al (2007) could be suggested:

1. Sequences for the shoulder muscles MRI – T2W; T1W; STIR as the basic sequences, followed by FatSat and contrast imaging where appropriate.
2. Planes: transverse plane with the limbs aligned along the body and parallel to each other; and dorsal plane.
3. Concurrent use of a wider field of view and a narrow one centered on the lesion.

4 Magnetic resonance imaging of the proximal thoracic limb muscles in dogs with brachial plexus mass lesions

4.1 Introduction

The brachial plexus is the complex network of nerves that supplies motor, sensory, and sympathetic innervation to the thoracic limb. The anatomical delineation of the human brachial plexus includes 5th cervical (C5) to 1st thoracic (T1) nerve roots, while in dogs there are contributions from 6th cervical (C6) to 2nd thoracic (T2) roots, which form three trunks, six divisions, three cords, and five main motor/sensory branches (Figure 4-1). In humans, variations in the relationship between roots, trunks, and muscles are believed to be more the rule than the exception (Orebaugh & Williams, 2009). The anatomical variations in the brachial plexus anatomy in humans and small animals have clinical significance for surgeons, radiologists, anaesthetists, neurosurgeons and neurologists from a diagnostic and therapeutic point of view (Chaudhary et al., 2012). One example of a situation where this variation may be important is following local anaesthesia of peripheral nerves for surgery of the distal aspect of the thoracic limb, with persistent neurological deficits reported following intraneural injection in man (Jeng & Rosenblatt, 2011) and in the dog (Hofmeister et al., 2007; Trumpatori et al., 2010).

Typically in man, the formation of the brachial plexus begins just distal to the scaleneus muscles (Johnson et al., 2010), but may lie more cranially or caudally. Another common variation is the contribution to the brachial plexus from 4th cervical (C4) and T2 roots (Johnson et al., 2010). In dogs reported variations include a contributing branch of the fifth cervical and lack of the first and second thoracic nerves (Evans & De Lahunta, 2012). However, no significant variations in the branching patterns were found in beagle dogs when the following nerves were examined: the suprascapular, subscapular, radial, cranial pectoral, axillary, caudal pectoral, ulnar and median (Nakamura et al., 2004).

The general approach to the anatomical assessment of the brachial plexus consists of topographical evaluation of different structures, including the glenoid cavity, axillary artery and muscles (McFarland et al., 2001). Topographical studies in humans suggest that there is a strong association between segmental variation of the axillary artery and variation of the brachial plexus (Yang et al., 2009). The relationship between the nerves and muscles is also influenced by the location or shape of the muscles, with abnormal

position of the subscapular muscle a predisposing factory for the development of nerve entrapment (Breisch, 1986).

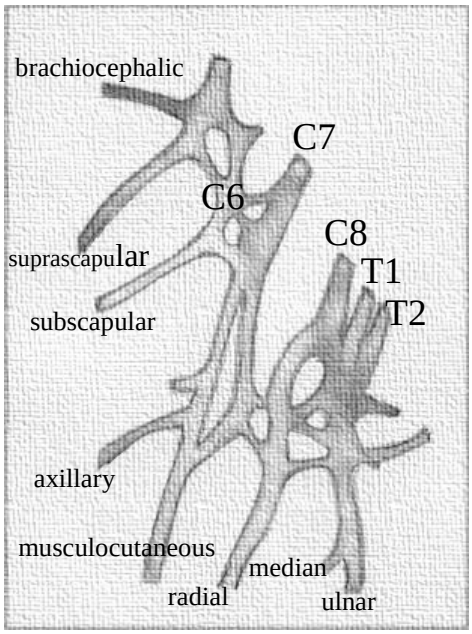

Figure 4-1 Schematic representation of the anatomy of the brachial plexus of a dog demonstrating the nerve roots C6 to T2 contributing to the cords from which the peripheral nerves arise.

There are three cords in the canine brachial plexus. These cords lie as intermediate nerve trunks between the ventral branches of the spinal nerves that form the plexus and the named nerves that innervate structures of the limb (Evans & de Lahunta, 2012).

ROOTS	NERVE	MUSCLES INNERVATED
C5,6	Brachiocephalic	Cleidobrachialis
C6,7	Subscapular	Subscapularis
C5,6,7	Suprascapular	Supraspinatus Infraspinatus
C6,7,8	Axillary	Deltoideus, Teres major, Teres major, Sub-scapularis
C7,8,T1,T2	Radial	Triceps, Extensors of the elbow, carpus and digits
C7	Musculocutaneous	Biceps brachii, Coracobrachialis, Brachialis, Sup. Pectoral
C8,T1, T2	Median	Pronator teres, Quadratus, Carpal and digital flexors
C8,T1, T3	Ulnar	Carpal and digital flexors
C7	Long thoracic	Serratus ventralis
C7,T1	Thoracodorsal	Latissimus dorsi
C8,T1	Lateral thoracic	Cutaneous trunci
C8,T1, T2	Caudal pectoral	Deep pectoral

Table 4-1 Nerve roots giving rise to specific peripheral nerves of the brachial plexus and the muscles innervated by them.

4.1.1 Peripheral Nerves of the Brachial Plexus

The brachial plexus gives rise to a number of peripheral nerves. These can be categorised in a variety of ways, they are approached from cranial to caudal in this text.

The brachiocephalic nerve is derived mainly from C6, with a possible contribution from C5 nerve. It forms two small branches that enter the brachiocephalic muscle. A branch of the brachiocephalic nerve joins C7 nerve to form the suprascapular nerve. The suprascapular nerve (C5, C6, C7) travels between the supraspinatus and infraspinatus muscles, providing innervation to these two muscles. The musculocutaneous nerve (C7) provides sensory innervation to the craniomedial aspect of the antebrachium and motor innervation to the coracobrachialis, biceps brachii and brachialis muscles. The subscapular nerve arises from C6-C7 and innervates the subscapular muscle. It can be single or double. The axillary nerve is formed by C6-C7-C8, passes caudal to the shoulder joint to reach the lateral aspect of the limb. It innervates the teres major, teres minor, deltoideus muscles and part of' the subscapular muscle. The radial nerve (C7, C8, T1, T2) innervates the triceps muscle, and the carpal and digital extensors (extensor carpi radialis, common and long digital extensors and extensor carpi ulnaris). The radial nerve branches enter the triceps muscle distal to the shoulder joint, then continues deep to the biceps muscle and the medial head of the triceps muscle, spirals around the disto-caudal part of humerus and turns to the

lateral aspect of the brachium between the muscle brachialis and lateral head of triceps muscle. The median nerve (C8, T1, T2) innervates the flexors of the carpus and digits (flexor carpi radialis and superficial and deep digital flexors). It travels along the medial side of the limb. The ulnar nerve (C8, T1, T2) provides sensory innervation to the caudal aspect of the elbow joint capsule and caudolateral aspect of the antebrachium and motor innervation to the flexors of the carpus and digits (flexor carpi ulnaris and deep digital flexor) (Lemke & Creighton, 2008). The ulnar nerve is united with the median nerve before deviating towards the olecranon to cross the caudal aspect of elbow joint. The dorsal thoracic nerve arises primarily from the eighth cervical spinal nerve and supplies the latissimus dorsi muscle. The lateral thoracic nerve, originating from spinal cord segments C8–T1, supplies motor innervation to the cutaneous trunci muscle. The long thoracic nerve innervates the serratus ventralis muscle. The long thoracic nerve arises from C7, and is formed before the brachial plexus (Sharp & Wheeler, 2005; de Lahunta & Evans, 2010; Platt & Garosi, 2012; Evans & de Lahunta, 2012).

The axillary artery and vein are the only major vessels located in the axillary space (Mahler & Adogwa, 2008). The vertebral artery runs medial to the ventral branches of C6-8 as they emerge from their respective intervertebral foramina. The costocervical artery runs next to the ventral branch of T1 as it emerges from the intervertebral foramen and wraps around the medial surface of the first rib. The vertebral ganglion is located within the thoracic inlet near the origin of the vertebral artery and provides most, if not all, of the postganglionic sympathetic innervation to the heart (Evans & de Lahunta, 2012).

4.1.2 Brachial plexopathies

Brachial plexopathies are considered either traumatic or non-traumatic in origin, with trauma accounting for about 50% of cases in man, and frequently result from road traffic accidents (Sureka et al., 2009). Non-traumatic pathologies include radiation fibrosis, chronic inflammatory demyelinating polyneuropathy, brachial neuritis (as a result of soft tissue inflammation), neurogenic tumours and metastatic tumours. The brachial plexus can be affected in cases of breast cancer, because one of the major lymphatic drainage routes is through the apex of the axilla (Hyodoh & Akiba, 2002). Hypertrophic neuritis is a tumour-like chronic inflammatory process, which may be focal or multifocal and is mainly a demyelinating neuropathy (Stumpo et al., 1999). The underlying cause of brachial plexus neuritis is often not determined, but may be associated with viral or bacterial infection and vaccination (Sureka et al., 2009).

In man scapula wing appearance (winging) was reported in cases with spinal accessory nerve damage (trapezius palsy), dorsal scapular nerve damage (rhomboideus palsy), long thoracic nerve damage (serratus ventralis palsy) (Martin & Fish, 2008; Meininger et al., 2011).

In dogs traumatic injuries to the forelimb often cause damage to multiple nerves of the brachial plexus, most often to the radial nerve, although caudal-, cranial- and complete-brachial plexus avulsions are possible. Similar to human patients, brachial plexus avulsion in dogs is often the result of road traffic accidents (Wheeler & Wright, 1986). Inflammatory conditions include such entities as idiopathic neuropathy (Cummings et al., 1973) and hypertrophic neuritis (Ródenas et al., 2013). Cases of neuritis following foreign body penetration with a chronic granulomatous and fibrosing steatitis, perineuritis and neuritis with Wallerian-like degeneration have been described (Walmsley et al., 2009).

Diagnosis of shoulder neuropathy is challenging in man and in veterinary patients due to the frequently non-specific clinical signs. One of the more common of these in human patients, suprascapular neuropathy, may be related to primary nerve lesion (stretching into a fibrous or osteofibrous space), due to extrinsic compression, or damage secondary to scapula fracture or humeral head dislocation (Blum et al., 2013). Diagnosis is based on the pattern of muscle denervation on electromyography (EMG) and MRI (Blum et al., 2013).

4.1.3 Peripheral nerve sheath tumours

The term malignant peripheral nerve sheath tumour (MPNST) was proposed by the World Health Organization to replace previous terminology, such as “malignant schwannoma,” “malignant neurilemmoma,” “neurogenic sarcoma,” and “neurofibrosarcoma”. It includes any malignant tumour arising from a peripheral nerve or its attendant sheath, excluding epineurium or the vasculature of peripheral nerves (Gupta & Maniker, 2007; Vilanova et al., 2007). These tumours are reported to range in appearance from tumours with features of a neurofibroma to those of a fibrosarcoma (Weiss & Goldblum, 2001); hence, the diagnosis of MPNST lacks specific morphological, immunohistochemcial or molecular features (Rodriguez et al., 2012). In man four types of neurogenic tumours of the brachial plexus are identified: benign schwannoma; neurofibroma, associated with neurofibromatosis type I; benign hybrid tumours and malignant peripheral nerve sheath tumour (MPNST) (Es et al., 2010).

In veterinary medicine, the variable histological appearance and interspecies differences, on the one hand, and similarity in biological behaviour, on the other hand, have led to a generic grouping within the nerve sheath tumour category (Simpson et al., 1999; Bagley, 2010). Most tumours of peripheral nerves, excluding sympathetic ones, result from neoplastic transformation of periaxonal Schwann cells, from endo- or epineurally located fibroblasts within the nerve sheath (Withrow & Vail, 2007), from connective tissue elements associated with the peripheral nerve, or from the axon and cell body (Bagley, 2010).

In contrast to man, canine peripheral nerve sheath tumours are predominantly malignant (Kraft et al., 2007). For the diagnosis of malignant peripheral nerve sheath tumour, one of the following criteria must be met: (1) arises from a peripheral nerve; (2) arises from a pre-existing benign or other malignant peripheral nerve sheath tumour; (3) displays histological features of Schwann cell or perineural cell differentiation by immunohistochemistry or electron microscopy. They occur in or near the nerve trunk, recur locally and spread haematogenously, with the lungs being the most common site for metastatic deposition in man (Huang et al., 2003). Malignant PNST in dogs display aggressive behaviour to intratumoral tissue, with extensive necrotic areas and cellular pleomorphism (Tavasoly et al., 2013).

Histologic criteria for MPNST were defined as spindle cell tumours intimately associated with a peripheral nerve and its perineureum, with or without Antoni bodies A or B (Kraft et al., 2007).

The shapes of neurogenic tumours have been described macroscopically and by imaging techniques in man and animals:

1- Fusiform thickening of one or more nerve trunks is caused by the tumour entering and exiting the nerve. The tumour frequently spreads proximally and distally along the nerve. Detection of the nerve entering and exiting a mass has been suggested as diagnostic of a neurogenic neoplasm (Murphey et al., 1999).
2- Plexiform neurofibromas represent diffuse involvement of a long nerve segment with tortuous expansion and gross appearance as a”bag of worms”.
3- Dumbbell shape in the paraspinal area with the extention into neural foramina (Lin & Martel, 2001).
4- Globoid mass (Sharp & Wheeler, 2005).
5- A tubular mass has been described using ultrasound (Rose et al., 2005).
6- Diffuse and mass variations on MR images (Kraft et al., 2007).

Peripheral nerve tumours in dogs are found in the extremities (Brehm et al., 1995); in the diaphragm (Patterson & Perry, 2008); in the thorax being derived from the cells of the nerve sheath or from the ganglionic cells or paraganglionic cells of the autonomic nervous system (Essman et al., 2002; Woo et al., 2008); extradurally within the vertebral canal and without external extension through the foramen (Oliveira et al., 2013); in the spinal nerve roots (Olegário et al., 2012) and which can extend into the vertebral canal through the intervertebral foramen (DeLahunta & Glass, 2009); in the spleen (Bergmann, et al., 2009); in the liver (Park et al., 2011); in the eye (Sato et al., 2005); in the trigeminal nerve (Saunders et al., 1998); subcutaneously (Sawamoto et al., 1999); in the skin, tongue and large intestine (Schoniger & Summers, 2009).

Despite such widespread occurrence, the most common location for peripheral nerve sheath tumours in dogs is the brachial plexus or associated nerves (Simpson et al., 1999).

4.1.4 Brachial plexus tumours in dogs

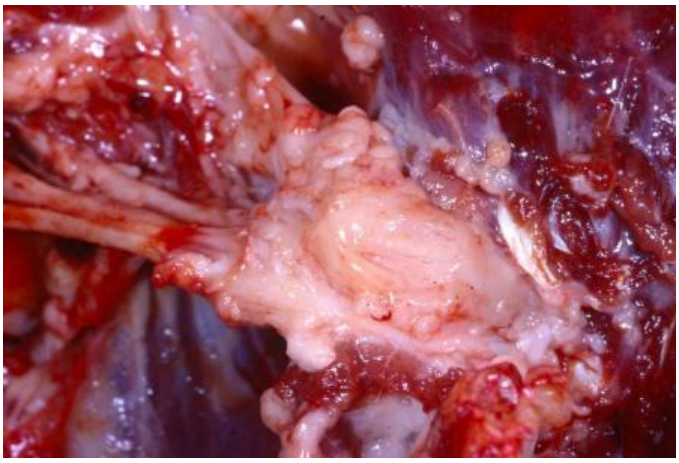

Figure 4-2 Gross pathological specimen of a brachial plexus tumour. (http://ocw.tufts.edu/Content/72/imagegallery/1362320/1369021/1378360)

In addition to neurogenic tumours (schwannoma, neurofibroma, etc.), the brachial plexus can be affected by other soft tissue tumours, for example lymphoma and bone neoplasia (Lorenz et al., 2011), as well as being a site of metastatic spread (Naude & Miller, 2006).

One classification system divided neurogenic tumours according to their anatomical localisation into three groups: tumors involving nerves distal to the brachial or lumbosacral plexus (Peripheral Group), tumours involving nerves of the brachial or lumbosacral plexus (Plexus Group), and tumors involving the vertebral canal (Root Group) (Brehm et al.,

1995). In a study assessing 51 dogs with both brachial and lumbar plexus tumours, 29 dogs (56.8%) belonged to the proximal group and 18 (35.3%) belonged to the peripheral group, with C7, C8 and T1 roots affected most frequently (Chevoir et al., 2012). It has been noted that during tumour growth there is a tendency for multiple nerve involvement (Anor, 2004). C6-T2 spinal cord segment lesions, and damage to the associated peripheral nerves, produce lower motor neuron signs in the affected thoracic limb, accompanied by loss of muscle tone and neurogenic muscle atrophy (Lorenz et al., 2011).

Author	No	Diagnosis	Tumour shape	Muscle atrophy	Clinical Signs
Naude & Miller, 2006	1	C4-6 chemodectoma MTS		Deltoideus, infraspinatus, supraspinatus	Progressive 3week lameness Neck pain Neurological deficits inconclusive
Da Costa et al., 2008	4	MPNST		Over scapula & humerus	Progressive lameness 2-8 month duration Flexor reflex ↓
Kim et al.,2003	1	MPNST C6, C7		Over shoulder	Monoparesis progressing to tetraparesis, LMN deficits, 2 month duration
Chevoir et al., 2012	40	PNST		33 dogs: 29 dogs: ext.carpi rad,triceps 26 dogs: flexor carpi 22 dogs: flexor digitorum 12 dogs: epaxial muscles	Lameness 12 dogs, hyperesthesia 14 dogs, cutaneous trunci reflex loss 9 dogs, neurological deficits
Platt et al, 1999	1	PNST Radial nerve	Fusiform on MRI postcontrast	Diffuse	Progressive lameness of 2 months duration Reduction of the extensor carpi and withdrawal reflexes
Rose et al, 2005	5	PNST C6-C7	Tubular US	Extensive	Progressive lameness, Horner's syndrome, conscious proprioceptive deficits
		PNST axilla	Tubular US		Lameness, triceps withdrawal
		PNST axilla	Tortuous US		Lameness
		Rabdomyiosarcoma involving BP	Mass US	Evident	Lameness, pain
		PNST C6,7, 8, T1, axilla	Tubular US branching infiltrative	Evident	Lameness Conscious proprioceptive deficits
Rudich et al, 2004	24	PNST Schwannomas Sarcomas Myxosarcoma Neurofibrosarcoma	Linear along the nerve root-CT	Scapular area and limb - 83% of dogs	Progressive lameness 5 dogs – neck pain Concurrent disease: elbow osteochondrosis, biceps tendonitis, ulnar carpal fracture
Simpson et al, 1999	1	PNST	Bulbous mass	Infraspinatus, supraspinatus,	Lameness of 2 months duration

cont

		C5-6, C6-7, Roots, axilla		deltoideus, triceps, antebrachial, biceps	Neck pain
Ferreira et al, 2005	1	Lung carcinoma apical lobe of the left lung thoracic inlet		Over the scapula and humerus.	Lameness of 2 months duration No neurological deficits Horner's syndrome Cutaneous trunci reflex loss
Kraft et al, 2007	18	PNST	8/18 - smooth or nodular, diffuse linear nerve thickening;	Muscular atrophy 18/18	18/18 intermittent or progressive forelimb lameness, monoparesis
					9/18 pain upon axillary palpation
					4/18 cervical pain
			6/8 - vertebral canal involvement;		13/18 lower motor neuron signs 5/13 hemiparetic 5/18 Horner's syndrome
			10/18 - nodular mass in axilla		
Walmsley et al., 2009	1	Foreign body neuritis	Not mass lesion: MRI: not conclusive Histology: multiple roots thickening; chronic granulomatous and fibrosing steatitis, perineuritis, neuritis, Wallerian degeneration	Spinatus	Lameness Reduced withdrawal Partial Horner's syndrome
Wheeler et al., 1986	15	Brachial plexus avulsion	No mass lesion	10/11 - atrophy of muscles not innervated by the radial n (spinatus)	8/11 cutaneous trunci reflex loss 6/11 Horner's syndrome
	6	Neurofibrosarcoma		Muscle atrophy: muscles not considered appreciably atrophied on clinical examination.	Chronic lameness, sensory loss, cutaneous trunci reflex loss or Horner's syndrome, pain on palpation and manipulation of the limb

Table 4-2 Literature overview of dogs with thoracic limb monoparesis.

The most consistently reported clinical sign in dogs with brachial plexus tumours was slow progressive chronic lameness (80% of cases reported by Chevoir et al. (2012), 100% cases reported by Kraft et al., (2007) and muscle atrophy, which can be localised, generalised or unevenly distributed over the limb (Platt et al., 1999; Costa et al., 2008). If the tumour originated in a peripheral nerve, the clinical signs were usually limited to chronic intermittent or progressive forelimb lameness, and initially diagnosed as an orthopaedic or musculoskeletal problem (Rose et al., 2005; Kraft et al., 2007; Bagley, 2010). Moreover, a concurrent musculoskeletal or orthopaedic problem can complicate the diagnosis (Bagley, 2010).

Muscle atrophy can be severe or subtle, and may not be evident during clinical assessment alone. Furthermore, atrophy can be detected in muscles other than those expected (Wheeler & Wright., 1986). However, the pattern of muscle involvement should match the distribution of the peripheral nerves (Bredella et al., 1999).

Unilateral muscle atrophy has been considered one of the most characteristic features of nerve sheath tumours (Platt et al., 1999; Da Costa et al., 2008). However, it also occurs in a variety of other conditions, such as foreign body, hypertrophic neuritis and brachial plexus trauma. These conditions require a dramatically different approach, hence severe muscle atrophy and monoparesis without an obvious orthopaedic reason should prompt on MRI or CT examination (Rudich et al., 2004).

Progressive growth of a tumour may result in invasion of the spinal canal and development of upper motor neuron deficits in the ipsilateral hindlimb and ipsilateral Horner's syndrome (Rose et al., 2005). Compression of the cervical spinal cord will lead to neurological deficit in all four limbs (Simpson et al., 1999; Kim et al., 2003). Compression of vascular structures and tumour metastatic spread to lungs and lymph nodes can produce systemic signs (Kostov et al., 2008).

4.1.5 MRI and other diagnostic methods

4.1.1.1 MRI and peripheral nerve sheath tumour appearance

Brachial plexus imaging techniques have been divided into two categories: structural neurography mainly with the use of STIR sequences; and microstructural neurography, which depends on diffusion tensor imaging to define the degree and direction of water diffusion within the nerve fibres (Mallouhi et al., 2012). This method is useful in

differentiating the dense cellular tumour tissue from inflammatory and infectious changes or scar tissue (Judmaier, 2013). Nerve tissue function can be assessed using functional MRI. Spectroscopy can give an insight into the biochemistry of nervous tissue. A novel method under investigation is magnetization transfer imaging, and is based on the ratio of protein-bound and free water protons in the nerve tissue (Judmaier, 2013).

The fat suppressing sequences are of special diagnostic importance because they show the water content within the anatomical structures, and can depict enlargement of small nerves due to oedema (Judmaier, 2013). It was suggested that a water bag (500 ml normal saline) placed on the right and the left side of the neck above the shoulder region can increase signal to noise ratio to obtain higher resolution images of the brachial plexus in man (Collins et al., 1995). Blood flow compromise accompanies a nerve compression and ischemia initiates inflammatory changes causing muscle oedema and fibrosis (Collins et al., 1995).

There are limitations in the assessment of pathologies of smaller nerves with MRI, especially in patients with degenerative nerve diseases. Nevertheless, MRI can be of great diagnostic value even in these cases, as denervation of musculature causes signal hyperintensity in the muscle, which can serve as valuable aid to diagnosis (Judmaier, 2013). On the other hand, muscle hyperintensity is a non-specific finding in both human and veterinary patients, and can occur in traumatic, inflammatory and neoplastic conditions (Linda et al., 2010; Eminaga et al., 2013). The imaging methods are of great importance in tumour location, margin detection, distribution, spinal cord and thoracic cavity involvement (Chevoir et al., 2012). Imaging is also useful to define the relationship of the nerve sheath tumour with adjacent neural, vascular, and muscular structures (Platt et al., 1999; Li et al., 2008).

Nerve-sheath tumours have an isointense signal on T1-weighted images and a hyperintense signal on T2-weighted images relative to the spinal cord with contrast uptake ranging from homogeneous to a peripheral ring-like enhancement. In man the most characteristic pattern on fluid-sensitive sequences has been described by many authors as a “target lesion” that reflects pathologic anatomy of the lesion: the decreased signal centrally represents fibrous Antoni A tissue, while the increased signal in the periphery represents myxomatous Antoni B tissue (Wippold et al., 2007). This MRI appearance was suggested to be pathognomic and diagnostic for nerve sheath tumours

(Beall et al., 2007). Often tumour heterogeneity has been explained by a higher ratio of type B to type A tissue, which can reflect hemosiderin deposits and cystic formation seen within type B tissue (Wippold et al., 2007).

In a study on MRI brachial plexus tumours in 18 dogs the periphery of the nerve sheath tumour was hyperintense (relative to muscle) on STIR and T2W images, isointense on T1W pre-contrast images; and contrast uptake was non-uniform and sometimes minimal or mild (Kraft et al., 2007). Tumours that reach the vertebral canal may cause bone resorption and enlargement of the intervertebral foramen (Lorenz et al., 2011).

However, other conditions may mimic these signs: nerve abscess or granuloma, foreign bodies, lymphoma, hypertrophic neuropathy, brachial plexus neuritis, hypertrophic neuritis or nerve thickening associated with foraminal stenosis (Chevoir et al., 2012).

4.1.1.2 MRI and neurogenic muscle atrophy

Early stages of muscle denervation are accompanied by an increase in vascular supply as well as extracellular fluid, probably due to increased muscle cell membrane permeability. These events are responsible for the T2W signal hyperintensity (Wessig et al., 2004; Kamath et al., 2008). In experimental mice, T2 abnormalities were persistent until the renervation phase (Wessig et al., 2004). The point at which T2 values began to decrease depended on the degree of nerve injury. In the irreversible neurotmesis group, T2 values remained high throughout the study period (Pfirrmann, 2008). In the subacute phase, a denervated muscle has a relative increase in both the amount of fat and the extracellular water content (Kamath et al., 2008). The T2W signal intensity in experimental settings was found to be well correlated with the severity of acute nerve damage (Yamabe et al., 2008). Chronic denervation is often best seen on T1-weighted spin-echo images as loss of muscle bulk and widespread areas of increased signal intensity resulting from fatty infiltration (Kamath et al., 2008).

MRI changes in ipsilateral limb muscle consist of hyperintense signal on T2W, STIR, and T1W images, with mild contrast uptake, and are suggestive of neurogenic atrophy, oedema, fatty infiltration and fibrosis (Kraft et al., 2007). The primary nerve abnormality may not always be visible on MRI. Nevertheless, MRI features of compressive neuropathy include direct signs involving the nerve and indirect signs related to muscle denervation (Yanny & Toms, 2010). This is why signal intensity changes in the muscles innervated by the injured nerve may be used to determine the

presence of nerve damage and localise the cause (Bredella et al., 1999). T1W and T2W images with and without fat saturation are useful in identifying denervation atrophy, with T2W showing oedema, suggestive of an acute to subacute process, and T1W images depicting atrophy and fatty infiltration, suggestive of a chronic process (Bredella et al., 1999). MRI in neuritis cases shows plexus enlargement with diffuse T2W hyperintensity in affected nerves and T2W hyperintensity in the affected muscles (Sureka et al., 2009).

4.1.1.3 Computed Tomography

It has been suggested that masses as small as 1.0cm can be identified on contrast enhanced CT scans (Rudich et al., 2004). However, the lack of the sensitivity of the CT compared with the sensitivity of MRI, for the detection of peripheral nerve tumours, especially in the absence of muscular atrophy, has been reported (Chevoir et al., 2012). Small or diffuse tumours may be hard to detect, and it can also be difficult to assess nerve structures that are oriented obliquely to the transverse imaging plane (Kraft et al., 2007).

4.1.1.4 Ultrasonography

Ultrasound has been shown to be a promising diagnostic tool in detecting brachial plexus tumours, though it is not always possible to image the entire tumour (Rose, 2005).

4.1.1.5 Electromyography

Electromyography (EMG) is widely used to detect muscles denervation by the presence of spontaneous electrical activity (Jones, et al., 1975; Wheeler & Wright, 1986). However, abnormal electrical activity could also be seen with certain myopathies and denervation may be the result of any pathological process involving loss of lower motor neurons (Simpson et al., 1999). An epaxial muscle EMG study may predict proximal extension of PNSTs in dogs with the specificity of 100% for the thoracic limbs, but with the sensitivity as low as 53% (Chevoir et al., 2012).

Aims of this study

1- To describe the appearance of the brachial plexus tumours on MRI images
2- To evaluate the detectability of the mass lesions on different MRI sequences
3- To measure the muscle atrophy in terms of size reduction and T1W/T2W signal intensity changes in the serratus ventralis, rhomboideus, triceps, biceps, supraspinatus, infraspinatus and subscapularis muscles.

4.2 Materials and methods

The electronic patient database of the University of Glasgow Small Animal Hospital was searched to identify dogs with a presumptive diagnosis of brachial plexus neoplasia and where an MRI study of the brachial plexus was performed. Histological confirmation was not included as part of the inclusion criteria as this was rarely available.

T1W and T2W transverse images were used to determine muscle signal intensity and to perform muscle area measurements which were compared to the unaffected contralateral side. The dorsal plane was used for these measurements if the field of view on the transverse plane was inadequate. Sagittal plane images were used as a reference for defining the level of the transverse images in relation to the vertebral column. If it was not possible to measure muscle area on the above sequences then STIR or T1FS sequences were used for muscle area measurements as well as tumour description. Muscle area and muscle signal intensity measurements were performed using ImageJ Software (http://rsbweb.nih.gov/ij/).

Statistical analysis was performed using GraphPad and the Mann-Witney and Spearman test was used. Descriptive statistics were reported as median, upper and lower quartiles and range.

4.3 Results

Nineteen dogs with a presumptive diagnosis of brachial plexus neoplasia and 1 dog with lymphoma involving the brachial plexus were extracted from the hospital database: 5 Labradors, 2 Jack Russell terriers, one of each – Chihuahua, Golden retriever, Collie, Greyhound, Staffordshire terrier, Weimaraner, German shepherd, Dalmatian, Dandy Dinmont, cross bred and two dogs where the breed and gender were not recorded. There were 11 males, 6 females with a mean age of 8years (range 2-13years) among the recorded dogs.

4.3.1 Descriptive appearance of the mass lesions affecting the brachial plexus

Tumour shape			Tumour numbers		Thoracic cavity	Vertebral canal	Spinal cord	
globoid	tubular	fusiform	multiple	single	involvement	invasion	involvement	compression
10	3	6	9	10	7	9	6	3

Table 4-3 Brachial plexus lesions - mass characteristics.

Thirteen out of 19 lesions presented as a mass: 9 had a round /globoid shape; 3 had a tubular shape and 6 were fusiform in shape and confined to the nerve resembling nerve thickening. In 9 out of 19 cases the lesions were multiple, with involvement of the thoracic cavity in 7 out of 9 cases. In 9 cases invasion of the vertebral canal was noted as follows: 5 fusiform mass lesions, 3 – globoid and 1 tubular; while spinal cord compression was obvious in 3 out of 9 cases. Localisation of the mass was defined as immediately adjacent to the spine and potentially affecting multiple nerve roots or a single root. The localisation could also affect nerve trunks and peripheral nerves in the axilla area. The mass could also arise in the region of the axilla, involve multiple nerves and extend into the vertebral canal.

4.3.1.1 Mass lesion shape: globoid, tubular or fusiform

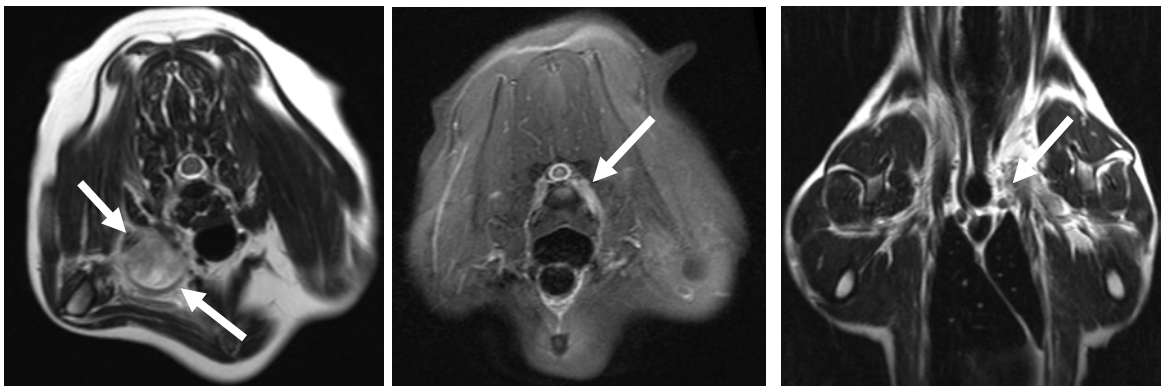

A B C

Figure 4-3 MRI appearance of brachial plexus mass lesions. Examples of a globoid (arrows) (A); fusiform (B) and tubular (C) mass lesions. A- T2W transverse; B- STIR transverse; C- T2W dorsal images.

4.3.1.2 Mass lesion appearance: multiple or single

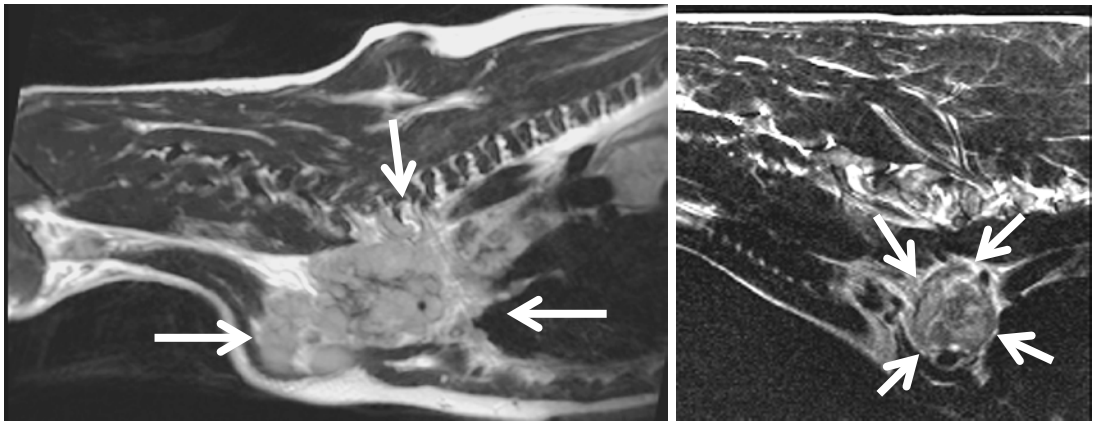

A B

Figure 4-4 MRI images - A –T2W parasagittal image of a lobulated mass involving roots, trunks and nerves and extending into thoracic cavity; B T2W parasagittal image depicting a single globoid shaped mass in the axilla.

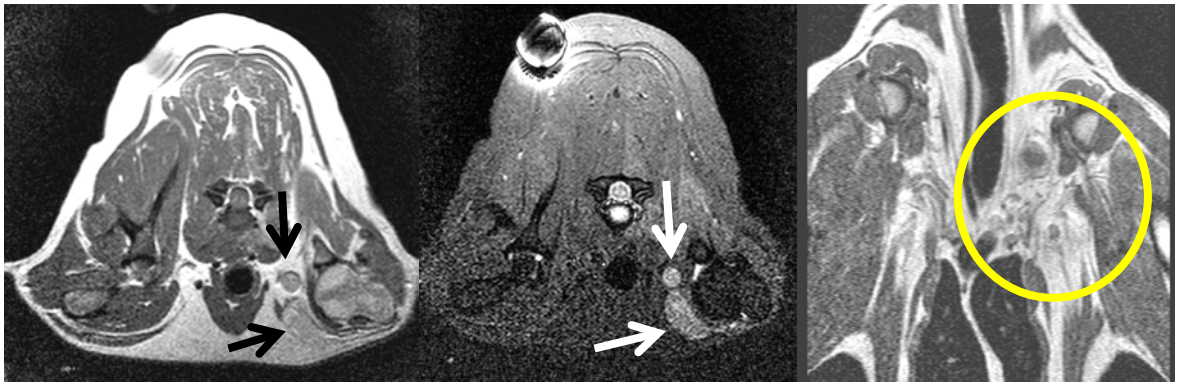

A B C

Figure 4-5 MRI transverse T1W with contrast (A), STIR (B) and dorsal T1W with contrast (C) images demonstrating multiple mass lesions in the axilla.

4.3.1.3 Thoracic cavity involvement or local mass effect

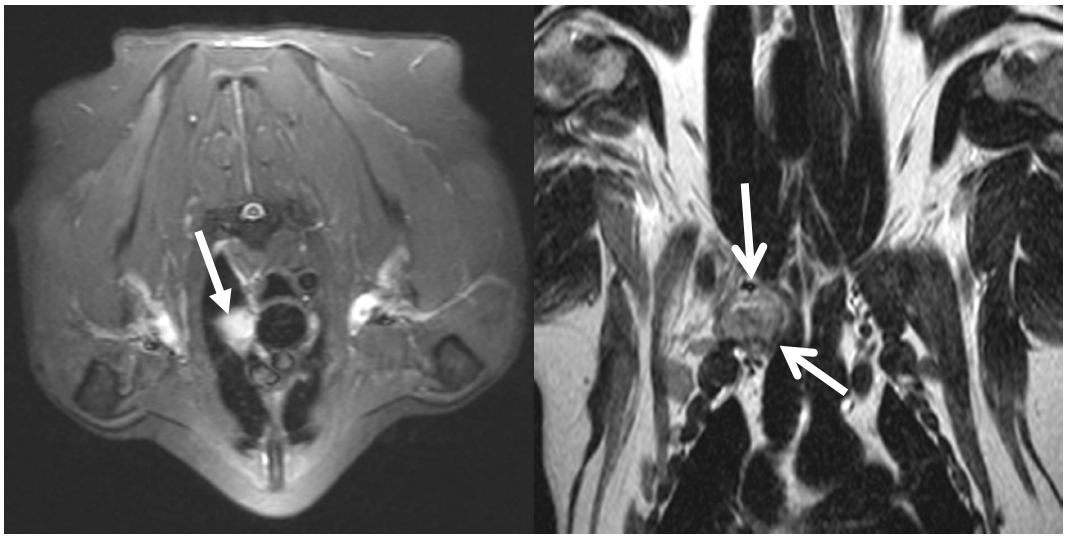

A B

Figure 4-6 MR images showing thoracic cavity involvement. (A) STIR transverse image. (B) T2W dorsal with a single large mass (arrowed).

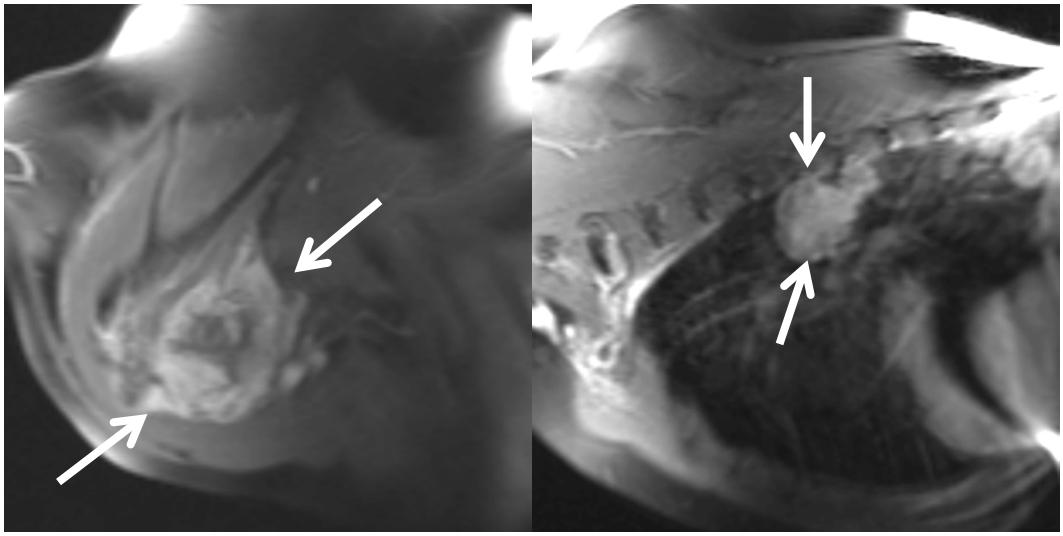

A B

Figure 4-7 MR T1W FatSat with contrast paramedial sagittal images revealing a multi-lobulated mass lesion (arrowed) – in the axilla (A) and thoracic cavity (B)

4.3.1.4 Vertebral canal involvement

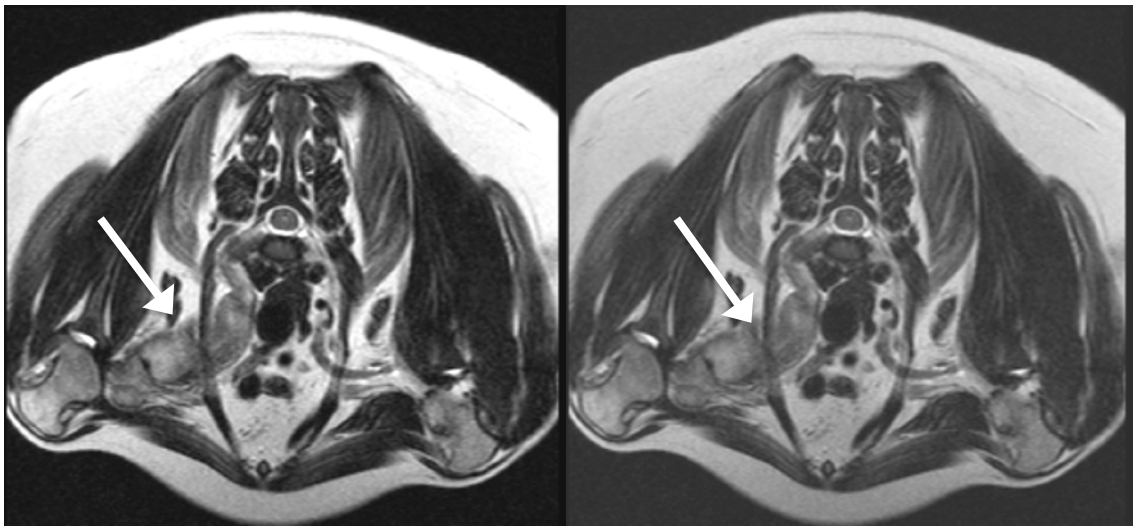

A B

Figure 4-8 MRI T2W (A) and T1W (B) transverse images of a tubular mass extending from the axilla to the vertebral canal (arrows).

4.3.1.5 Spinal cord compression

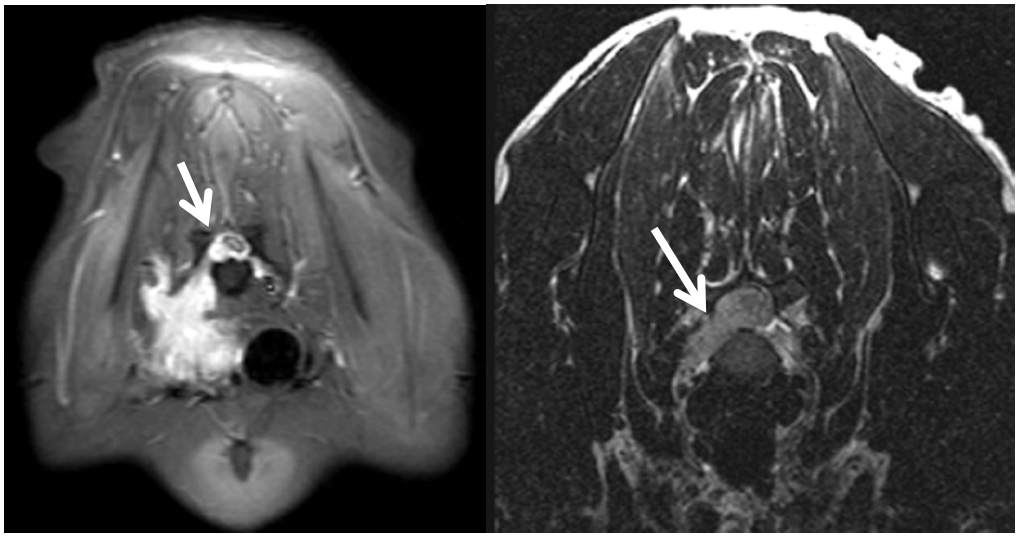

A B

Figure 4-9 MR images. A - STIR transverse image shows a mass extending from the brachial plexus into the vertebral canal and compressing the spinal cord (arrowed); B - T2W transverse image shows a mass (arrowed) invading the vertebral canal.

4.3.1.6 Mass effect

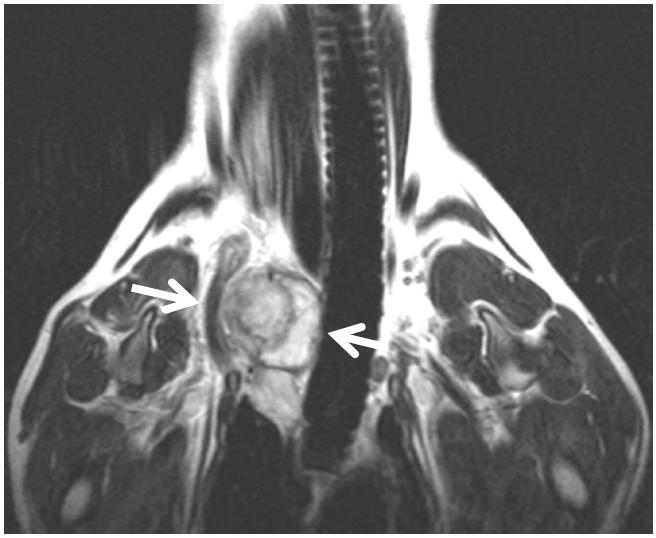

Figure 4-10 MR T2W dorsal image of a globoid mass of the brachial plexus compressing adjacent soft tissue structures.

4.3.2 Sequences for a mass lesion detection

Case No	T2	T1	T1FS	STIR	GAD uptake	Contrast distribution
231891	hyperintense	Isointense	isointense	NA	good	Patchy
229399	isointense*	isointense*	slightly	hyperintense**	slight	Uniform
207533	slightly	isointense*	NA	hyperintense**	no uptake	no uptake
215396	hyperintense	slightly	NA	hyperintense**	good	Patchy
224672	hyperintense	Isointense	slightly	NA	good	Patchy
226376	slightly	Isointense*	slightly	hyperintense**	slight	Patchy
227446	hyperintense	Isointense	slightly	NA	good	Patchy
228522	hyperintense	hyperintense	hyperintense	hyperintense**	good	Patchy
228891	hyperintense	isointense*	slightly	hyperintense**	good	Patchy
235379	hyperintense**	Isointense	NA	NA	good	Patchy
142533	slightly	isointense*	NA	hyperintense**	good	Uniform
213333	slightly	isointense*	NA	NA	good	Uniform
213529	slightly	Isointense	NA	hyperintense**	good	Uniform
205557	hyperintense	slightly	NA	hyperintense**	good	Patchy
220807	hyperintense	Slightly	NA	hyperintense**	slight	Uniform
217064	hyperintense	isointense*	NA	hyperintense**	good	Patchy
217085	hyperintense	isointense*	NA	hyperintense**	good	Uniform
228945	slightly	slightly	slightly	NA	slight	Uniform
220833	hyperintense	Slightly	NA	NA	NA	NA

Table 4-4 MRI mass lesion detection with different sequences. T1W with fat suppression (T1FS) – without gadolinium. GAD – any sequence with gadolinium. Hyperintense signal- strongly shows the lesion. Slightly (hyperintense) – less bright signal, but still detectable. Isointense – signal equal to the signal from the muscles; a lesion still can be detected due to the mass effect and visible mass margins. Isointense* lesion cannot be differentiated from the surrounding tissues on the image because there is no mass effect. **- the best detectability.

The best results were achieved with STIR sequence images (12/12 cases), followed by the T2W sequence images (12/19- hyperintence; 6/19 slightly hyperintence; 1/19 – isointense). On T1W images mass lesions were slightly hyperintense in 5 out of 19 cases and isointense in 12 out of 19 cases. The contrast uptake ranged from slight to good in 17 out of 18 cases and no uptake in 1 case. The contrast distribution was patchy with areas of hypo- and hyperintensity in 10 out of 18 cases, and homogenous in 9 out of 18.

4.3.3 The effect of brachial plexus mass lesions on muscle signal intensity and area changes

The following muscles were selected for signal intensity and area determination on the basis that they could readily be distinguished from adjacent muscles on at least one imaging plane and were included within the field of view: serratus ventralis, rhomboideus, subscapularis, supraspinatus/infraspinatus, deltoideus, biceps and triceps. The following muscle changes were recorded in the transverse and dorsal plane: size reduction and T1W and T2W hyperintensity - diffuse, focal or patchy around the mass lesion.

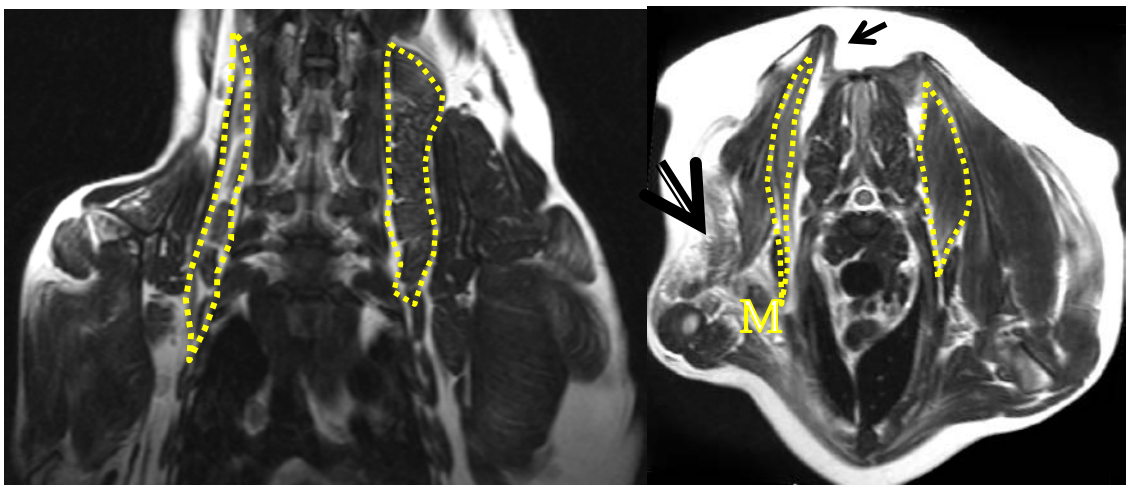

A B

Figure 4-11 MR images. T2W dorsal (A) and transverse (B) image depicting the serratus ventralis muscle size reduction in comparison to the contralateral muscle (dotted line). On the transverse image the scapula wing and the rhomboideus size reduction (small arrow) can be seen, as well as fat infiltration and atrophy of the triceps m. (large arrow) ipsilaterally to the lesion. M-mass lesion.

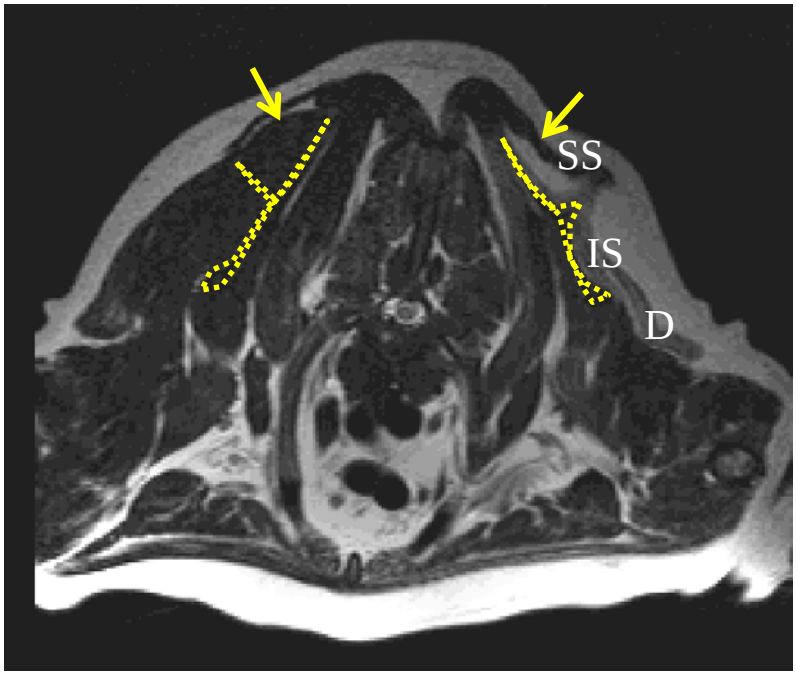

Figure 4-12 MR image. T2W transverse image shows atrophy and fat replacement of the supraspinatus (SS) (arrowed), infraspinatus (IS) and deltoideus (D) muscles at the affected side.

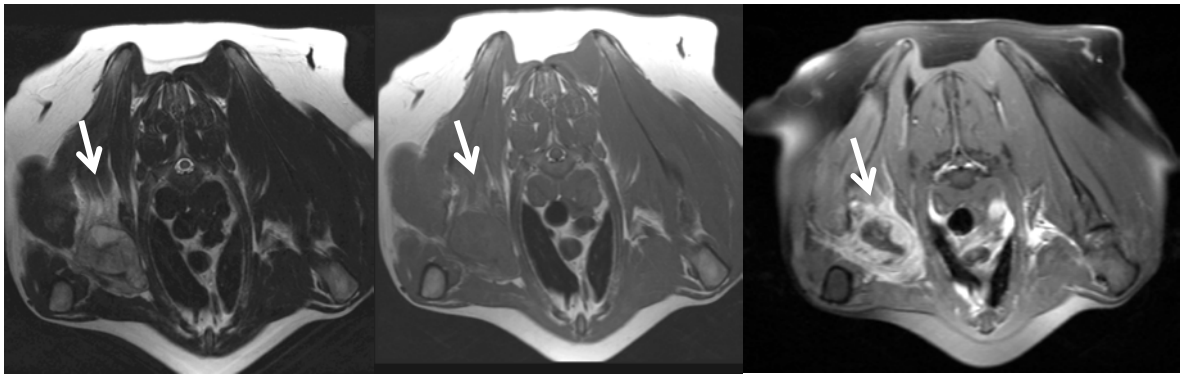

Figure 4-13 MR images. T2W (A), T1W (B) and post contrast T1 FatSat (C) with transverse images showing signal hyperintensity surrounding a mass (arrowed) on the T2W sequence, with slight contrast enhancement on the T1W image and more obvious identification of the mass on post contrast T1 FatSat images.

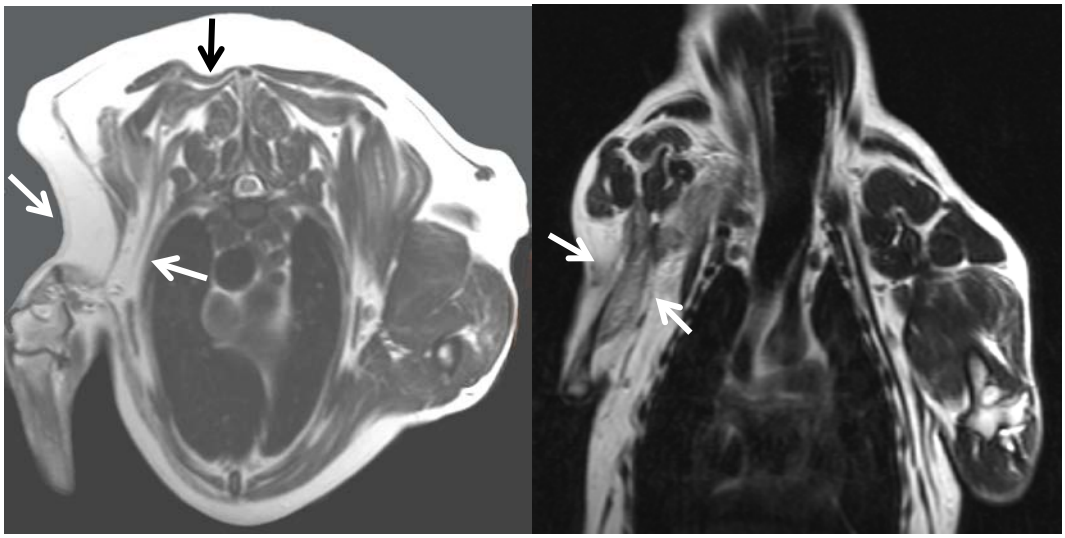

Figure 4-14 T1W transverse and T2W dorsal images of the same dog demonstrating pronounced right thoracic limb muscle atrophy with fatty replacement: triceps, biceps brachii, serratus ventralis and rhomboideus muscles and asymmetry with the scapula deviating dorsally (wing appearance).

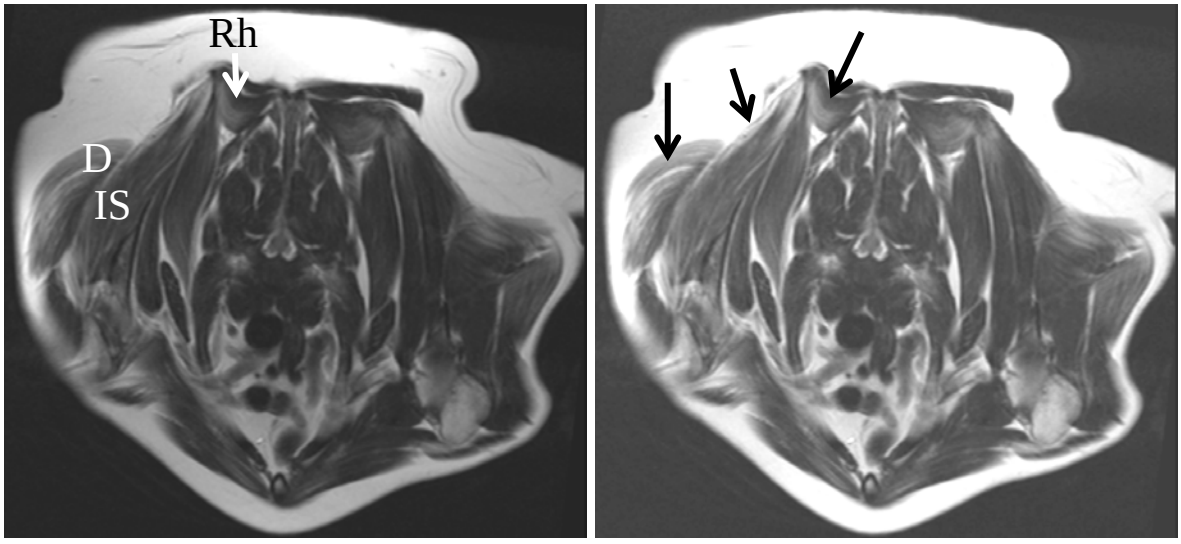

Figure 4-15 MR images. T2W (A) and T1W (B) transverse images of a dog with a brachial plexus mass lesion depicting signal hyperintensity in the muscles rhomboideus (Rh, arrow), deltoideus (D), infraspinatus (IS) muscles in both sequences as well as dorsal deviation of the scapula.

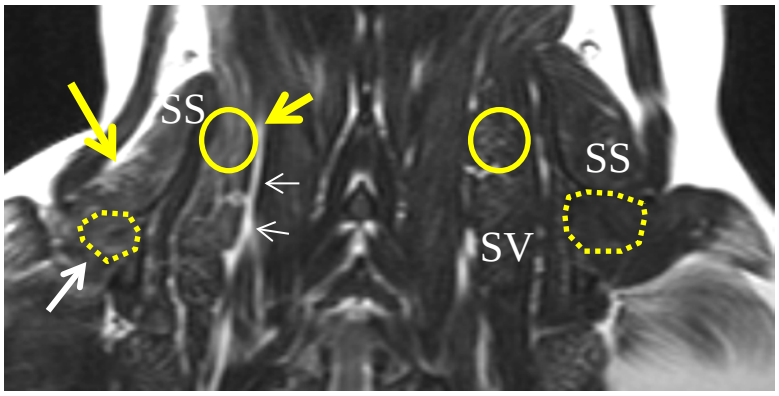

Figure 4-16 MR image. On this T2W dorsal image the following changes are evident ipsilateral to a brachial plexus mass lesion: focal area of signal hyperintensity (longer arrow) in the supraspinatus muscle and size reduction (SS); loss of the normal marbling appearance (circle and short arrow) in the serratus ventralis muscle (SV); reduction in size of the infraspinatus muscle (dotted circle and arrow); intermuscular fat deposition (small arrows).

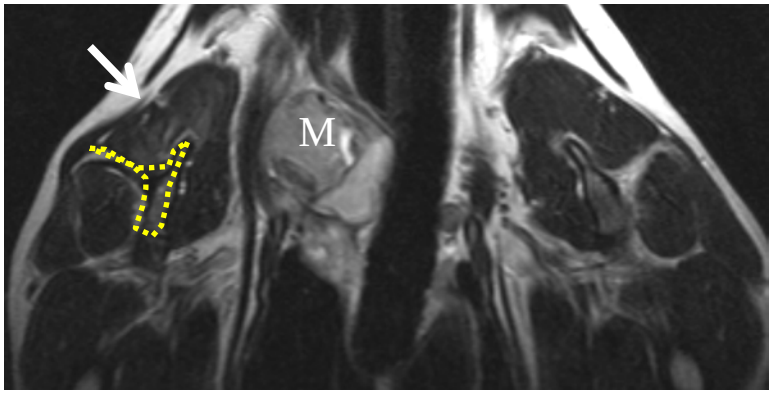

Figure 4-17 This T2W MR dorsal image shows a mass (M) compressing surrounding soft tissues. Involvement of the suprascapular nerve is suspected, which is compatible with the supraspinatus muscle hyperintensity (solid arrow). Dotted line localizes the scapula.

4.3.3.1 The serratus ventralis muscle.

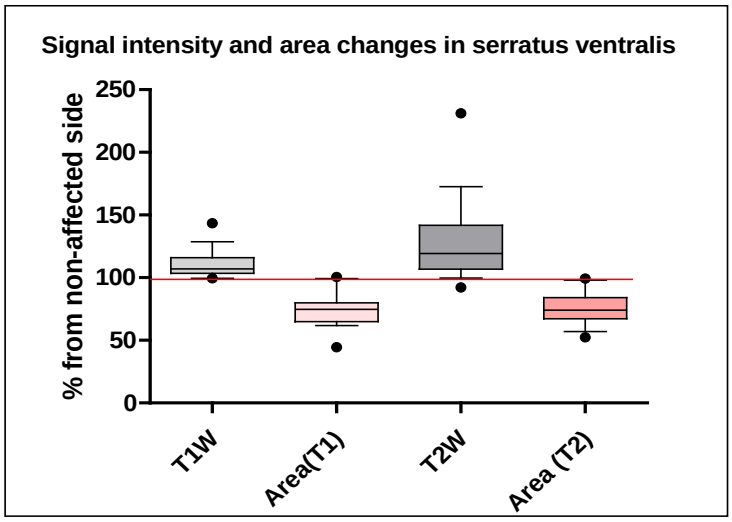

Figure 4-18 Box & whisker plot shows the serratus ventralis muscle. T1W and T2W signal intensity and area changes. Both sequences were expressing signal hyperintensity. The T1 and T2W medians were significantly different with T2 signal hyperintensity much higher (P value =0.0307). The area of the muscle measured on T1 and T2 images was not significantly different (P value 0.9847). The area of the serratus ventralis muscle on the affected side was less than non-affected (less than 100%).

4.3.3.2 The supraspinatus/infraspinatus muscle

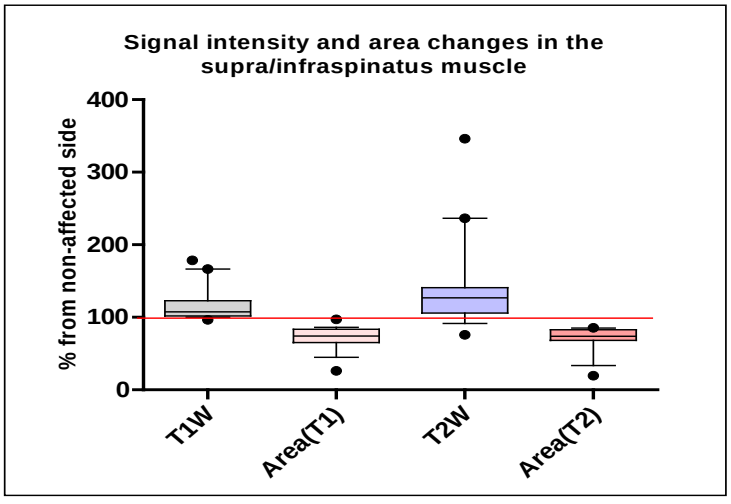

Figure 4-19 Box & whisker plot. T1W and T2W signal intensities of the supra/infraspinatus muscles of the affected side were not significantly different (P = 0.1218). Comparison of the area showed significant reduction in cross-sectional area (P<0.0001).

4.3.3.3 The subscapularis muscle

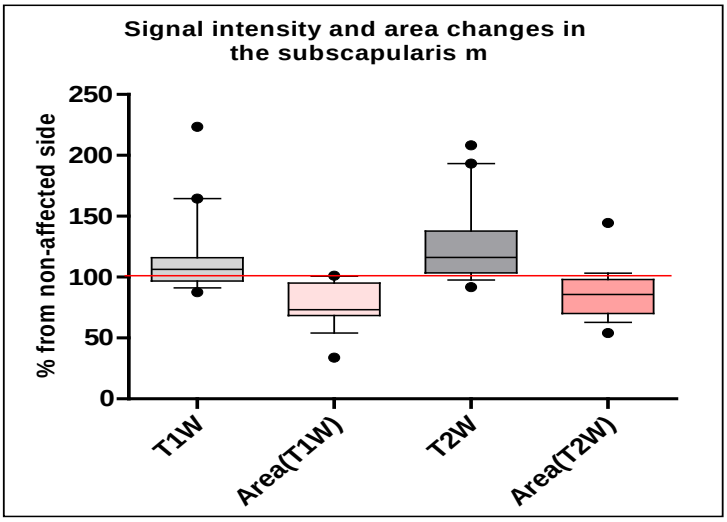

Figure 4-20 Box & whisker plot of signal intensity and area changes in the subscapularis muscle. T1W and T2W signal intensities were not significantly different (P = 0.0961).

4.3.3.4 The triceps muscle

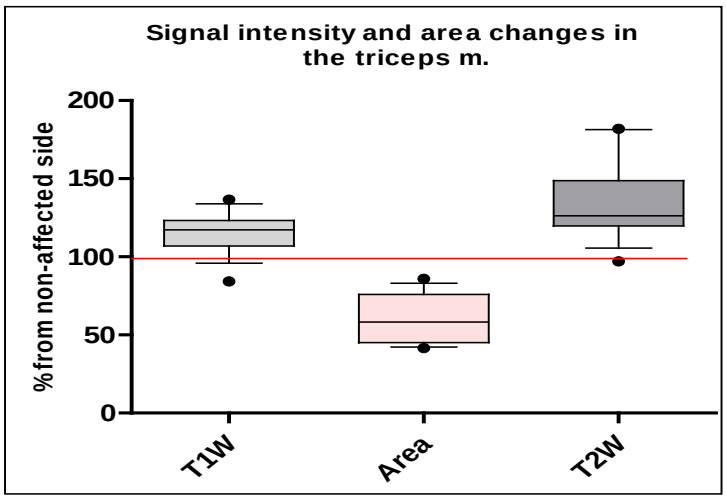

Figure 4-21 Box & whisker plot represents T1W and T2W signal intensity and area changes (T2W images) in the triceps muscle with significant increase in T1W and T2W signal intensity and a reduction in cross sectional muscle area (P=0.0270).

4.3.3.5 The biceps muscle

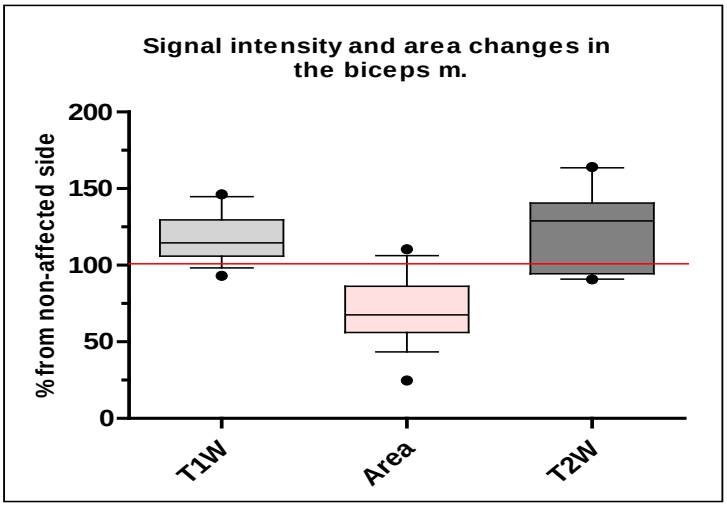

Figure 4-22 Box & whisker plot of T1W and T2W signal intensity and area changes (STIR images) in the muscle biceps brachii. There was no significant difference between T1W and T2W values when comparing signal intensity (P=0.6620)

4.3.3.6 The rhomboideus muscle

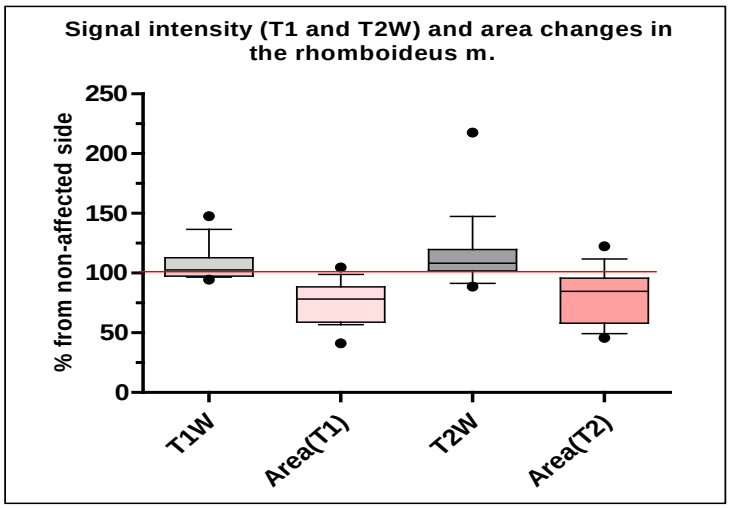

Figure 4-23 Box & whisker plot showing T1W and T2W signal intensity and area changes in the muscle rhomboideus with no significant difference when comparing signal intensity (P=0.2232).

4.3.3.7 The deltoideus muscle

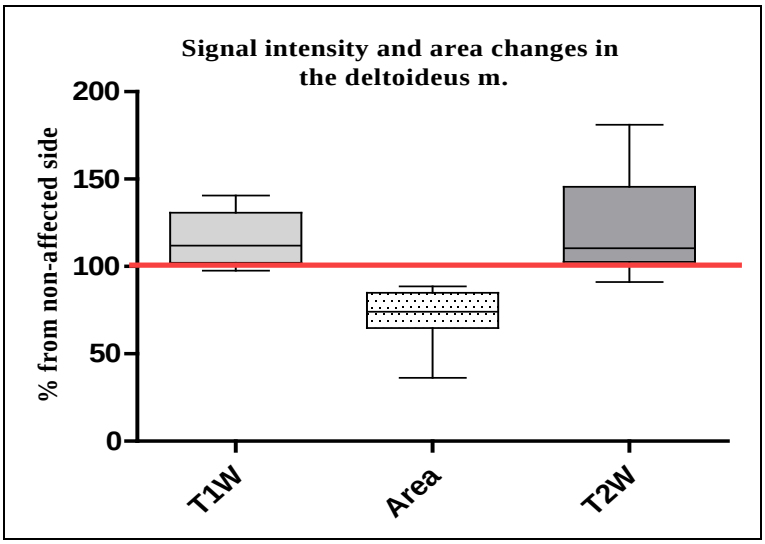

Figure 4-24 Box & whisker plot shows T1W, T2W and area changes (T1FatSat) images) in the deltoideus m. There is no significant difference when comparing changes in signal intensity (P=0.8103)

4.3.3.8 Signal intensity and area analysis in all 7 muscles.

The overall effect of brachial plexus mass lesions, and by presumption the effect of muscle denervation, on T1W and T2W MRI signal intensity in muscle and muscle area was determined for all measured muscles in the affected limbs, as compared to the control contralateral limb.

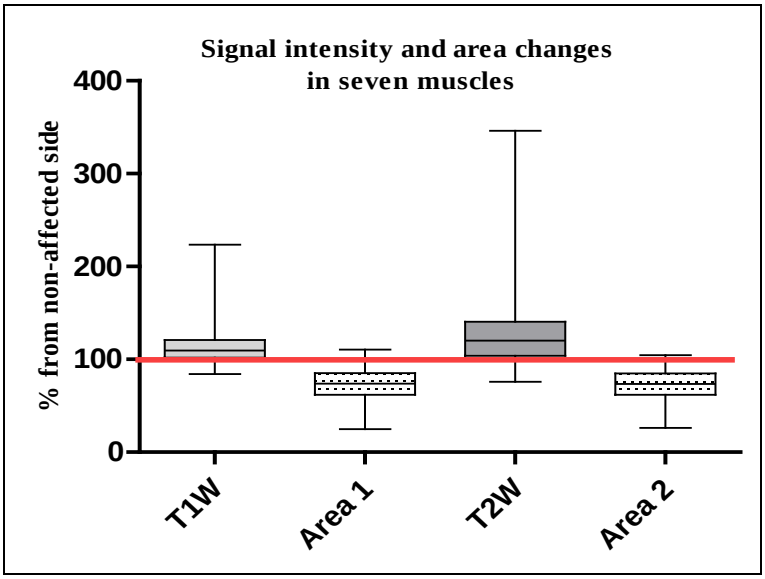

Figure 4-25 Box & whisker plot illustrating T1W and T2W signal intensity and muscles area changes (% from contralateral side) calculated in 7 muscles of each of the 19 dogs.

There was good correlation between T1W and T2W signal intensity changes (Spearman test, r=0.2747, P=0.0035), though the medians were significantly different (P<0.05) when examined with the two-tailed Mann-Whitney test. There were a lack of correlation (Spearman test) between the increase in signal intensity and reduction in area (T1/area P value = 0.0545; T2/area P value = 0.0856).

4.4 Discussion

The brachial plexus provides motor and sensory innervation to the thoracic limb. It can be affected by neurogenic as well as non-neurogenic tumours, inflammation/infection and trauma. Brachial plexus assessment represents a challenge in human and veterinary patients because of similarity of clinical presentation of different plexopathies, and many of these conditions cannot be localised without diagnostic imaging (Tagliafico et al., 2012). In dogs progressive thoracic limb lameness/monoparesis with muscle atrophy is a typical clinical observation in brachial plexopathies and especially brachial plexus tumours (Jones et al., 1995; Kraft et al., 2007). MRI can identify the exact site of insult depending on the muscles involved, and provides information about the duration of denervation, and often directly depicts the cause (Yanny & Toms, 2010).

It has been established in man that the muscle response to a pathological process is limited to a few non-specific patterns on MRI: abnormal signal intensity (May et al., 2000); change in symmetry, size and shape ranging from atrophy to pseudohypertrophy (Costa et al., 2012).

4.1.2 **T2W signal intensity**

In the early stages of denervation, increased signal intensity can be observed on T2W, short tau inversion recovery (STIR) and sequences with fat saturation. T2W relaxation time prolongation is usually explained by the oedema (Deroide et al., 2012), caused by the increased muscle cell membrane permeability, increased capillary bed, impaired drainage or tumour infiltration (tumourogenic oedema) (Wessig et al., 2006). Costa et al (2012) characterised the types of oedema as (1) patchy focal; (2) patchy throughout a single muscle; (3) diffuse oedema in a single muscle; (4) oedema in adjacent muscles; (5) symmetric oedema in nonadjacent muscles; and (6) asymmetric oedema. T2W signal hyperintensity in human cases of muscle denervation can persist for up to one year (Costa et al., 2012). It has been observed in experimental settings in rodents that muscle changes can be detected on MRI starting from 3 to 7 days post-denervation (Küllmer et al., 1998); and that in the irreversible neurotmesis group of animals T2W signal intensity remained high throughout the study and did not decrease, in contrast to the animals with reversible nerve damage (Yamabe et al., 2008).

4.1.3 **T1W signal intensity**

T1W signal abnormalities are typically caused by fat deposition, and less commonly, by methhaemoglobin, proteinaceous fluid or mineral deposits as well as calcium containing lesions. T1W hyperintensity can be patchy in early stages of fat infiltration; or can reflect complete fatty replacement in the chronic stage; it can be focal due to fat deposits or scars, or uniform from the loss of marbling which is especially suspicious for a tumour (Costa et al., 2012).

In the present study T1W and T2W signal intensity and muscle area were measured in 7 muscles in each of the 19 dogs with a presumptive diagnosis of brachial plexus tumour: serratus ventralis, rhomboideus, subscapularis, supraspinatus/infraspinatus, triceps, biceps, deltoideus. The reported complaints of progressive unilateral thoracic limb lameness (100% of dogs) ranged from 7 days to 12 months in duration. Taking into account the chronic progressive character of this condition, it may be assumed that

under certain circumstances the owner's perspective of illness duration can be misleading. Muscle atrophy was clinically evident in 13 cases (68.4%), and was confirmed by EMG in 9 out of 11 cases (81%) – in the biceps, triceps, extensor carpi radialis and flexors muscles, whereas the MRI scans showed a higher number of muscles affected and variable combination of signal intensities and area changes. The median values of T2W signal intensity were higher than T1W in the muscles serratus ventralis and triceps muscles, but in the other five muscles the T2W and T1W signal intensity was not significantly different. Peritumoral oedema and T2W hyperintensity of the surrounding area is a well recognised state in brain and soft tissue tumours in man. The proposed major pathogenetic mechanisms are ischemia from compression, venous stasis and venous congestion, excretion and secretion, and hydrodynamic disturbances (Bitzer et al., 2002). As an example, the extent of peritumoral T2W hyperintensity area due to oedema and tumour infiltration in human patients with soft tissue sarcoma was up to 7cm (White et al., 2005).

4.1.4 **Muscle size**

Fatty infiltration is usually associated with muscle atrophy, however, it may cause muscle hypertrophy or pseudohypertrophy. Petersilge et al (1995) have suggested that true hypertrophy is characterised by the absence of signal changes on T1W and T2W sequences and unchanged muscles contours, while in a muscle with pseudohypertrophy areas of increased T1W signal are distributed through the normal muscle and diffuse mottled distribution of fat can be detected. Not only fat infiltration can contribute to the phenomenon of pseudohypertrophy, but oedema as well (Wessig et al., 2006).

Muscle atrophy with fatty infiltration may be found in non-neurologic conditions resembling chronic denervation on MR images (May et al., 2000). The median muscle area was reduced by 22 to 27% (73-78% of the control) in five muscles (serratus ventralis, supra/infraspinatus, subscapularis, rhomboideus and deltoideus); 42% reduction was calculated in the triceps and 33% in the biceps muscle. In the majority of images the scapula was displaced dorsally creating the appearance of a wing-like shape (Figure 4-11B) and correlated with atrophy of the serratus ventralis and rhomboideus muscles, which may be caused by long thoracic nerve or spinal nerve damage. Correspondingly, in man scapula wing appearance in neurological cases can be caused by: spinal accessory nerve damage (trapezius palsy), dorsal scapular nerve damage

(rhomboideus palsy), and long thoracic nerve damage (serratus ventralis palsy) (Martin & Fish, 2008; Meininger et al., 2011).

4.1.5 **Atrophy staging**

Histopathological and MRI staging of muscle atrophy in man and in animals is usually based on the classification into acute/ subacute and chronic changes. It has been demonstrated with the use of CT in dogs with sciatic nerve crush injury that muscle atrophy with fat infiltration appeared after 1 to 2 weeks post-denervation and became significant after three weeks (Orima & Fujita, 1997). In contrast to these findings, others have found abnormal signal intensity as early as 4 days after experimental denervation in rats (Kamath et al., 2008).

Adami et al (2006) in experimental permanent sciatectomy in rats have reported three phases of denervation – early fast atrophy (one month duration, 50% reduction of fibre diameter), intermediate slow atrophy (four to six months duration, 20% reduction) and a final phase of complete atrophy after seven to nine months (steady state, loss of muscle fibres and increase in fat and collagen) (Adami et al., 2006). In man, the acute stage is thought to last about one month (oedema, T2W and STIR increase), subacute – six months (T2W and STIR hyperintensity) and chronic – after six months (fatty infiltration and muscle trophy – T1W and T2W hyperintensity) (Kamath et al., 2008).

Regarding morphological staging of muscle atrophy, it has been established that the response of a given muscle fibre to denervation may not be consistent in all muscles, and can be fibre-specific in various stages of denervation (Tomanek & Lund, 1973; Borisov et al., 2001).

In the present study T2W intensity was higher than T1W in only two muscles – serratus ventralis and triceps and was not different in the rest of the muscles. It can be speculated that muscle atrophy stages after acute injury and chronic gradual nerve compression/destruction could be different in their order of progression and severity, although more investigations are needed. The noted concomitant T1W and T2W signal hyperintensity can be caused by a complex pathophysiological condition in chronic denervation without a regeneration phase. This could include a combination of oedema, fat atrophy, inflammation and different degree of muscle size reduction. The actual muscle size can be overestimated due to the oedema effect.

4.1.6 **Mass lesions characteristics**

The majority of the mass lesions were more readily detected on the STIR images, followed by T2W and T1FS with contrast. Contrast uptake exhibited a patchy pattern as was previously reported. The mass lesions in 17 out of 19 cases were located in the axilla and in two cases – paravertebrally. In 9 out of 19 cases (47.4%) more than one lesion was detected, with thoracic cavity involvement in 7 out of 9 cases (77.7 %). In 10 out of 19 (52.6%) cases the masses were globoid in shape with the size ranging from 10x21 to 78.5x44.3 mm; 3 out of the 19 masses (15.78%) were tubular in shape, and 6 cases with fusiform nerve enlargement (31.5%). Mass extension into the vertebral canal was noted in 9 out of 19 cases (47.4%), and 3 out of 9 with spinal cord compression 33.3%). The length of the mass lesion (in cases of multiple masses - the length of the largest one) ranged from 1 to 4 vertebrae.

4.1.7 **Conclusion**

The present study is an example of chronic muscle response to chronic denervation evaluated on the MR images. The complex effects of a lesion affecting the brachial plexus such as mass effect, compression and destruction of nerves and compromised vascular supply induce a combination of denervation and disuse atrophy in the muscles of the shoulder region. It can be speculated that a mixed pattern with T1W and T2W identical signal hyperintensities may indicate ongoing degeneration and partial regeneration or concomitant oedema, fatty atrophy and tumour infiltration effects. It can be suggested that experimental staging into early/acute (T2W) and chronic (T1W) phases cannot be directly extrapolated on these cases. The limitation of the study is the absence of histological data and the small group size.

5 General Discussion

Magnetic resonance imaging allows the visualisation of soft tissue structures at a level of detail not previously possible. In particular, MRI allows the assessment of the normal anatomy and the influence of body condition, signalment and disease on these structures. This study sought to evaluate the utility of MRI for the assessment of muscle within the proximal thoracic limb of the dog, in health and disease. The effect of disease was examined in dogs with suspected mass lesions of the brachial plexus as a model of chronic denervation with the opposite normal limb acting as the control. One of the features of chronic denervation is infiltration of affected muscles with fat. Prior to understanding the effect of disease on the MRI anatomy and signal intensity of muscle, it was important to first examine the effect of body condition score (BCS) (as a measure of obesity) on normal muscle anatomy and signal intensity. This study therefore sought to examine the MRI appearance of two soft tissue compartments: fat (subcutaneous, intermuscular and intramuscular) in the lumbar and cervical areas as a measure of BCS in a group of dogs (Chapter 2). After quantification of the effect of differences in body condition, the anatomy of the skeletal muscles of the proximal thoracic limb where no pathology was present was examined using MRI (Chapter 3). Finally, the effect of chronic denervation on the MRI appearance of the skeletal muscles of the proximal thoracic limb was defined in cases of brachial plexus mass lesions (Chapter 4).

Lipids (fat) are important components of all mammalian cells with complex biological functions (Adibhatla & Hatcher, 2007), playing a role in a variety of pathological conditions such as diabetes and insulin resistance, obesity related hypertension, orthopaedic diseases and life-span reduction (German, 2006; Toll et al., 2010; Corbee, 2012). The crucial role of lipids in tissue physiology and cell signalling has been established in many neurological disorders and neurodegenerative diseases in man (Wenk, 2005). Ectopic fat deposition in organs such as the liver, pancreas and heart and in skeletal muscle may induce pathological changes in these organs that have been explained by lipotoxicity (Basso & Thiene, 2005; Herpen & Schrauwen-Hinderling, 2008; Tamilarasan et al., 2012). Intramuscular fat accumulation with reduction in muscle mass is one of the characteristic features of muscle atrophy secondary to denervation and disuse (Powers et al., 2007), after spinal cord injury (Scelsi, 2001; Gorgey & Dudley, 2007), intervertebral disc degeneration, whiplash injury (Elliott et

al., 2005; Elliott et al., 2006; Cagnie et al., 2009), in inherited muscle defects, in ageing (Vettor et al., 2009) and in myopathies of different aetiologies in humans and companion animals (Hanson et al., 1998; Platt et al., 2006; Kobayashi et al., 2009; Olby et al., 2011). It induces ultrastructural damage by a combination of activation of the proteosomal system, increased apoptosis and impairment of muscle regeneration potential (Tamilarasan et al., 2012). MRI for body composition evaluation is widely used in man and less so in veterinary patients (Khoury et al., 2008). MRI of skeletal muscles is believed to be a sensitive tool for the detection of acute and chronic muscle atrophy due to denervation and disuse, and as a measure of motor unit integrity in a peripheral nerve injury and regeneration model (Zhang et al., 2008). It has been increasingly used in the diagnosis of shoulder pathology in man and in dogs (Kraft et al., 2007; Williams et al., 2009). The first aim of this study was to determine the effect of changes in BCS on the amount and pattern of subcutaneous, intermuscular and intramuscular fat deposition as measured by MRI in the cervical and lumbar regions. BCS was assessed according to the 9-point body condition scoring system and was compared to body fat percentage estimations calculated from girth measurements. BCS demonstrated a good overall correlation with body fat percentage and with the thickness and amount of the dorsal subcutaneous fat in the lumbar area. Subjectively the pattern of fat distribution was different in the cervical region with increasing BCS, when compared to the lumbar region: in the lumbar region the fat was largely deposited subcutaneously, while in the cervical region fat was deposited between muscles as well as subcutaneously. Consistent with this observation in the cervical area there was a correlation between BCS and the amount of dorsal and ventral subcutaneous fat, and the total amount of fat (subcutaneous and intermuscular). This finding is of particular interest because the cervical area is not typically included in the 9-point BCS scale or girth measurement methods for the estimation of body fat percentage. With increasing BCS fat is not only deposited subcutaneously and between muscles, but also within muscles and one effect of this would be to alter the MRI signal hyperintensity. Fat appears hyperintense on both T1W and T2W MR images. When the correlation between BCS and muscle hyperintensity on MRI was examined there was a good correlation between T1W signal intensity and increasing BCS. This correlation was less strong for the cervical musculature. The results of this section of the study demonstrated that the 9-point BCS and body fat percentage estimation by means of girth measurements demonstrated similar levels of accuracy when the two methods were compared. These methods have been shown to be reliable tools for the qualitative

assessment of body composition in dogs, particularly for the classification of obesity. However, these methods do not take into account breed differences with regard to body composition, nor the ability to detect ectopic fat depots. MRI is able to provide a more objective measure of subcutaneous fat thickness, body fat distribution and the degree of muscle fatness, and thus can serve as a tool for discrimination between normality and disease when combined with clinical data.

Having established the effect of increasing BCS on subcutaneous, intermuscular and intramuscular fat deposition and MRI muscle hyperintensity, the MRI assessment of the skeletal muscle anatomy of the proximal thoracic limb was investigated. In order to achieve this, MRI studies of the shoulder region from 32 dogs were assessed. It was apparent from this work that limb position at the time of the MRI study was a major factor influencing the appearance of this region. In particular, the MRI appearance of the proximal thoracic limb musculature depended on the angle between the spine of scapula and the plane of the MRI sequence. Whether the limb was in extension or flexion influenced the ability to confidently detect certain individual muscles (absence/ presence/ partial detection). The appearance of an individual muscle was also influenced by the orientation of the MRI plane perpendicular or transverse to the orientation of the muscle fibres. Identification of the major muscle groups was most reliable when the MRI plane planning was aligned parallel to the spine of the scapula and the limb was directed caudally along the body, rather than when aligned to the vertebral column. In terms of MRI planes, the individual muscles were easiest to distinguish on images transverse to the spine of the scapula, although the dorsal plane was also highly informative and provided additional information when combined with the transverse plane. T1W and T2W sequences were highly useful for evaluation of muscle size and structure, but the STIR sequence was important for the detection of normal and abnormal peripheral nerve structures. Asymmetry of limb position as well as MRI artefacts such as identity chips, zip artefact and motion artefact were found to interfere with image analysis. Whilst little can be done to overcome the problem of ID chip or motion artefact, it was clear from the retrospective analysis of the MRI studies that factors unrelated to imaging had a dramatic effect on the quality of the MR study and the most important of these was the position of the animal in the MRI unit. Consequently, one of the outcomes of this part of the study was the suggestion that more attention was paid to positioning of the animals on the MRI table from an imaging perspective, to minimise variation in the appearance and detection of individual muscle

groups. Thus it could be argued that an extension of a proposed protocol (Kraft et al., 2007) for imaging of the shoulder would produce more reliable and repeatable images of the region. To such an end:

1- The basic MRI sequences for evaluation of the muscles of the proximal thoracic limb should include T1W, T2W, STIR, FatSat and sequences with contrast where appropriate.
2- The imaging planes should include dorsal and transverse planes, relative to the spine of the scapula, with the limbs aligned along the body and parallel to each other, and using the sagittal plane for reference.
3- The field of view should include a wide field of view, plus a narrow one centered on the lesion.

Having defined the effect of body condition score on the normal MRI appearance of muscle, and described the normal MRI anatomy of this region, the final part of this study evaluated the effect of chronic denervation on the MRI appearance of muscle. This was achieved by retrospective evaluation of the MRI studies performed in 19 dogs with a presumptive diagnosis of brachial plexus neoplasia. First, the MR changes in the shoulder region muscles were assessed. A mixed pattern of T1W and T2W signal hyperintensity, varying degrees of fat infiltration (from detectable T1 hyperintensity to complete fat substitution of the muscle) and reduction in muscle size (from 24.82% to 78% of the control side) were identified. In two muscles, the serratus ventralis and the triceps, the amount of T2W hyperintensity was significantly higher than the T1W hyperintensity. The magnitude of this effect in these two muscle groups may be due to different stages of atrophy in the muscles of the shoulder region, or due to a combination of denervation and disuse. The retrospective nature of the study did not allow atrophy staging (T1W hyperintensity in the chronic phase, T2W hyperintensity in the acute phase) which has previously been established in experimental settings (Adami et al., 2006). Brachial plexus mass lesions create complex pathophysiological effects, with on-going degeneration and partial regeneration (due to muscle fibre sprouting), oedema, fatty infiltrate and tumour mass effects. The anatomical and physiological complexity of the proximal thoracic limb and its pattern of muscle innervation predisposes to involvement of multiple muscles in the event of brachial plexus lesions. The importance of the diagnostic capabilities of MRI for evaluation of this region was supported by the fact that more muscles demonstrated changes on MRI, than were detected clinically or by electromyography (EMG). The evaluation of fatty infiltrate into the denervated muscle was included in this study. It has been shown in

experimental rodent models and in human patients that the distribution of fatty streaks within a muscle is not evenly distributed, but adopts a random pattern and may not be adequately visualised on a single imaging plane. Based on this it has been suggested that the evaluation of fatty infiltration into muscle should be standardised (Williams et al., 2009).

The data presented in this study is an example of the response of muscle to chronic denervation as evaluated on MR images. The limitations of this part of the study were the relatively low number of animals in what is a heterogeneous disease and the absence of histological data. MRI of brachial plexus mass lesions has previously been evaluated (Platt et al., 1999; Kraft et al., 2007). The majority of the mass lesions were more readily detected on the STIR images, followed by T2W and T1 FatSat with contrast. The mass lesions were located paravertebrally and in the axilla. The masses varied in shape from a globoid mass to a tubular mass or fusiform nerve thickening. The globoid lesions produced a marked mass effect and induced surrounding soft tissue hyperintensity. The lesions exhibited a non-uniform contrast uptake. In 9 out of 19 cases more than one lesion was detected, and in 7 out of 19 cases the mass extended into the thoracic cavity. Mass extension into the vertebral canal was noted in 9/19 cases (47.4%), and in 6 of these spinal cord involvement was evident, with detectable spinal cord compression in 3/6 cases. Other disease processes may resemble a brachial plexus tumour: nerve abscesses or granulomas, foreign bodies, lymphoma, hypertrophic neuropathy, brachial plexus neuritis, hypertrophic neuritis or nerve thickening associated with foraminal stenosis (Chevoir et al., 2012). The diagnosis of a brachial plexus tumour becomes more problematic when there is fusiform nerve enlargement.

On the basis of the present study there are a number of additional questions, which have arisen. The study demonstrated a good correlation between BCS, SCF thickness and muscle T1W signal hyperintensity. It would be interesting to perform similar analyses based on abdominal and visceral fat deposition and T1W signal intensity in other groups of muscles. It would also be interesting to assess alterations in muscle signal intensity and the development of muscle atrophy in acute denervation conditions, disuse atrophy and metabolic myopathies. This could allow more detailed understanding of muscle atrophy staging and the differentiation between different conditions. A valuable addition to these studies would be the availability of histopathological data.

6 References

Abellan Van Kan, G., Cedarbaum, J.M., Cesari, M., Dahinden, P., Fariello, L. et al. (2011). Sarcopenia: biomarkers and imaging. Journal of Nutrition, Health & Aging, 15(10), 834-846.

Acevedo, L.M. & Rivero, J.-L.L. (2006). New insights into skeletal muscle fibre types in the dog with particular focus towards hybrid myosin phenotypes. Cell and Tissue Research, 323(2), 283–303.

Adami, N., Biral, D., Caccavale, S., & Rossini, K. (2006). Histology of the long term denervated rat muscle. Basic Applied Myology, 16 (3&4), 113–114.

Adibhatla, R.M. & Hatcher, J.F. (2007). Role of lipids in brain injury and diseases. Future Lipidology, 2(4), 403–422.

Agnello, K.A., Puchalski, S.M., Wisner, E.R., Schulz, K.S. & Kapatkin, A.S. (2008). Effect of positioning, scan plane, and arthrography on visibility of periarticular canine shoulder soft tissue structures on magnetic resonance images. Veterinary Radiology & Ultrasound, 49(6), 529–539.

Al-Attar, S.A., Pollex, R.L., Robinson, J. F., Miskie, B.A., Walcarius, R. et al. (2007). Quantitative and qualitative differences in subcutaneous adipose tissue stores across lipodystrophy types shown by magnetic resonance imaging. BMC Medical Imaging, 7, 3.

Allam, M., Lee, D., Nulsen, F. & Fortune, E. (1952). The anatomy of the brachial plexus of the dog. Anatomical Record, 114(2), 173–179.

Anor, S. (2004) Monoparesis. In: BSAVA Manual of Canine and Feline Neurology. Eds. S.R. Platt & N.J. Olby. 3rded. BSAVA, Gloucester, 265–279.

Bagley, R.S. (2010). Spinal neoplasms in small animals. Veterinary Clinics of North America: Small Animal Practice, 40(5), 915–927.

(Bakshi et al., 1999). Fluid-Attenuated inversion-recovery MR imaging in acute and subacute cerebral intraventricular haemorrhage. American journal of neuroradiology, 20(4), 629-636

Basso, C. & Thiene, G. (2005). Adipositas cordis, fatty infiltration of the right ventricle, and arrhythmogenic right ventricular cardiomyopathy. Just a matter of fat? Cardiovascular Pathology, 14(1), 37–41.

Bastard, J., Maachi, M. & Lagathu, C. (2006). Recent advances in the relationship between obesity, inflammation, and insulin resistance. European Cytokine Network, 17, 4–12.

Baulain, U. (1997). Magnetic resonance imaging for the in vivo determination of body composition in animal science. Computers and Electronics in Agriculture, 17(2), 189–203.

Beall, D.P., Googe, D.J., Emery, R.L., Thompson, D.B., Campbell, S.E. et al. (2007). Extramedullary intradural spinal tumors: a pictorial review. Current Problems in Diagnostic Radiology, 36(5), 185–198.

Bergmann, W., Burgener, I.A., Roccabianca, P., Rytz, U. & Welle, M. (2009). Primary splenic peripheral nerve sheath tumour in a dog. Journal of Comparative Pathology, 141(2-3), 195–198.

Biering-Sorensen, B., Kristensen, I.B., Kjaer, M., Biering-Sorensen, F. (2009). Muscle after spinal cord injury. Muscle & Nerve, 40(4), 499-519.

Bierry, G., Kremer, S., Kellner, F., Abu Eid, M., Bogorin, A. et al. (2008). Disorders of paravertebral lumbar muscles: from pathology to cross-sectional imaging. Skeletal Radiology, 37(11), 967–977.

Bishop, T.M., Glass, E.N., de Lahunta, A., & Shelton, G.D. (2008). Imaging diagnosis - masticatory muscle myositis in a young dog. Veterinary Radiology & Ultrasound, 49(3), 270–272.

Bitar, R., Leung, G., Perng, R., Tadros, S., Moody, A.R. et al. (2006). MR pulse sequences: what every radiologist wants to know but is afraid to ask. Radiographics, 26(2), 513–537.

Bitzer, M., Klose, U., Geist-Barth, B., Nägele, T., Schick, F. et al. (2002). Alterations in diffusion and perfusion in the pathogenesis of peritumoral brain edema in meningiomas. European Radiology, 12(8), 2062–2076.

Bjornvad, C. R., Nielsen, D. H., Armstrong, P. J., McEvoy, F., Hoelmkjaer, K. M. et al. (2011). Evaluation of a nine-point body condition scoring system in physically inactive pet cats. American Journal of Veterinary Research, 72(3), 433–437.

Bley, T.A., Wieben, O., François, C.J., Brittain, J.H. & Reeder, S. B. (2010). Fat and water magnetic resonance imaging. Journal of Magnetic Resonance Imaging, 31(1), 4–18.

Blum, A., Lecocq, S., Louis, M., Wassel, J., Moisei, A. et al. (2013). The nerves around the shoulder. European Journal of Radiology, 82(1), 2–16.

Boettcher, M., Machann, J., Stefan, N., Thamer, C., Häring, H.-U. et al. (2009). Intermuscular adipose tissue (IMAT): association with other adipose tissue compartments and insulin sensitivity. Journal of Magnetic Resonance Imaging , 29(6), 1340-1345.

Borisov, A.B., Dedkov, E.I., & Carlson, B.M. (2001). Interrelations of myogenic response, progressive atrophy of muscle fibres, and cell death in denervated skeletal muscle. Anatomical Record, 264(2), 203–218.

Bredella, M., Tirman, P., & Fritz, R. (1999). Denervation syndromes of the shoulder region: MR imaging with electrophysiologic correlation. Skeletal Radiology, 28(10), 567–572.

Brehm, D., Vite, C., Steinberg, H., Haviland, J. & van Winkle, T. (1995). A retrospective evaluation of 51 cases of peripheral nerve sheath tumours in the dog. Journal of American Animal Hospital Association, 31(4), 349–359.

Breisch, E. A. (1986). A rare human variation : the relationship of the axillary and inferior subscapular nerves to an accessory subscapularis muscle. Anatomical Record, 216(3), 440–442.

Bruce, W.J, Spence, S., Miller, A. (1997). Teres minor myopathy as a cause of lameness in a dog. Journal of Small Animal Practice, 38(2), 74-77.

Buhschwein, A., Flatz, K., Zoellner, M., Kostlin, R., Matis, U., 2008. Magnetic resonance imaging of musculature and tendons in small animal practice. Imaging technique and appearance of different diseases and traumatic injuries. Tieraerztliche Praxis Ausgabe Kleintiere Heimtiere 36, 249-262.

Burkholder, W.J. (2000). Use of body condition scores in clinical assessment of the provision of optimal nutrition. Journal of the American Veterinary Medical Association, 217(5), 650-654.

Burkholder, W.J., & Toll, P. W. (1997). In: Obesity: Management of Obesity. Hill's Pet Nutrition. 1-42.

Cagnie, B., Barbe, T., Vandemaele, P., Achten, E., Cambier, D. et al. (2009). MRI analysis of muscle/fat index of the superficial and deep neck muscles in an asymptomatic cohort. European Spine Journal, 18(5), 704–709.

Carlson, B. (2008). Muscle regeneration in animal models. In: Skeletal Muscle Repair and Regeneration Vol 3. Eds S. Schiaffino & T. Partridge. Springer Netherlands, Dordrecht. 163-179.

Carroll, K. W. & Helms, C.A. (2002). Magnetic resonance imaging of the shoulder: a review of potential sources of diagnostic errors. Skeletal Radiology, 31(7), 373–383.

Chaudhary, P., Singla, R., Kalsey, G., & Arora, K. (2012). A four trunked brachial plexus and a post fixed brachial plexus: a conjunction or a co-incidence? Report of three cases. Clinical Anatomy, 25(5), 593–600.

Chavhan, G.B., Babyn, P.S., Thomas, B., Shroff, M.M. & Haacke, E.M. (2009). Principles, techniques, and applications of T2*-based MR imaging and its special applications. Radiographics, 29(5), 1433–1449.

Chevoir, M., Thibaud, J.L., Labruyère, J., Uriarte, A., Fornel-Thibaud, P.D. et al. (2012). Electrophysiological features in dogs with peripheral nerve sheath tumors . Journal of American Veterinary Medical Association, 241(9), 1194–1201.

Collins, J., Shaver, M., Disher, A., & Miller, T. (1995). Compromising abnormalities of the brachial plexus as displayed by magnetic resonance imaging. Clinical Anatomy, 8(1), 1–16.

Corbee, R.J. (2013). Obesity in show dogs. Journal of Animal Physiology and Animal Nutrition, 97(5), 904–910.

Cornier, M.-A., Després, J.-P., Davis, N., Grossniklaus, D.A, Klein, S. et al. (2011). Assessing adiposity: a scientific statement from the American Heart Association. Circulation, 124(18), 1996–2019.

Costa, A.F., Di Primio, G.A, & Schweitzer, M.E. (2012). Magnetic resonance imaging of muscle disease: a pattern-based approach. Muscle & Nerve, 46(4), 465–481.

Cuddon, P. (2002). Acquired canine peripheral neuropathies. Veterinary Clinics of North America: Small Animal Practice, 32(1), 207-249.

Cummings, J.F., Lorenz, M.D., de Lahunta, A. & Washington, L.D. (1973). Canine brachial plexus neuritis: a syndrome resembling serum neuritis in man. Cornell Veterinarian, 63(4), 589–617.

Da Costa, R.C., Parent, J.M., Dobson, H., Ruotsalo, K., Holmberg, D. et al. (2008). Ultrasound-guided fine needle aspiration in the diagnosis of peripheral nerve sheath tumors in 4 dogs. Canadian Veterinary Journal, 49(1), 77–81.

Davies, D.R. & Irwin, P. J. (2003). Degenerative neurological and neuromuscular disease in young rottweilers. Journal of Small Animal Practice, 44(9), 388–394.

Dawson, R.M., Latif, Z., Haacke, E. M. & Cavanaugh, J.M. (2013). Magnetic resonance imaging-based relationships between neck muscle cross-sectional area and neck circumference for adults and children. European Spine Journal, 22(2), 446-452.

Degardin, A., Morillon, D., Lacour, A., Cotten, A., Vermersch, P. et al. (2010). Morphologic imaging in muscular dystrophies and inflammatory myopathies. Skeletal Radiology, 39(12), 1219–1227.

Delauche, A.J., Cuddon, P.A., Podell, M., Devoe, I.M., Powell, H.C. et al. (1998) Nemaline rods in canine myopathies: 4 case reports and literature review. Journal of Veterinary Internal Medicine, 12(6), 424-430.

Delfaut, E. & Beltran, J. (1999). Fat suppression in MR imaging: techniques and pitfalls. Radiographics, 19(2), 373–382.

Delp, M.D. & Duan, C. (1996). Composition and size of type I, IIA, IID/X, and IIB fibres and citrate synthase activity of rat muscle. Journal of Applied Physiology, 80(1), 261-270.

Deroide, N., Bousson, V., Daguet, E., Dumurgier, J., Tin, S. N.W. et al. (2012). Muscle magnetic resonance imaging sensitivity does not decrease in chronic, mild, or proximal lower limb neuropathies. Muscle & Nerve, 45(5), 659–667.

Dewey, C.A. (2008) Practical Guide to Canine and Feline Neurology. 2nd ed. Blackwell Ames. 706.

de Lahunta, A. & Evans, H. (2010) Guide to Dissection of the Dog. 7th ed. Saunders Elsevier, St. Louis. 17-27, 82, 121-129.

de Lahunta, A. & Glass, E. (2009) Veterinary Neuroanatomy and Clinical Neurology. 3rd ed. Saunders Elsevier, St.Louis. 86, 88-91, 101-105.

de Risio, L., McConnell, J., De Stefani., A., Matiasek, L., Feliu-Pascual, A., Shelton, G. (2009). Imaging diagnosis – acute necrotizing myopathy in a dog. Veterinary Radiology and Ultrasound, 50(6), 639-643.

Diez, M. (2006). Body condition scoring in cats and dogs. Focus, 16(1), 39–40.

Dirk P. (2001). Historical perspectives: plasticity of mammalian skeletal muscle. Journal of Applied Physiology, 90(3), 1119-1124.

Doppler, K., Mittelbrown, M., Bornemann, A. (2008). Myogenesis in human denervated muscle biopsies, Muscle & Nerve, 37(1), 79-83.

Dorsten, C.M. & Cooper, D.M. (2004). Use of body condition scoring to manage body weight in dogs. Contemporary topics in laboratory animal science. Contemporary Topics in Laboratory Animal Science, 43(3), 34-37.

Dyer, K.R., Duncan, I.D., Hammang, J.P. & Dubielzig, R.R. (1986) Peripheral neuropathy in two dogs: correlation between clinical, electrophysiological and pathological findings. Journal of Small Animal Practice, 27(3), 133-146.

Elliot, D. (2006). Techniques to assess body composition in dogs and cats. Focus, 16(1), 16–20.

Elliott, J.M., Galloway, G.J., Jull, G.A., Noteboom, J.T., Centeno, C.J. et al. (2005). Magnetic resonance imaging analysis of the upper cervical spine extensor musculature in an asymptomatic cohort: an index of fat within muscle. Clinical Radiology, 60(3), 355–363.

Elliott, J., Jull, G., Noteboom, J.T., Darnell, R., Galloway, G. et al. (2006). Fatty infiltration in the cervical extensor muscles in persistent whiplash-associated disorders: a magnetic resonance imaging analysis. Spine, 31(22), 847–855.

Eminaga, S., Cherubini, G.B., Villiers, E., Targett, M., & Caine, A. (2013). STIR muscle hyperintensity in the cervical muscles associated with inflammatory spinal cord disease of unknown origin. Journal of Small Animal Practice, 54(3), 137–42.

Es, H.W., Bollen, T.L. & Heesewijk, H. P. (2010). MRI of the brachial plexus: a pictorial review. European Journal of Radiology, 74(2), 391–402.

Essman, S.C., Hoover, J.P., Bahr, R.J., Ritchey, J.W. & Watson, C. (2002). An inthrathoracic malignant peripheral nerve sheath tumour in a dog. Veterinary Radiology & Ultrasound, 43(3), 255–259.

Evans, H., & de Lahunta, A. (2012). Miller's Anatomy of the Dog. 4th ed. Elsevier St. Louis. 210-214, 233-241, 618-628.

Evans, J., Levesque, D. & Shelton, G.D. (2004). Canine inflammatory myopathies: A clinicopathologic review of 200 Cases. Journal of Veterinary Internal Medicine, 18(5), 679–691.

Ferrante, M.A. (2004). Brachial plexopathies: classification, causes, and consequences. Muscle & Nerve, 30 (5), 547–568.

Ferreira, A., Peleteiro, M., Correia, J., Jesus, S., & Goulão, A. (2005) Small-cell carcinoma of the lung resembling a brachial plexus tumour. Journal of Small Animal Practice, 46(6), 286-290.

Freeman, L.M. (2012). Cachexia and sarcopenia: emerging syndromes of importance in dogs and cats. Journal of Veterinary Internal Medicine, 26(1), 3-17.

Fuglevand, A.J. & Segal, S.S. (1997). Simulation of motor unit recruitment and microvascular unit perfusion : spatial considerations. Journal of Applied Physiology, 83(4), 1223–1234.

Fusco, J., Marcellin-Little, D. J., Levine, D., Canapp, S. O. (2007). The canine shoulder: selected disorders and their management with physical therapy. Clinical Techniques in Small Animal Practice, 22(4), 171-182.

Garcia, J. (2000). MRI in inflammatory myopathies. Skeletal Radiology, 28(8), 425-438.

Gavin, P. R. & Bagley, R. S. (2009) Practical Small Animal MRI. 1st ed. Wiley-Blackwell, Ames. 8-10, 10-21, 227-230.

German, A. (2006). The growing problem of obesity in dogs and cats. Journal of Nutrition, 136, 1940S–1946S.

Gerth, N., Sum, S., Jackson, S. & Starck, J.M. (2009). Muscle plasticity of Inuit sled dogs in Greenland. Journal of Experimental Biology, 212(8), 1131–1139.

Goodpaster, B.H., Stenger, V.A., Boada, F., McKolanis, T., Davis, D. et al. (2004). Skeletal muscle lipid concentration quantified by magnetic resonance imaging. American Journal of Clinical Nutrition, 79(5), 748–754.

Gorgey, A.S. & Dudley, G.A. (2007). Skeletal muscle atrophy and increased intramuscular fat after incomplete spinal cord injury. Spinal Cord, 45(4), 304–309.

Granger, N. (2011). Canine inherited motor and sensory neuropathies: an updated classification in 22 breeds and comparison to Charcot-Marie-Tooth disease. Veterinary Journal, 188(3), 2742-2785.

Gupta, G. & Maniker, A. (2007). Malignant peripheral nerve sheath tumors. Neurosurgical Focus, 22(6), 1–8.

Hanson, S.M., Smith, M.O., Walker, T. L. & Shelton, G.D. (1998). Juvenile-onset distal myopathy in Rottweiler dogs. Journal of Veterinary Internal Medicine, 12(2), 103-108.

Harder, C., De Jong, J., Bos, C., Van Meel, M., Bystrov, D. et al. (2008). Consistent automated scan planning of shoulder. In: Proceedings 16th scientific meeting International Society for Magnetic Resonance in Medicine, Toronto, 3665.

Hayashi, N., Masumoto, T., Abe, O., Aoki, S., Ohtomo, K. et al. (2002). Accuracy of abnormal paraspinal muscle findings on contrast-enhanced MR images as indirect signs of unilateral cervical root-avulsion injury. Radiology, 223(2), 397–402.

Herpen, N.A. & Schrauwen-Hinderling, V.B. (2008). Lipid accumulation in non-adipose tissue and lipotoxicity. Physiology & Behaviour, 94(2), 231–241.

Hodson-Tole, E.F. & Wakeling, J.M. (2008). Motor unit recruitment patterns 2: the influence of myoelectric intensity and muscle fascicle strain rate. Journal of Experimental Biology, 211(12), 1893–1902.

Hofmeister, E.H., Kent, M. & Read, M.R. (2007). Paravertebral block for forelimb anaesthesia in the dog- an anatomic study. Veterinary Anaesthesia and Analgesia, 34(2), 139–342.

Hu, H.H. (2011). Body and organ fat quantification. Assessment of abdominal adiposity and organ fat with magnetic resonance imaging. In: Advances in CT and MRI Techniques; Preconference-workshop of the Obesity Society 2011 meeting, Orlando, Florida.

Hu, H. H., Nayak, K.S. & Goran, M.I. (2011) Assessment of abdominal adipose tissue and organ fat content by magnetic resonance imaging. Obesity Reviews, 12(5), 686-695.

Huang, L., Espinoza, C. & Welsh, R. (2003). Malignant peripheral nerve sheath tumour with divergent differentiation. Archive of Pathology & Laboratory Medicine, 127(3), 147–150.

Hutchinson, K. J., Linderman, J.K. & Basso, D.M. (2001). Peripheral neuropathy in two dogs: correlation between clinical, electrophysiological and pathological findings. Journal of Neurotrauma, 18(10), 1075-1089.

Hyodoh, K., Hyodoh, H. & Akiba, H. (2002). Brachial Plexus : normal anatomy, pathological conditions. Current Problems in Diagnostic Radiology, 31(5), 179–188.

Ishioka, K., Okumura, M., Sagawa, M., Nakadomo, F., Kimura, K. et al. (2005). Computed tomographic assessment of body fat in beagles. Veterinary Radiology & Ultrasound, 46(1), 49–53.

Jackman, R.W. & Kandarian, S.C. (2004). The molecular basis of skeletal muscle atrophy. American Journal of Physiology. Cell Physiology, 287(4), 834–843.

Jeng, C. & Rosenblatt, M. (2011). Intraneural injections and regional anesthesia: the known and the unknown. Minerva Anestesiologica, 77, 54–58.

Jeon, K.W., Pette, D. & Staron, R.S. (1997). Mammalian skeletal muscle fibre type transitions. International Review of Cytology, 170, 143–223.

Jeusette, I., Greco, D., Aquino, F., Detilleux, J., Peterson, M. et al. (2010). Effect of breed on body composition and comparison between various methods to estimate body composition in dogs. Research in Veterinary Science, 88(2), 227–232.

Johnson, E.O., Vekris, M., Demesticha, T., & Soucacos, P.N. (2010). Neuroanatomy of the brachial plexus: normal and variant anatomy of its formation. Surgical and Radiologic Anatomy, 32(3), 291–297.

Johnston, D. (1985). Tendons, skeletal muscles, and ligaments in health and disease. In: Textbook of Small Animal Orthopedics. Ed. D.M. Nunamaker. International Veterinary Information Service (www.ivis.org) New York.

Jones, B.R, Alley, M.R., Johnstone, A.C., Jones, J. M. Cahill, J.I. et al. (1995). Nerve sheath tumours in the dog and cat. New Zealand Veterinary Journal, 43(5), 190–196.

Jones, B.R., Alley, M.R, Johnstone, A., Jones, J.M., McPherson, J.I. et al. (1975). Malignant schwannoma of the brachial plexus in a dog. Australian Veterinary Journal, 51(1), 40–42.

Judmaier, W. (2013). Introduction to Magnetic Resonance Imaging of the Peripheral Nervous System: General Considerations and Examination Technique. In: Atlas of Peripheral Nerve Ultrasound. Eds. S. Peer & H. Gruber. Springer-Verlag Berlin. 17–28.

Kamath, S., Venkatanarasimha, N., Walsh, M. & Hughes, P.M. (2008). MRI appearance of muscle denervation. Skeletal Radiology, 37(5), 397–404.

Kan, V. G. A., Cedabraum, J.M., Cesari, M., Dahinden, P., Fariello, R.G., Fielding, R.A. et al. (2011). Sarcopenia: Biomarkers and imaging (International conference on sarcopenia research). The Journal of Nutrition, Health and Aging, 15(10), 834-846.

Khoury, V., Cardinal, E. & Brassard, P. (2008). Atrophy and fatty infiltration of the supraspinatus muscle: sonography versus MRI. American Journal of Roentgenology, 190(4), 1105–1111.

Kim, D.Y., Cho, D., Lee, J. & Taylor, H.W. (2003). Malignant peripheral nerve sheath tumour with divergent mesenchymal differentiations in a dog. Journal of Veterinary Diagnostic Investigation, 15(2), 174–178.

Kim, S., Hong, S. & Jun, W. (2011). MRI imaging mapping of skeletal muscle denervation in entrapment and compressive neuropathies MR imaging mapping of skeletal muscle denervation in entrapment and compressive neuropathies. Radiographics, 31(2), 319–332.

Kobayashi, M., Nakamura, A., Hasegawa, D., Fujita, M., Orima, H. et al. (2009). Evaluation of dystrophic dog pathology by fat-suppressed T2-weighted imaging. Muscle & Nerve, 40(5), 815–826.

Kornegay, J., Childers, D., Bogan, D.J., Bogan, J.R., Nghiem, P. et al. (2012) The paradox of muscle hypertrophy in muscular dystrophy. Physical Medicine and Rehabilitation. Clinics of North America, 23(1), 149-172.

Kostov, M., Mijovic, Z., Visnjic, M., Mihailovic, D., Stojanovic, M. et al. (2008). Malignant peripheral nerve sheath tumour in a dog presenting as a pseudo aneurysm of the left jugular vein : a case report. Veterinarni Medicina, 53(12), 685–689.

Kover, G., Szendro, Z., Romvari, R., Jensen, J., Sorensen, P. et al. (1998). In vivo measurement of body parts and fat deposition in rabbits by MRI. World Rabbit Science, 6(2), 231–235.

Kraft, S., Ehrhart, E.J., Gall, D., Klopp, L., Gavin, P. et al. (2007). Magnetic resonance imaging characteristics of peripheral nerve sheath tumours of the canine brachial plexus in 18 dogs. Veterinary Radiology & Ultrasound, 48(1), 1–7.

Kramer, M., Gerwing, M., Hach, V. & Schimke, E. (1996). Sonography of the musculoskeletal system in dogs and cats. Veterinary Radiology & Ultrasound, 38(2), 139–149.

Kube, S., Vernau, K., LeCouter, R., Mixisin, A. & Shelton, D. (2006). Congenital myopathy with abundant nemaline rods in a cat. Neuromuscular Disorders, 16(3), 188-191.

Küllmer, K., Sievers, K.W., Reimers, C.D., Rompe, J.-D., Müller-Felber, W. et al. (1998). Changes of sonographic, magnetic resonance tomographic, electromyographic, and histopathologic findings within a 2-month period of examinations after experimental muscle denervation. Archives of Orthopaedic and Trauma Surgery, 117(4-5), 228–234.

Laflamme, D. (1997). Development and validation of a body condition score system for dogs. Canine Practice, 22(4), 10–15.

Lemke, K.A. & Creighton, C.M. (2008). Paravertebral blockade of the brachial plexus in dogs. Veterinary Clinics of North America: Small Animal Practice, 38(6), 1231–41,

Li, C.-S., Huang, G.-S., Wu, H.-D., Chen, W.-T., Shih, L.-S. et al. (2008). Differentiation of soft tissue benign and malignant peripheral nerve sheath tumors with magnetic resonance imaging. Clinical Imaging, 32(2), 121–127.

Li, G., Lee, P., Mori, N., Yamamoto, I., Kawasumi, K. et al. (2012). Supplementing five-point body condition score with body fat percentage increases the sensitivity for assessing overweight status of small to medium sized dogs. Veterinary Medicine: Research and Reports, 3, 71–78.

Lin, J., & Martel, W. (2001). Cross-sectional imaging of peripheral nerve sheath tumors. American Journal of Roentgenology, 176(1), 75-82.

Linda, D., Harish, S., Stewart, B., Finlay, K., Parasu, N. et al. (2010). Multimodality imaging of peripheral neuropathies of the upper limb and brachial plexus. Radiographics, 30(5), 1373–1400.

Liney, G. (2005). MRI from A to Z: A Definitive Guide for Medical Professionals. 1sted. Cambridge University Press, Cambridge. 260.

Lorenz, M.D., Coates, J. & Kent, M. (2011). Handbook of Veterinary Neurology, 5th ed. Elsevier Saunders St. Louis. 94-105.

Lovitt, S., Moore, S.L. & Marden, F.A. (2006). The use of MRI in the evaluation of myopathy. Clinical Neurophysiology, 117(3), 486–495.

Lund, E., Armstrong, P., Kirk, C. & Klausner, J. (2006). Prevalence and risk factors for obesity in adult dogs from private US veterinary practices. International Journal of Applied Research in Veterinary Medicine, 4(2), 177-186.

Lutz, S., Sewell, A.C., Reusch, C.E. & Kook, P.H. (2013). Clinical and laboratory findings in border collies with presumed hereditary juvenile cobalamin deficiency. Journal of the American Animal Hospital Association, 49(3), 197–203.

Mahler, S.P. & Adogwa, A.O. (2008). Anatomical and experimental studies of brachial plexus, sciatic, and femoral nerve-location using peripheral nerve stimulation in the dog. Veterinary Anaesthesia and Analgesia, 35(1), 80–89.

Makrogiannis, S., Serai, S., Fishbein, K.W., Schreiber, C., Ferrucci, L. et al. (2012). Automated quantification of muscle and fat in the thigh from water-, fat-, and nonsuppressed MR images. Journal of Magnetic Resonance Imaging , 35(5), 1152–1161.

Mallouhi, A., Marik, W., Prayer, D., Kainberger, F., Bodner, G. et al. (2012). 3T MR tomography of the brachial plexus: structural and microstructural evaluation. European Journal of Radiology, 81(9), 2231–2245.

Marchadier, A., Vidal, C., Tafani, J.-P., Ordureau, S., Lédée, R. et al. (2011). In: Quantitative CT imaging for adipose tissue analysis in mouse model of obesity. R. Summers & B. van Ginneken (Eds.). SPIE Medical Imaging 2011. Orlando, Florida, 796320–796328.

Martin, R.M. & Fish, D.E. (2008). Scapular winging: anatomical review, diagnosis, and treatments. Current Reviews in Musculoskeletal Medicine, 1(1), 1–11.

Mawby, D.I., Bartges, J.W., D'Avignon, A., Laflamme, D.P., Moyers, T.D. et al. (2004). Comparison of various methods for estimating body fat in dogs. Journal of the American Animal Hospital Association, 40(2), 109–114.

May, D., Disler, D., Jones, E., Balkisoon, A. & Manaster, B. (2000). Abnormal signal intensity in skeletal muscle at MR imaging: patterns, pearls, and pitfalls. Radiographics, 20 Spec No (suppl 1), 295–315.

McFarland, E.G., Caicedo, J.C., Guitterez, M.I., Sherbondy, P.S. & Kim, T.K. (2001). The anatomic relationship of the brachial plexus and axillary artery to the glenoid: implications for anterior shoulder surgery. American Journal of Sports Medicine, 29(6), 729–733.

McGreevy, P.D., Thomson, P.C., Pride, C., Fawcett, A., Grassi, T. et al. (2005). Prevalence of obesity in dogs examined by Australian veterinary practices and the risk factors involved. Veterinary Record, 156(22), 695–702.

McMahon, C.J., Wu, J.S. & Eisenberg, R.L. (2010). Muscle edema. American Journal of Roentgenology, 194(4), 284–292.

Mehta, J.R., Braund, K.G., McKerrell, R.E. & Toivio-Kinnucan, M. (1989). Analysis of muscle elements, water, and total lipids from healthy dogs and Labrador retrievers with hereditary muscular dystrophy. American Journal of Veterinary Research, 50(5), 640–644.

Meininger, A., Figuerres, B. & Goldberg, B. (2011). Scapula winging: an update. Journal of American Academy of Orthopedic Surgeons, 19(8), 453–462.

Michel, K.E., Sorenmo, K. & Shofer, F.S. (2004). Evaluation of body condition and weight loss in dogs presented to a veterinary oncology service. Journal of Veterinary Internal Medicine, 18(5), 692–695.

Mitchell, A., Scholz, A., Wange, P. & Song, H. (2001). Body composition analysis of the pig by magnetic resonance imaging. Journal of Animal Science, 79(7), 1800–1813.

Mokrusch, T. (2002). MRI-Changes of skeletal muscle after denervation and LIB electrical stimulation. Basic Applied Myology, 12(6), 273–276.

Mohamed, M., Heasely, D.C., Yagmurlu, B., Yousem, D.M.(2004). Fluid-attenuated inversion recovery MR imaging and subarachnoid hemorrhage: not a panacea. American journal of neuroradiology, 25(4), 545-550.

Monti, R., Roy, R. & Edgerton, V. (2001). Role of motor unit structure in defining function. Muscle & Nerve, 24(7), 848–866.

Monziols, M., Collewet, G., Bonneau, M., Mariette, F., Davenel, A. et al. (2006). Quantification of muscle, subcutaneous fat and intermuscular fat in pig carcasses and cuts by magnetic resonance imaging. Meat Science, 72(1), 146–154.

Murphey, M. D., Smith, W. S., Smith, S. E., Mark, J. & Temple, H. T. (1999). Imaging of musculoskeletal neurogenic tumours : radiologic-pathologic correlation. Radiographics, 19(5), 1253–1280.

Murphy, W.A, Totty, W.G. & Carroll, J.E. (1986). MRI of normal and pathologic skeletal muscle. American Journal of Roentgenology, 146(3), 565–574.

Nakamura, M., Tomizawa, N., Tohyama, K. & Hara, S. (2004). Morphological variations in brachial plexus of beagle dogs : evaluation of utility as sources of allogeneic nerve grafts. Journal of Veterinary Medical Science, 66(7), 767–772.

Napier, N., Shortt, C. & Eustace, S. (2006). Muscle edema: classification, mechanisms, and interpretation. Seminars in Musculoskeletal Radiology, 10(4), 258–267.

Naude, S. & Miller, D.B. (2006). Magnetic resonance imaging findings of a metastatic chemodectoma in a dog. Journal of South African Veterinary Association, 77(3), 155–159.

O'Neill, D.G., Elliott, J., Church, D.B., McGreevy, P.D., Thomson, P.C. et al. (2013). Chronic kidney disease in dogs in UK veterinary practices: prevalence, risk factors, and survival. Journal of Veterinary Internal Medicine, 27(4), 814–821.

Okada, E., Matsumoto, M., Ichihara, D., Chiba, K. & Toyama, Y. (2011). Cross-sectional area of posterior extensor muscles of the cervical spine in asymptomatic subjects: a 10-year longitudinal magnetic resonance imaging study. European Spine Journal, 20(9), 1567–1573

Olby, N.J., Sharp, N.J.H., Nghiem, P.E., Keene, B.W., DeFrancesco, T.C. et al. (2011). Clinical progression of X-linked muscular dystrophy in two German Shorthaired Pointers. Journal of the American Veterinary Medical Association, 238(2), 207–212.

Olegário, E., Zanoni, F.P., Ferioli, R.B., Siliane, M., De Souza, B. et al. (2012). Canine malignant peripheral nerve sheath tumour involving nerve roots of the third lumbar spinal cord segment. Semina: Ciências Agrárias, Londrina, 33(6), 2397–2402.

Oliveira, M., Fuente, C.D. LA, Pumarola, M. & Anor, S. (2013). Imaging diagnosis: cranial cervical intraspinal schwannoma in a dog. Veterinary Radiology & Ultrasound, doi: 10.1111/vru.12071.

Orebaugh, S.L. & Williams, B.A. (2009). Brachial plexus anatomy: normal and variant. Scientific World Journal, 9, 300–312.

Orellana-James, N., Ginja, M., Regueiro, M., Oliveira, P., Gama, A. et al. (2013). Subacute and chronic MRI findings in bilateral canine fibrotic contracture of the infraspinatus muscle. Journal of Small Animal Practice, 54(8), 428-431.

Orima, H. & Fujita, M. (1997). Computed tomographic findings of experimentally induced neurogenic muscular atrophy in dogs. Journal of Veterinary Medical Science, 59(8), 729–731.

Paciello, O., Maiolino, P., Fatone, G. & Papparella, S. (2003). Mitochondrial myopathy in a German Shepherd dog. Veterinary Pathology, 40(5), 507-511.

Park, J.-W., Woo, G.-H., Jee, H., Jung, D.-W., Youn, H.-Y. et al. (2011). Malignant peripheral nerve sheath tumour in the liver of a dog. Journal of Comparative Pathology, 144(2-3), 223–226.

Pathria, M. & Boutin R. (2005). Magnetic resonance imaging of muscle. In: Musculoskeletal Diseases. Eds J. Hodler, C.L. Zollikofer & G.K. von Schulthess. Springer Zurich. 48-53.

Patterson, C.C. & Perry, R.L. (2008). Malignant peripheral nerve sheath tumour. Journal of the American Animal Hospital Association, 44(1), 36-40.

Petersilge, C.A., Pathria, M.N., Gentili, A., Recht, M.P. & Resnick, D. (1995). Denervation hypertrophy of muscle: MR features. Journal of Computer Assisted Tomography, 19(4), 596–600.

Pette, D. (2001). Plasticity in skeletal, cardiac and smooth muscle. Historical perspectives: plasticity of mammalian skeletal muscle. Journal of Applied Physiology, 90(3), 1119–1124.

Pette, D. & Staron, R.S. (2001). Transitions of muscle fibre phenotypic profiles, Histochemistry & Cell Biology, 115(5), 359–372.

Pfirrmann, C.W.A. (2008). Science to Practice : Can MR imaging be used to predict the degree and prognosis of peripheral nerve injuries ? Radiology, 247(2), 301–302.

Phoenix, J., Betal, D., Roberts, N., Helliwell, T.R. & Edwards, R.H. (1996). Objective quantification of muscle and fat in human dystrophic muscle by magnetic resonance image analysis. Muscle & Nerve, 19(3), 302–310.

Piercy, R.J., Hinchcliff, K.W., Morley, P.S., Di Silvestro, R.A., Reinhart, G.A. et al. (2001). Vitamin E and exertional rhabdomyolysis during endurance sled dog racing. Neuromuscular Disorders, 11(3), 278–286.

Platt, S. (2002). Neuromuscular complications in endocrine and metabolic disorders. Veterinary Clinics of North America: Small Animal Practice, 32(1), 125-146.

Platt, S. & Garosi, L. (2012). Small Animal Neurological Emergencies. Manson Publishing London. 672.

Platt, SR, Graham, J., Chrisman, C.L., Collins, K., Chandra, S. (1999). Magnetic resonance imaging and ultrasonography in the diagnosis of a malignant peripheral nerve sheath tumor in a dog. Veterinary Radiology & Ultrasound, 40(4), 367–71.

Platt, S.R., McConnell, F.J., Garosi, L.S., Ladlow, J. et al. (2006) Magnetic resonance imaging in the diagnosis of canine inflammatory myopathies in three dogs. Veterinary Radiology & Ultrasound, 47(6), 532-537.

Podell, M. (2002). Inflammatory myopathies. Veterinary Clinics of North America: Small Animal Practice. 32(1), 147-167.

Polak, J.F., Jolesz, F.A. & Adams, D.F. (1988) NMR of skeletal muscle differences in relaxation parameters related to extracellular/intracellular fluid spaces. Investigative Radiology, 23(2), 107-112.

Polster, J.M., & Schickendantz, M.S. (2010). Shoulder MRI: what do we miss? American Journal of Roentgenology, 195(3), 577–584.

Powers, S.K., Kavazis, A.N. & McClung, J.M. (2007). Oxidative stress and disuse muscle atrophy. Journal of Applied Physiology, 102(6), 2389–2397.

Preedy, V. & Peters, T. (2002). Skeletal Muscle: Pathology, Diagnosis and Management of Disease. Cambridge University Press, London. 716.

Psatha , M., Wu, Z., Gammie, F.M., Ratkevicius, A., Wackerhage, H. et al. (2012) A longitudinal MRI study of muscle atrophy during lower leg immobilization following ankle fracture. Journal of Magnetic Resonance Imaging, 35(3), 686-956.

Pumarola, M., Moore, P.F. & Shelton, G.D. (2004). Canine inflammatory myopathy: analysis of cellular infiltrates. Muscle & Nerve, 29(6), 782–789.

Radin, M.J., Sharkey, L.C., & Holycross, B.J. (2009). Adipokines: a review of biological and analytical principles and an update in dogs, cats, and horses. Veterinary Clinical Pathology, 38(2), 136–156.

Rasouli, N., Molavi, B., Elbein, S.C. & Kern, P.A. (2007). Ectopic fat accumulation and metabolic syndrome. Diabetes, Obesity, Metabolism, 9(1), 1–10.

Ródenas, S., Summers, B., Saveraid, T., Denning, A. & Marioni-Henry, K. (2013). Chronic hypertrophic ganglioneuritis mimicking spinal nerve neoplasia: clinical, imaging, pathologic findings, and outcome after surgical treatment. Veterinary Surgery, 42(1), 91–98.

Rodriguez, F.J., Folpe, A.L., Giannini, C. & Perry, A. (2012). Pathology of peripheral nerve sheath tumors: diagnostic overview and update on selected diagnostic problems. Acta Neuropathologica, 123(3), 295–319.

Rose, S., Long, C., Knipe, M. & Hornof, B. (2005). Ultrasonographic evaluation of brachial plexus tumors in five dogs. Veterinary Radiology & Ultrasound, 46(6), 514–517.

Ross, R, Goodpaster, B., Kelley, D. & Boada, F. (2000). Magnetic resonance imaging in human body composition research. From quantitative to qualitative tissue measurement. Annals of the New York Academy of Sciences, 904, 12–17.

Rucinsky, R., Cook, A., Haley, S., Nelson, R., Zoran, D.L. et al (2010). Diabetes management guidelines for dogs and cats. Journal of American Animal Hospital Association, 46(3), 215–224.

Rudich, S.R., Feeney, D.A., Anderson, K.L. & Walter, P.A. (2004). Computed tomography of masses of the brachial plexus and contributing nerve roots in dogs. Veterinary Radiology & Ultrasound, 45(1), 46–50.

Sacha, J., Cockman, M.D., Dufresne, T.E. & Trokhan, D.P. (2003). Quantification of regional fat volume in rat MRI. In: Medical Imaging: Physiology and Function: Methods, Systems, and Applications, Proceedings SPIE5031, 289–297.

Sagawa, M., & Nakadomo, F. (2002). Correlation between plasma leptin concentration and body fat content in dogs. American Journal of Veterinary Research, 63(1), 7–10.

Samara, A., Ventura, E.E., Alfadda, A.A. & Goran, M.I. (2012). Use of MRI and CT for fat imaging in children and youth: what have we learned about obesity, fat distribution and metabolic disease risk? Obesity Reviews, 13(8), 723–732.

Sanderson, S.L. (2010). Body Condition Score Techniques for Dogs. NAVC Clinician's Brief, 4(March), 6–9.

Sato, T., Yamamoto, A., Shibuya, H., Sudo, H., Shirai, W. et al. (2005). Intraocular peripheral nerve sheath tumour in a dog. Veterinary Ophthalmology, 8(4), 283–286.

Saunders, J.H., Poncelet, L., Clercx, C. & Snaps, F.R. (1998). Probable trigeminal nerve schwannoma in a dog. Veterinary Radiology & Ultrasound, 39(6), 539–542.

Sawamoto, O., Yamate, J., Kuwamura, M., Hagiwara, R. & Kurisu, K. (1999). A canine peripheral nerve sheath tumor including peripheral nerve fibres. Journal of Veterinary Medicine Science, 61(12), 1335–1338.

Scelsi, R. (2001). Muscle pathology after spinal cord injury: our 20 year experience and results on skeletal muscle changes in paraplegics, related to functional rehabilitation. Basic Applied Myology, 11(2), 75–85.

Schaefer, S.L. & Forrest, L.J. (2006). Magnetic resonance imaging of the canine shoulder: an anatomic study. Veterinary Surgery, 35(8), 721–728.

Schiaffino, S. & Reggiani, C. (2011). Fibre types in mammalian skeletal muscles. Physiological Reviews, 91(4), 1447–1531.

Schoniger, S., & Summers, B.A. (2009). Localized, plexiform, diffuse, and other variants of neurofibrome in 12 dogs, 2 horses, and a chicken. Veterinary Pathology, 46(5), 904-915.

Schreurs, N.M., Garcia, F., Jurie, C., Agabriel, J., Micol, D. et al. (2008). Meta-analysis of the effect of animal maturity on muscle characteristics in different muscles, breeds, and sexes of cattle. Journal of Animal Science, 86(11), 2872–2887.

Scordilis, P.J., Grenier, J.-M. & Wessely, M.A. (2005). Shoulder MRI. Part 1: A basic overview. Clinical Chiropractic, 8(2), 93-101.

Scott, W., Stevens, J. & Binder–Macleod, S. (2001). Human skeletal muscle fibre type classifications. Physical Therapy, 81(11), 1810–1816.

Sharir, A., Milgram, J. & Shahar, R. (2006). Structural and functional anatomy of the neck musculature of the dog (Canis familiaris). Journal of Anatomy, 208(3), 331–351.

Sharp, N.J.H. & Wheeler, S. J. (2005). Small Animal Spinal Disorders: Diagnosis and Surgery. 2nd ed. Elsevier Mosby Edinburgh. 722.

Shelton, G.D., Nyhan, W., Kass, P., Barshop, B., Haas, R. (1998). Analysis of organic acids, amino acids, and carnitine in dogs with lipid storage myopathy. Muscle & Nerve, 21(9), 1202-1205.

Shelton, G.D. (2004). Rhabdomyolysis, myoglobinuria, and necrotizing myopathies. Veterinary Clinics of North America: Small Animal Practice, 34(6), 1469–1482.

Shelton, G.D. (2007). From dog to man: the broad spectrum of inflammatory myopathies. Neuromuscular Disorders , 17(9-10), 663–670.

Shelton, G.D. (2010). Routine and specialized laboratory testing for the diagnosis of neuromuscular diseases in dogs and cats. Veterinary Clinical Pathology, 39(3), 278–295.

Shen, W., Wang, Z., Punyanita, M., Lei, J., Sinav, A. et al. (2003). Adipose tissue quantification by imaging methods: a proposed classification. Obesity Research, 11(1), 5–16.

Silva, R., Uosyte, R., Clements, D.N., Bergkvist, G.T., & Schwarz, T. (2013). Computed tomography and positive contrast computed tomographic arthrography of the canine shoulder: normal anatomy and effects of limb position on visibility of soft tissue structures. Veterinary Radiology & Ultrasound, 54(5), 470–477.

Simpson, D. J., Beck, J. A., Allan, G. S. & Culvenor, J. A. (1999). Diagnosis and excision of a brachial plexus nerve sheath tumour in a dog. Australian Veterinary Journal, 77(4), 5–7.

Slupe, J. L., Freeman, L. M. & Rush, J. E. (2008). Association of body weight and body condition with survival in dogs with heart failure. Journal of Veterinary Internal Medicine, 22(3), 561–565.

Son, H.R., d'Avignon, D.A. & Laflamme, D P. (1998). Comparison of dual-energy x-ray absorptiometry and measurement of total body water content by deuterium oxide dilution for estimating body composition in dogs. American Journal of Veterinary Research, 59(2), 529–532.

Souccar, C., Lapa, A., Do Valle, J. (1982). The influence of testosterone on neuromuscular transmission in hormone sensitive mammalian skeletal muscles. Muscle & Nerve, 5(3), 232-237.

Stahl, C., Wacker, C., Weber, U., Forterre, F., Hecht, P. et al. (2010). MRI features of gastrocnemius musculotendinopathy in herding dogs. Veterinary Radiology & Ultrasound, 51(4), 380–385.

Steiss, J. E. (2002). Muscle disorders and rehabilitation in canine athletes. Veterinary Clinics of North America: Small Animal Practice, 32(1), 267–285.

Stone, R., Berghoff, N., Steiner, JM. & Zoran, D. (2009). Use of a bioelectric impedance device in obese and lean healthy dogs to estimate body fat percentage. Veterinary Therapeutics, 10(1-2), 59–70.

Stringer, E.M., Stoskopf, M.K., Simons, T., O'Connell, A.F. & Waldstein, A. (2010). Ultrasonic measurement of body fat as a mean of assessing body condition in free-ranging Raccoons (Procyon lotor). International Journal of Zoology, 1–6.

Stumpo, M., Foschini, M.P., Poppi, M., Cenacchi, G., & Martinelli, P. (1999). Hypertrophic inflammatory neuropathy involving bilateral brachial plexus. Surgical Neurology, 52(6), 458–465.

Sureka, J., Cherian, R.A., Alexander, M. & Thomas, B.P. (2009). MRI of brachial plexopathies. Clinical Radiology, 64(2), 208–218.

Tagliafico, A., Succio, G., Serafini, G. & Martinoli, C. (2012). Diagnostic accuracy of MRI in adults with suspect brachial plexus lesions: A multicentre retrospective study with surgical findings and clinical follow-up as reference standard. European Journal of Radiology, 81(10), 2666–2672.

Tamilarasan, K.P., Temmel, H., Das, S.K., Al Zoughbi, W., Schauer, S. et al. (2012). Skeletal muscle damage and impaired regeneration due to LPL-mediated lipotoxicity. Cell Death & Disease, 3(7), 1–8.

Tang, H., Vasselli, J., Wu, E. & Gallagher, D. (2000). In vivo determination of body composition of rats using magnetic resonance imaging. Annals of the New York Academy of Sciences, 904, 32–41.

Tavasoly, A., Javanbakht, J., Khaki, F., Hosseini, E. & Bahrami, A. (2013). Ulnar malignant peripheral nerve sheath tumor diagnosis in a mixed-breed dog as a model to study human : histologic, immunohistochemical and clinicopathologic study. Diagnostic Pathology, 8(86), 1–6.

Thibaud, J.-L., Monnet, A., Bertoldi, D., Barthélémy, I., Blot, S. et al. (2007). Characterization of dystrophic muscle in golden retriever muscular dystrophy dogs by nuclear magnetic resonance imaging. Neuromuscular disorders , 17(7), 575–584.

Thomas, E.L., Parkinson, J.R., Frost, G.S., Goldstone, A.P., Doré, C. J. et al. (2012). The missing risk: MRI and MRS phenotyping of abdominal adiposity and ectopic fat. Obesity, 20(1), 76–87.

Toll, P.W., Yamka, R.M., Schoenherr, W.D. & Hand, M.S. (2010). Obesity: In: Small Animal Clinical Nutrition. Eds. M.S. Hand, C.D. Thatcher, R.L. Remillard, P. Roudebush & B.J. Novotny. 5th ed. Mark Morris Institute Topeka, 501–529.

Tomanek, R.J. & Lund, D.D. (1973). Degeneration of different types of skeletal muscle fibres I. Denervation. Journal of Anatomy, 116(3), 395–407.

Trayhurn, P. & Wood, I.S. (2004). Adipokines: inflammation and the pleiotropic role of white adipose tissue. British Journal of Nutrition, 92(3), 347–355.

Trumpatori, B.J., Carter, J.E., Hash, J., Davidson, G.S., Mathews, K. G. et al. (2010). Evaluation of a midhumeral block of the radial, ulnar, musculocutaneous and median (RUMM block) nerves for analgesia of the distal aspect of the thoracic limb in dogs. Veterinary Surgery, 39(7), 785–796.

Vettor, R., Milan, G., Franzin, C., Sanna, M., De Coppi, P. et al. (2009). The origin of intermuscular adipose tissue and its pathophysiological implications. American Journal of Physiology. Endocrinology and Metabolism, 297(5), E987–998.

Vilanova, J.C., Woertler, K., Narváez, J.A, Barceló, J., Martínez, S.J. et al. (2007). Soft-tissue tumours update: MR imaging features according to the WHO classification. European Radiology, 17(1), 125–138.

Vitale, C. & Olby, N.J. (2007) Neurologic dysfunction in hypothyroid, hyperlipidemic Labrador Retrievers. Journal of Veterinary Internal Medicine, 21(6), 1316-1322.

Volpi, E., Nazemi, R., Fujita, S. (2004). Muscle tissue changes with aging. Current Opinion in Clinical Nutrition and Metabolical Care, 7(4), 405-410.

Walmsley, G., Scurrell, E., Summers, B., Mahoney, P., Penning, V. et al. (2009). Foreign body induced neuritis masquerading as a canine brachial plexus nerve sheath tumor. Veterinary Comparative Orthopaedics and Traumatology, 22(5), 427–429.

Watson, C.J. & Schenkman, M. (1995). Physical therapy management of isolated serratus anterior muscle paralysis. Physical Therapy, 75(3), 194–202.

Watson, P.J. (2003). Exocrine pancreatic insufficiency as an end stage of pancreatitis in four dogs. Journal of Small Animal Practice, 44(7), 306–312.

Wattjes, M.P., Kley, R.A. & Fischer, D. (2010). Neuromuscular imaging in inherited muscle diseases. European Radiology, 20(10), 2447–2460.

Weiss, S. & Goldblum, J. (2001), Malignant tumours of the peripheral nerves. In: Enzinger and Weiss's Soft Tissue Tumors. 4th ed. Elsevier Mosby, St. Louis. 1622.

Wenk, M.R. (2005). The emerging field of lipidomics. Nature Reviews: Drug Discovery, 4(7), 594–610.

Wessig, C., Kenn, W., Koltzenburg, M. & Bendszus, M. (2006). Denervation hypertrophy may mimic local tumor spread on magnetic resonance imaging. Muscle & Nerve, 34(1), 108–110.

Wessig, C., Koltzenburg, M., Reiners, K., Solymosi, L. & Bendszus, M. (2004). Muscle magnetic resonance imaging of denervation and reinnervation : correlation with electrophysiology and histology. Experimental Neurology, 185(2), 254–261.

Wheeler, S.J. & Wright, J.A. (1986). The diagnosis of brachial plexus disorders in dogs : a review of twenty-two cases. Journal of Small Animal Practice, 27(3), 147–157.

White, L.M., Wunder, J.S., Bell, R.S., O'Sullivan, B., Catton, C. et al. (2005). Histologic assessment of peritumoral edema in soft tissue sarcoma. International Journal of Radiation Oncology, Biology, Physics, 61(5), 1439–1445.

Wilkinson, M.J. & McEwan, N.A. (1991). Use of ultrasound in the measurement of subcutaneous fat and prediction of total body fat in dogs. Journal of Nutrition, 121(11 Suppl), S47–50.

Williams, M.D., Lädermann, A., Melis, B., Barthelemy, R. & Walch, G. (2009). Fatty infiltration of the supraspinatus: a reliability study. Journal of Shoulder and Elbow Surgery, 18(4), 581–587.

Windhorst, U. & Mommaerts, W. (1996). Physiology of skeletal muscle. In: Comprehensive Human Physiology Vol.1. Eds R. Greger & U.Windhorst. 1sted. Springer-Verlag, Berlin, 911-932.

Wippold, F.J., Lubner, M., Perrin, R.J., Lämmle, M. & Perry, A. (2007). Neuropathology for the neuroradiologist: Antoni A and Antoni B tissue patterns. American Journal of Neuroradiology, 28(9), 1633–1638.

Withrow, S. J., & Vail, D. M. (eds.). Withrow & MacEwen's Small Animal Clinical Oncology, 4th ed., p. 677. Saunders, Elsevier, St. Louis, MO, 2007.

Wokke, B.H., Bos, C., Reijnierse, M., van Rijswijk, C.S., Eggers, H. et al. (2013). Comparison of dixon and T1-weighted MR methods to assess the degree of fat infiltration in Duchenne muscular dystrophy patients. Journal of Magnetic Resonance Imaging , 38(3), 619-624.

Woo, O.H., Yong, H.S., Shin, B.K., Oh, Y.-W., Kim, H.K. et al. (2008). Wide spectrum of thoracic neurogenic tumors: a pictorial review of CT and pathological findings. British Journal of Radiology, 81(968), 668–676.

Yamabe, E.N., Toshiyasu, O., Koichi, K., Y., Ikegami, H. Toyama, Y. (2008). Peripheral nerve injury : diagnosis with MR imaging of denervated skeletal muscle - experimental study in rats. Radiology, 247(2), 409-417.

Yang, H.-J., Gil, Y.-C. & Lee, H.-Y. (2009). Intersegmental origin of the axillary artery and accompanying variation in the brachial plexus. Clinical Anatomy, 22(5), 586–594.

Yanny, S. & Toms, A. P. (2010). MR patterns of denervation around the shoulder. American Journal of Roentgenology, 195(2), W157–163.

Zachary, J. & McGavin, M. (2012) Skeletal Muscle. In: Pathologic Basis of Veterinary Disease. 5thed. Elsevier Mosby St. Louis. 891–919.

Zhang, J., Zhang, G., Morrison, B., Mori, S. & Sheikh, K. A. (2008). Magnetic resonance imaging of mouse skeletal muscle to measure denervation atrophy. Experimental Neurology, 212(2), 448–457.

Zierath, J.R. & Hawley, J.A. (2004). Skeletal muscle fibre type: Influence on contractile and metabolic properties. PLoS Biology, 2(10), e348.

7 Abbreviations

BCS	Body condition score
C4-C5	Cervical fourth and fifth vertebrae
CL	Clinically observed
CSF	Cerebrospinal fluid
CT	Computer tomography
DEXA	Dual energy X-ray absorptiometry
DICOM	Digital imaging and communication in medicine
DIXON	Chemical shift phenomenon in MRI
DNA	Deoxyribonucleic acid
EMG	Electromyography
Fat Sat	Fat saturation
HS	Hock-to-Stifle length
L1-L2	Lumbar first and second vertebrae
LMN	Lower motor neuron
M(mm)	Muscle (muscles)
MPNST	Malignant peripheral nerve sheath tumour
MRI	Magnetic resonance imaging
MTS	Metastasis
N(n)	Nerve
PACS	Picture archiving and communication system
PCcm	Pelvic circumference
PNST	Peripheral nerve sheath tumour
SCF	Subcutaneous fat
STIR	Short tau inversion recovery sequence
T1	Spin-lattice relaxation time
T2	Spin-spin relaxation time
TR/TE	Repetition time/echo time
US	Ultrasound